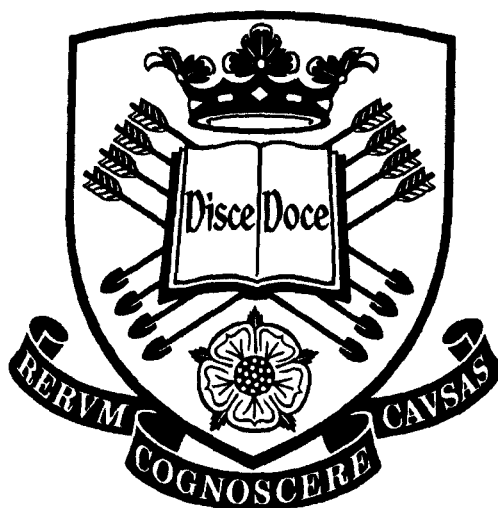


Modification of Epoxy Resins with Block Copolymers of Poly(ethylene oxide) and Poly(butylene oxide).

Gareth John Royston



The University of Sheffield
Department of Chemistry

A thesis submitted for the degree of Doctor of Philosophy, December
2006.

Abstract

Block copolymer modified epoxy resins have generated significant interest since it was demonstrated that the combination could lead to nanostructured thermosets through self-assembly.

In this work, samples of epoxy resin - formed by reaction of bisphenol-A diglycidyl ether (BADGE) and diethyltoluenediamine (DETDA) - and containing a range of copolymers composed of poly(ethylene oxide) (E) and poly(butylene oxide) (B), were prepared and characterized. Samples contained EB, EBE and BEB copolymers over a range of concentrations. Copolymers of low molecular weight and low B content were found not to microphase separate. BEB copolymers with high molecular weight and high B content were found to macrophase separate prior to, or during, cure.

FTIR spectroscopy during cure demonstrated that the reaction kinetics in these systems differ from those previously reported for similar systems.

Over moderate to high copolymer concentration the systems behaved as expected of a block copolymer in a solvent selective for one block. As concentration increased, transitions from BCC-Hex-Gyr-Lam phases were observed by SAXS.

At lower concentrations, in some systems, spherical micellar structures were formed, as demonstrated by TEM. SAXS analysis was performed on those systems producing sufficiently clear patterns. Some degree of reaction-induced microphase separation (RI μ PS) was observed in all cases. A linear increase in scattering intensity with extent of reaction was observed during RI μ PS. In some cases non-equilibrium structures were apparently observed, due to vitrification prior to completion of the RI μ PS process. The increase in the number of micelles as a function of concentration was analyzed and found to deviate from linearity as the system goes from a solution of copolymer in epoxy to swollen copolymer gel. The association number of the micelles was found to vary as a function of copolymer composition following a similar scaling law to that observed, by others, in aqueous solution.

Reaction-induced macrophase separation was observed in some BEB systems at elevated temperature, but not in similar EBE systems. The process was characterised by SALS and found to fit to the Cahn-Hilliard linear theory of spinodal decomposition. The systems were seen to vitrify before phase separation is complete, producing cured products that were phase separated into interpenetrating networks on the micron scale.

No significant improvement of mechanical properties of the resin was observed in those samples tested.

Declaration

I certify that this thesis, submitted for the degree of Doctor of Philosophy, is the result of my own work, except where otherwise acknowledged. Furthermore, I certify that no part of this work has been submitted towards a higher degree at any other university or institution.

Signed: 

Gareth Royston

Department of Chemistry, University of Sheffield, 26th April 2007.

Acknowledgements

Well, there are those that said it would never happen (I should know – for a while, I was one of them!) but it's finally done!

First and foremost I must thank my supervisor Patrick Fairclough for providing assistance, advice and encouragement throughout the last several years and for allowing me the chance to see this through.

I thank also Chiraphon Chaibundit and Withawat Minvanish, whom I have never met, but without whose labour over a hot vac line there would have been no copolymer with which to perform this work. Shaomin Mai also synthesised some of the polymers and, in addition, is thanked for help with SEM imaging and general assistance during my time in the group.

Thanks to Tony Ryan for advice and encouragement, to Sasha for help with the analysis of SAXS data, and to Andy Pryke for assistance with the rheometers.

Geoff Cope and Chris Hill of the Department of Biomedical Sciences prepared and imaged the TEM samples. Les Norton is thanked for help with the DMTA measurements.

Many thanks are due to Richard Wilkinson, without whose expertise nothing would ever get made, fixed, installed or serviced.

One of the things about being in one place for some time is that the list of people to thank on a personal level becomes almost limitless. Particular thanks are due to Ruth, Lyndsey, Nadejda, Christine and Colin, without whose friendship and support this day would probably never have come. As to the many others I must thank, a combination of the fear of causing offence by omission and the desire to get this blasted thing submitted leads me simply to thank all of those people who have provided me with friendship, advice, help and more during the completion of this work. Whether I know you from D49, Chemistry, Sheffield, or elsewhere, you all know who you are. Thank You.

Lastly, I save my most sincere thanks for my family for their unending patience and love.

1	INTRODUCTION	1
1.1	Epoxy Resin	2
1.1.1	Curing Reaction	2
1.1.2	Gelation	3
1.1.3	Curing Kinetics	5
1.1.4	Fracture Behaviour	7
1.1.5	Phase Separation	10
1.2	Block Copolymers	15
1.2.1	Behaviour in the Bulk	16
1.2.2	Behaviour in Solution	17
1.3	Nanostructured Block Copolymer - Epoxy Thermosets: A Brief Review	20
1.3.1	Non-reactive Modifiers	20
1.3.2	Reactive block copolymers	36
1.3.3	Fracture toughening	39
1.4	Aims	42
2	MATERIALS AND METHODS	43
2.1	Materials	43
2.1.1	Epoxy Resin	43
2.1.2	Cross-linking Agent	45
2.1.3	Block Copolymers	45
2.1.4	Preparation of Block Copolymer / Epoxy Blends	49
2.2	Experimental Techniques	51
2.2.1	Optical Microscopy	51
2.2.2	Transmission Electron Microscopy (TEM)	53
2.2.3	Scanning Electron Microscopy (SEM)	55
2.2.4	Fourier Transform Infra-Red Spectroscopy (FTIR)	56
2.2.5	Diferential Scanning Calorimetry (DSC)	58
2.2.6	Small Angle X-Ray Scattering (SAXS)	59
2.2.7	Small Angle Light Scattering (SALS)	64
2.2.8	Mechanical Testing	65

3	RESULTS AND DISCUSSION	70
3.1	Preliminary experiments	70
3.1.1	BADGE-PBO Cloud Point Curve	70
3.1.2	Determination of the gel point	72
3.1.3	Bridging behaviour in BEB triblocks	72
3.2	Observations during sample curing	74
3.2.1	Reaction Kinetics	74
3.2.2	Visual Observations	77
3.3	Microstructure of Cured Samples	83
3.3.1	Effect of concentration	83
3.3.2	The Micellar Regime	105
3.3.3	Reaction-Induced Macrophase Separation	124
3.4	Bulk Properties of Cured Samples	129
3.4.1	Glass Transition Temperature	129
3.4.2	Mechanical Properties	133
3.4.3	Other Observations	135
4	CONCLUSIONS AND FUTURE WORK	139
4.1	Summary & Conclusions	139
4.2	Future Work	143
	REFERENCES	145

1 Introduction

Hundreds of thousands of tonnes of epoxy resins and their associated hardeners are produced globally each year. Though they are familiar to many as structural adhesives, only a small part of total production is destined for that purpose. The major fraction will find use in surface coatings, electrical potting and insulation, and as the matrix in fibre reinforced composites, amongst other applications[1, 2]. The cured resins often have high service temperatures and are extremely hard wearing. However, these products also tend to be rather brittle and prone to fracture.

Block copolymers have been the subject of much research over the last three decades, largely due to the interesting behaviour of amphiphilic[†] species[3-7]. Here, the blocks show differing affinity towards a potential solvent and, frequently, a tendency to avoid mixing of dissimilar blocks with one another. This leads to the blocks arranging themselves into ordered structures with feature sizes determined by the lengths of the blocks – typically on the scale of nanometres.

The ability to combine block copolymers with epoxy resins and produce ‘nanostructured’ materials was first demonstrated in 1997 by Hillmyer *et al.* [8]. Further research, reviewed later, suggests significant potential for block copolymers in epoxy resins, both as toughening agents for epoxy resins and as templating agents for nanostructured materials.

[†] Amphiphilic \approx ‘loving both’, from Greek.

1.1 Epoxy Resin

Epoxy systems generally consist of an epoxy resin with two (possibly more) epoxide groups and a multifunctional curing agent. In this work, the common difunctional epoxy prepolymer BADGE and the tetrafunctional curing agent DETDA were used. The structures of these compounds are shown in Figure 1.1 and they are described in greater detail in Chapter 2.

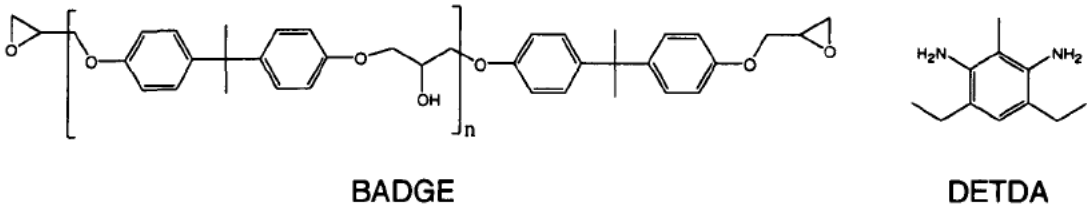


Figure 1.1 – Structures of epoxy resin (BADGE) and curing agent (DETDA) used in this work.

1.1.1 Curing Reaction

The epoxide group is a three membered planar ring. Geometrical constraints mean that the ring is highly strained with each of the three bond angles $\approx 60^\circ$ compared with a normal C-C-C bond angle of 109° and C-O-C angle of 112° [1]. Hence the epoxide group is highly susceptible to ring opening reactions. The mechanism of acid catalysed nucleophilic substitution to the ring is shown in Figure 1.2. Addition normally occurs to the less substituted carbon centre due to steric hindrance and the presence of electron donating substituents at the more highly substituted carbon.

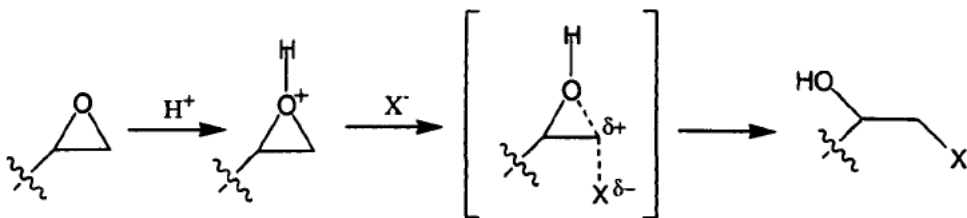


Figure 1.2 - Mechanism of acid-catalysed epoxide ring opening by a nucleophile.

1.1.2 Gelation

If, in a polymerizing system, one or more of the reactants has functionality greater than two it is clear that, rather than forming simple linear chains, a cross-linked network will be created. Once this network becomes effectively infinite, such that it extends throughout the reaction vessel, the physical properties of the reacting mixture change abruptly. Its viscosity becomes infinite and it begins to exhibit a complex viscoelastic response instead (Figure 1.3). Visually, this is observed as the transition from a free-flowing liquid to a semi-solid gel, hence the point at which the transition occurs is referred to as the gel point. Gelation occurs well before the reaction reaches completion. In an incompletely reacted system beyond the gel point the networked 'gel' fraction coexists with the liquid-like 'sol' fraction. The sol fraction is so called because it remains soluble in a suitable non-degrading solvent, whereas the gel fraction is insoluble.

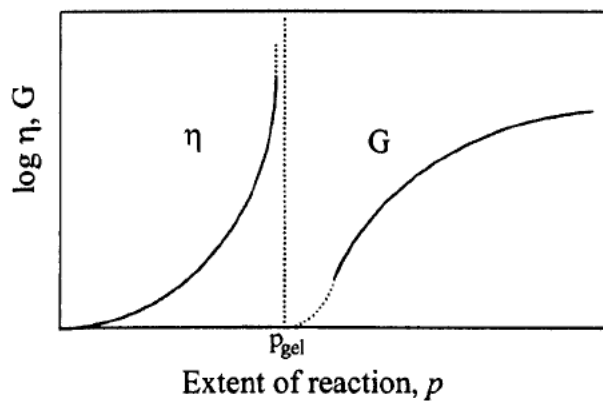


Figure 1.3 – Diagram showing transition from viscous liquid to viscoelastic gel at the gel point. G is the viscoelastic shear modulus and η the viscosity.

1.1.2.1 Flory-Stockmayer theory of network formation

Theoretical models for the process of gelation in cross linking systems have been developed by Flory[9, 10] and further extended by Stockmayer[11, 12]. Considering the reaction - depicted below - of a trifunctional cross-linker (A-groups) with a difunctional resin (B-groups). We define a branching coefficient, α , as the probability that a randomly selected functional group on a branch unit will be connected to

another branch unit by a chain of any length (as opposed to the chain ending at an unreacted or terminated group before reaching another branch point).

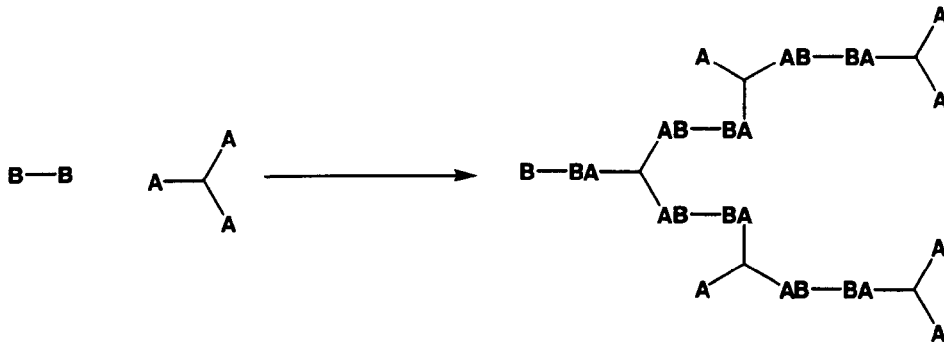


Figure 1.4 – The cross linking reaction between difunctional chain monomers and trifunctional cross-linking agent.

Travelling down a chain to a branch point, if $\alpha < \frac{1}{2}$ then there is a greater than even chance that each chain leading from the branch point will end in an unreacted group, rather than a branch point. Hence an infinite network will not form. If $\alpha > \frac{1}{2}$ then there is a greater than even chance of producing two new chains, which will in turn lead to 4α further chains, and so on. Hence formation of an infinite network becomes possible. The critical condition for gelation therefore occurs at $\alpha_c = \frac{1}{2}$. In systems where the cross-linker has functionality >3 this can be generalised to[9]:

$$\alpha_c = 1/(f - 1) \quad (1.1)$$

where f is the average functionality of the cross-linking agent.

Assuming the absence of intramolecular reactions and equal reactivity of all A and all B groups it can be shown that[9]:

$$\alpha = \frac{p_A p_B \rho}{1 - p_A p_B (1 - \rho)} \quad (1.2)$$

Where p_A and p_B are the extents of reaction of A- and B-groups respectively. The symbol ρ denotes the ratio of A groups on branch units to all A groups in the mixture

and arises because the theory as derived allows for the presence of difunctional A-A units as well as multifunctional units. Since, at least for the purpose of this model, all of the cross-linker in our system can be considered to be tetrafunctional, we can set $\rho = 1$. If we also define r as the ratio of A groups to B groups such that $p_B = rp_A$ we can reduce Equation 1.2 to:

$$\alpha = rp_A^2 \quad (1.3)$$

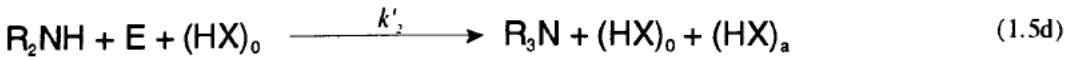
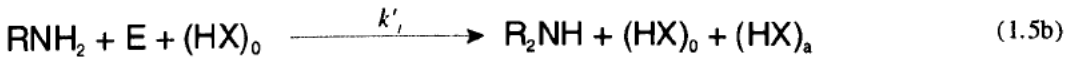
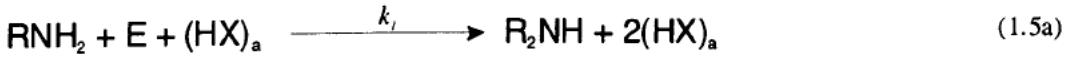
As long as the resin and cross-linker are mixed stoichiometrically so that there are equal numbers of A and B groups present at the beginning of the reaction, r is equal to one and therefore $\alpha = p^2$. Combining with Equation 1.1, we can therefore say that for a system containing only difunctional epoxy prepolymer and multifunctional cross-linker:

$$p_{gel} = \sqrt{\frac{1}{f-1}} \quad (1.4)$$

Therefore, theoretically, the gel point in our system should occur at $p = \sqrt{\frac{1}{3}} \approx 0.58$.

1.1.3 Curing Kinetics

The mechanism of cure of epoxy resins by amines has been shown to be catalysed by the hydroxyl groups present in the cured resin[13]. Hydrogen bonding from the hydroxyl hydrogen to the epoxide oxygen acts to withdraw electrons in a similar manner to the acid catalysed reaction depicted above. A scheme to describe the kinetics of the reaction of a primary amine with an epoxide has been derived by Horie[14] and is depicted below. It is assumed that there is initially some impurity present in the system which can act as a catalyst (for example, BADGE oligomers, rather than monomers, would provide hydroxyl groups.)



R_xN_y are the various amine species (primary, secondary and tertiary), E is an epoxide group, $(\text{HX})_0$ is some initial catalytic impurity and $(\text{HX})_a$ is the catalytic hydroxyl groups in the reacted resin.

Wisnarakkit and Gillham[15] have derived an equation to describe the reaction rate as a function of the extent of reaction, p :

$$\frac{dp}{dt} = k(1-p)^2(p+B) \quad (1.6)$$

where $k = (k_1 e_0^2) / 2$, $B = (k'_1 c_0) / (k_1 e_0)$, e_0 is the initial concentration of epoxide groups, c_0 is the initial concentration of catalyst $(\text{HX})_0$ and k_1 and k'_1 are the rate constants as shown in Equation 1.5.

Ishii and Ryan[16] have used isothermal DSC to show that the BADGE + DETDA system obeys these kinetics prior to the gel point by rearranging Equation 1.6 into the form of a straight line (Figure 1.5):

$$\frac{dp/dt}{(1-p)^2} = k'p + k''B \quad (1.7)$$

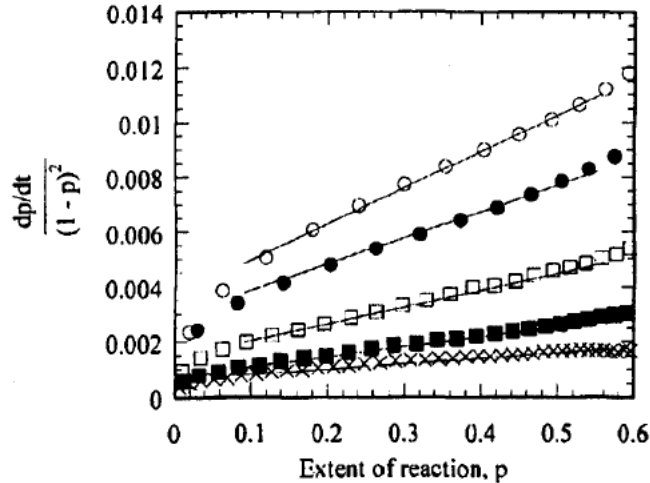


Figure 1.5 – Plot demonstrating the applicability of autocatalytic kinetics to reaction prior to the gel point in the neat BADGE + DETDA system. Series at various temperatures: from bottom to top 150, 160, 175, 195, 200 °C . Reproduced from [16].

1.1.4 Fracture Behaviour

Since epoxy resins are widely used in structural roles, their fracture behaviour is of great interest and has been reviewed in detail elsewhere[1, 2, 17].

Fracture occurs by one of two major modes (Figure 1.6). In ductile fracture, significant plastic deformation occurs prior to break. In highly ductile materials this may result in ‘necking’ of the specimen to a point. In moderately ductile materials fracture may occur *via* the formation of microvoids which slowly extend, coalesce and complete the fracture, thus leading to a rough fracture surface of fibrous appearance. In materials where plastic deformation is not favoured, including most cured epoxy resins, brittle fracture is the preferred mode. The lack of deformation prior to break leads to relatively flat fracture surfaces. The deformations which occur during ductile fracture absorb significant amounts of energy and can lead to crack deformation and blunting. Hence, ductile fracture occurs in a fairly ‘stable’ manner, requiring the constant application of force over a period of time in order to propagate the crack. By contrast, in brittle fracture, the crack normally propagates rapidly and may continue to do so even if the stress is removed from the sample, this is referred to as ‘unstable’ propagation. Brittle fracture of engineering materials can be

catastrophic since it may occur without warning and, once it has begun, failure is likely to occur before corrective action can be taken.

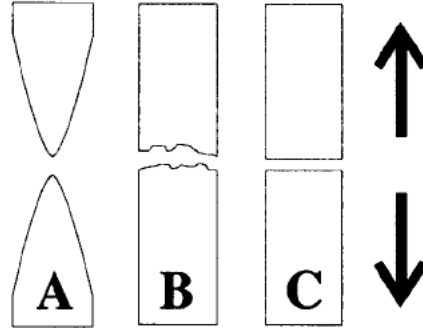


Figure 1.6 - Types of fracture. (A) Ductile fracture involving necking to a point. (B) Ductile fracture with surface roughening by plastic deformation. (C) Brittle fracture.

The fracture strength of epoxy resins, as with all materials, is much lower than its theoretical maximum value. Griffith[18] showed that this is due to the unavoidable presence of small defects in the material which result in local concentrations of stress.

In linear elastic fracture mechanics, models are based either on an analysis of energy or calculation of the localized stress field. In the former approach, an applied stress leads to an increase in potential energy in the system, once this energy exceeds that required for the creation of new fracture surfaces, a crack will propagate. This condition is quantified in the critical strain energy release rate, G_c :

$$G_c = \frac{P_c^2}{2B} \frac{\partial C}{\partial a} \quad (1.8)$$

where C is the compliance of the cracked body for a given crack length, a ; P_c is the load at onset of crack propagation and B is the specimen thickness in the fracture plane, orthogonal to the propagation direction.

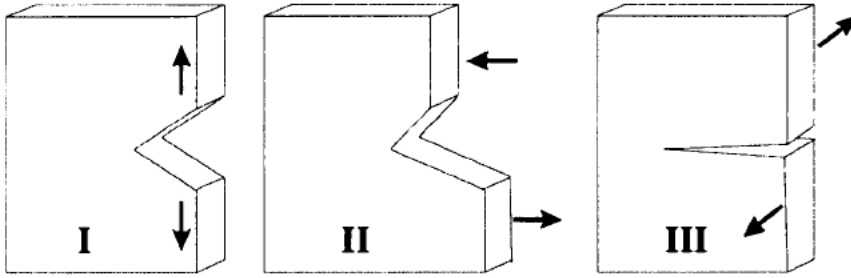


Figure 1.7 – Loading modes in fracture experiments. Mode I – opening; mode II – in-plane shear; mode III – anti-plane shear.

In the stress field analysis, the stress field around a sharp crack can be described by the stress intensity factor, K . In the case of a specimen under mode I loading (Figure 1.7), the critical stress intensity factor is given by:

$$K_{Ic} = Y\sigma_c \sqrt{a} \quad (1.9)$$

where Y is a geometrical factor, σ_c is the applied stress at onset of crack propagation, and a is the initial crack length. Experimental determination of K_{Ic} is discussed in Chapter 2; calculation of G_{Ic} from K_{Ic} is discussed in Section 1.3.3.

Stress can be dissipated by crack blunting as a result of plastic deformation, such as crazing or shear yielding. In crazing, microvoids form in a line and expand so that they take on the appearance of a fissure spanned by fibrous bridging filaments. Polymer chains within the filaments are strongly aligned. Because of the size of the voids, crazes often cause ‘stress-whitening’ of polymers due to the scattering of light. Shear yielding involves the alignment of polymer chains parallel to the plane of greatest shear. It leads to a redistribution of the stress field and crack blunting and is the major mechanism of plastic deformation in epoxy resins[1]. Shear yielding, crazing and crack propagation are all significant mechanisms of energy absorption.

Studies on thermoplastic- and rubber-toughened epoxies have suggested that toughening may occur by a variety of mechanisms. These include energy dissipation by debonding and cavitation of the additive particles. Huang and Kinloch[19, 20] have shown that the major mode of rubber toughening in a piperidine cured BADGE

system is shear yielding. The rubber particles create stress concentrations where shear yielding is favoured; this provides a mechanism for energy absorption and crack blunting.

1.1.5 Phase Separation

Binary polymer-solvent systems may show a number of different phase diagrams as shown in Figure 1.8.

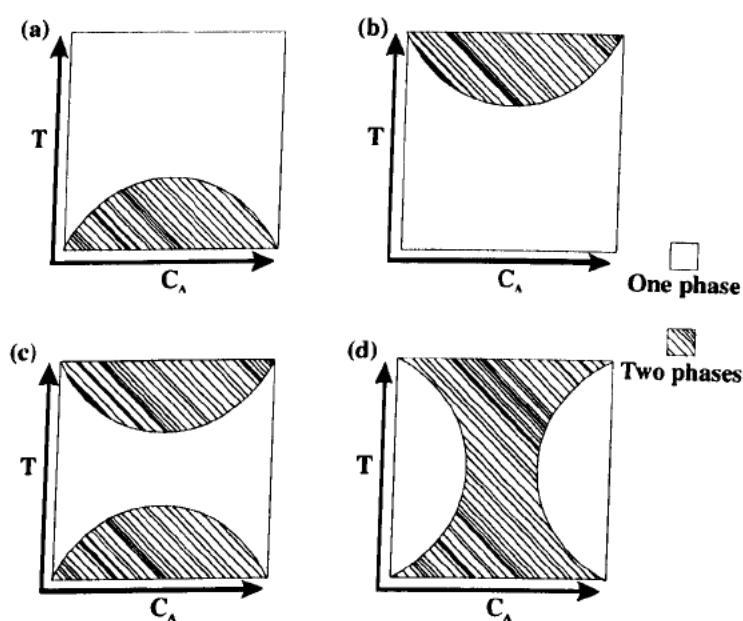


Figure 1.8 – Idealised phase diagrams for a binary polymer-solvent system. C_A is the concentration of one species. (a) Upper Critical Solution Temperature (UCST) behaviour. (b) Lower Critical Solution Temperature (LCST) behaviour. (c) Combined UCST and LCST. (d) ‘Hourglass’ diagram – a special case of (c).

The tendency of two components to mix can be expressed in terms of the Gibb’s free energy of mixing ($\Delta G^M = \Delta H^M - T\Delta S^M$). The familiar UCST behaviour is the consequence of the increase in entropic contribution with increasing temperature. LCST behaviour occurs in systems where significant hydrogen bonding occurs between solvent and solute. At high temperature the hydrogen bonds break, leading to a significant decrease in ΔH^M . Entropically driven LCST behaviour can also occur due to the much greater increase in molar volume exhibited on heating by the solvent

relative to the polymer. However this is only observed if it occurs before the boiling point of the solvent.

1.1.5.1 Flory-Huggins theory

For a solution of small molecules where the components are of comparable size and intermolecular forces between like and unlike molecules are identical, statistical considerations allow us to derive the free energy of mixing for a two component system, ΔG^M , as[21]:

$$\Delta G^M = -T\Delta S^M = -kT(N_1 \ln x_1 + N_2 \ln x_2) \quad (1.10)$$

where T is the temperature; ΔS^M is the entropy change of mixing; k is the Boltzmann constant, and N_i and x_i are, respectively, the number of molecules and mole fraction of component i .

The following assumptions are made in the derivation of equation 1.10: (i) no volume change occurs on mixing; (ii) all molecules are of equal size; (iii) all possible arrangements of molecules have the same energy (i.e. the enthalpy change of mixing, ΔH^M , is zero); (iv) the motion of components about their equilibrium positions remains unchanged on mixing.

A simple theory of mixing more suited to polymer systems was derived independently by Flory[22, 23] and Huggins[24-26]. In the solid state, a polymer is fixed in a single configuration; on dissolution it becomes free to adopt a much larger number of possible states. However, in polymers one must consider the number of possible configurations of the polymer chain available, remembering that some configurations will be unavailable due to volume being excluded by other chain elements. To allow for the difference in size, the polymer is considered as a chain of units of the same volume as a single solvent molecule. In an athermal system ($\Delta H = 0$) the enthalpy change of mixing is then found to be:

$$\Delta S^M = -k(N_1 \ln \phi_1 + N_2 \ln \phi_2) \quad (1.11)$$

where N_i and ϕ_i are, respectively, the number of molecules and volume fraction of species i .

The enthalpy change of mixing is considered to arise from the breaking of x solvent-solvent interactions and y polymer-polymer interactions and the subsequent formation of $(x + y)$ solvent-polymer interactions. The enthalpy change of mixing can then be written as:

$$\Delta H^M = kT\chi N_1\phi_2 \quad (1.12)$$

where χ is the Flory-Huggins interaction parameter and is specific for a given combination of polymer and solvent. In the original theory, χ was assumed to be purely enthalpic. In real world systems more satisfactory results are obtained if χ is defined as having temperature dependent (enthalpic) and temperature-independent (entropic) components. (i.e. $\chi = A + [B / T]$ where A and B are constants).

The free energy change of mixing can now be derived by combining equations 1.11 and 1.12:

$$\Delta G^M = kT[N_1 \ln \phi_1 + N_2 \ln \phi_2 + \chi N_1\phi_2] \quad (1.13)$$

Whilst the Flory-Huggins theory successfully predicts the observed behaviour of many polymer solutions, it is imperfect. Volume changes on mixing are not accounted for and it is incapable of predicting LCST behaviour. Alternative theories have been developed but will not be discussed here.

1.1.5.2 Mechanisms of phase separation

Figure 1.9 shows a sketch of a phase diagram and associated free energy plot for a binary system. The binodal line indicates where the two phases are in equilibrium (for each component, its chemical potentials in the two phases are equal). It corresponds to the intersection point of the free energy curve and the tangent which joins its minima. Experimentally the binodal curve corresponds to the cloud point curve of the system. The spinodal curve corresponds to the position of the inflexion points on the free energy curve.

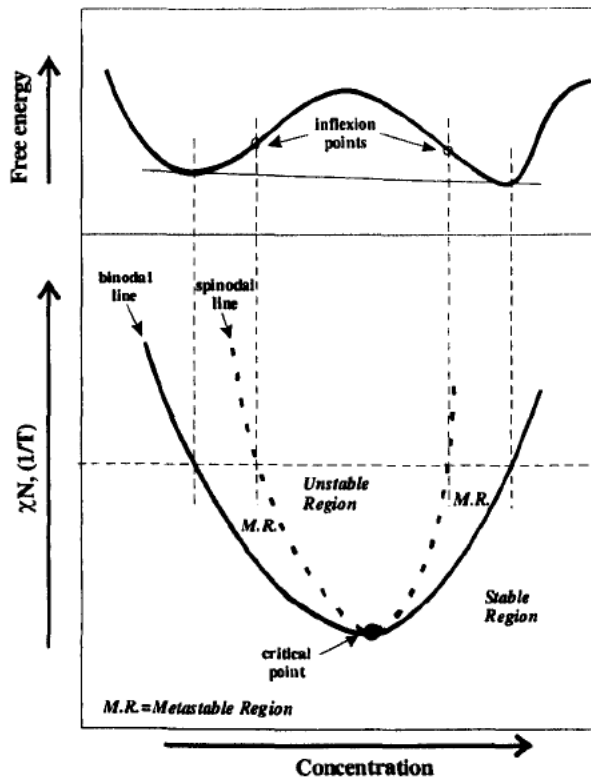


Figure 1.9 – Composition-temperature diagram and associated free energy plot for a binary system. The free energy plot is taken at the position of the horizontal dashed line on the composition diagram.

Inside the spinodal line the system is unstable and, unless kinetically inhibited, will phase separate by 'spinodal decomposition'. Spatially periodic fluctuations in the concentration of solute begin at small amplitude. Over time, solute diffuses into the solute rich phase and solvent into the solvent rich phase, thus the amplitude of the fluctuations increases. Spinodal decomposition usually results in a three dimensional

interconnected network with regular structure although, if not kinetically impeded, the domains usually coalesce to form spherical structures.

In the metastable region between the spinodal and binodal curves, 'nucleation and growth' occurs. Here, first an activation energy must be supplied to allow initial nuclei of polymer to form. Growth of the nucleus occurs by drawing molecules of polymer from the surrounding solution, resulting in a depleted layer, into which more polymer diffuses from solution due to the concentration gradient. Nucleation and growth normally leads to spherical domains with a range of diameters.

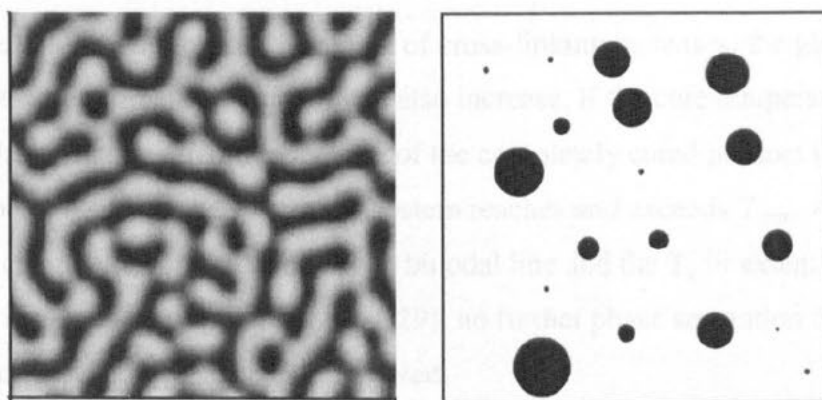


Figure 1.10 – (Left) Result of computer simulation showing morphology formed during spinodal decomposition. Reproduced from [27]. (Right) Typical morphology formed by nucleation and growth.

1.2 Block Copolymers

1.1.5.3 Reaction-Induced Phase Separation

As indicated in Figure 1.9 an increase in the degree of polymerization can also lead to phase separation. During polymerization the free energy is affected by the increase in the molar volume of the polymerizing component. The interaction between the modifier and the polymerizing component also changes as functional groups react. Reaction induced phase separation in thermosetting systems modified with various additives has been reviewed by Williams *et al.*[28].

The free energy of mixing in a pseudo-binary modified thermosetting polymer system can be written as[28]:

$$\Delta G^M = \left(RT/V_r \right) \left[\frac{\phi_P}{Z_P} \ln \phi_P + \frac{\phi_M}{Z_M} \ln \phi_M + \chi \phi_P \phi_M \right] \quad (1.14)$$

where V_r is some reference volume; ϕ_P and ϕ_M are the volume fractions of polymerizing system and modifier respectively (in the pseudo-binary system, prepolymer, cross-linker and cross linked polymer are considered as a single component); Z_P and Z_M are the molar volumes of each component normalized to V_r . Z_P will be a function of the extent of reaction and χ will normally follow an A+B/T type behaviour.

As the reaction progresses and the extent of cross-linking increases, the glass transition temperature of the system will also increase. If the cure temperature (T_{cure}) is below the glass transition temperature of the completely cured product ($T_{g\infty}$) then vitrification will occur when T_g for the system reaches and exceeds T_{cure} . After this point, indicated by the intersection of the binodal line and the T_g vs extent of reaction curve and named the 'Berghmans point' [29], no further phase separation can occur and the morphology will be kinetically fixed.

1.2 Block Copolymers

Copolymers are polymers composed of more than one type of monomer. In block copolymers, rather than being distributed throughout the chain, the monomers of the same type are grouped together to form two or more blocks. The blocks can be connected in a range of different geometries including linear di-, tri- and multi-blocks; star blocks; graft block copolymers and many others. A schematic representation of AB diblock and ABA triblock copolymers are shown below (where A & B represent different monomers).

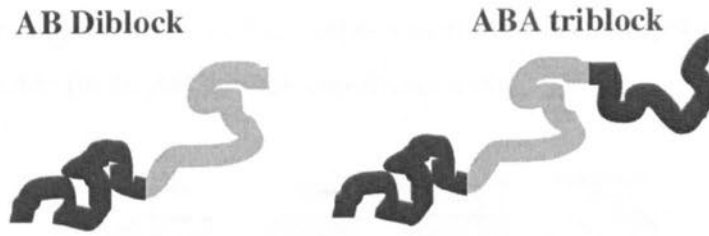


Figure 1.11 - Schematic representation of AB diblock and ABA triblock copolymers.

Block copolymers have been the subject of a great deal of research over the last thirty years because of their tendency to self-assemble into ordered structures on nanometre length scales and their use as amphiphiles. Much of this work has been reviewed and summarised in a number of recent monographs[3-7].

1.2.1 Behaviour in the Bulk

Dissimilar polymers are generally immiscible and will phase separate in the melt as described by Flory-Huggins and similar theories. In block copolymers, dissimilar blocks are thermodynamically driven to phase separate in the same way. However since the blocks are joined by chemical bonds they can only separate on length scales which are comparable to the molecular size. This is commonly referred to as 'microphase separation' as distinct from the 'macrophase' separation on larger length scales described above.

The tendency to demix is described by χN , where χ is the Flory-Huggins parameter and is proportional to the enthalpy of demixing and the temperature, as above. N is the degree of polymerization and is present because the entropic penalty associated with chain stretching scales with the size of the polymer. Chain stretching is necessary in order to fill space in microphase separated structures. If, in a diblock copolymer, both blocks occupy similar volumes at equilibrium then a structure composed of alternating lamellae of A and B blocks will be favoured. If the volumes occupied by the two blocks are not equal then chain stretching may be minimized by adopting some other morphology. Hence the final morphology adopted is highly dependent on the relative volume fractions of the blocks. Figure 1.12 shows an

example phase diagram and schematic representations of the morphologies which are known to be stable for an AB diblock copolymer melt.

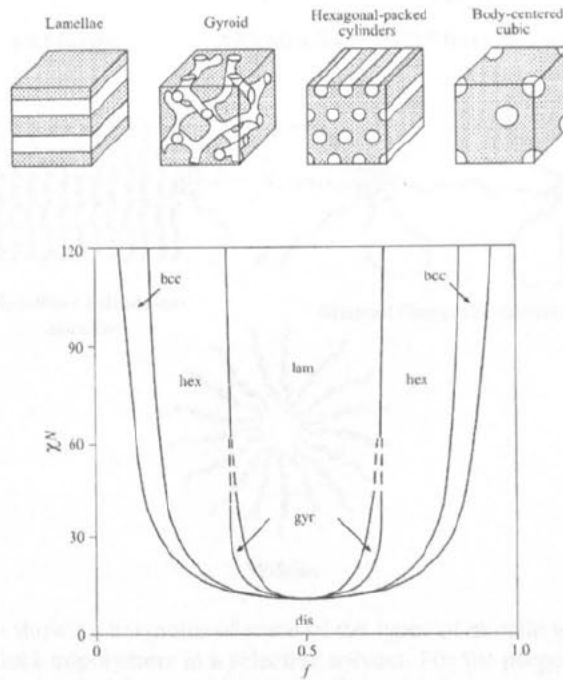


Figure 1.12 - Theoretical phase diagram for an AB diblock copolymer. f is the volume fraction of one block. Reproduced from ref [6].

When χN is high, the inter-phase boundaries will be sharply defined – this is the strong segregation limit (SSL). Closer to the order-disorder transition boundary, the boundaries are more diffuse. The concentration profile is more sinusoidal in appearance. This is the weak segregation limit (WSL).

1.2.2 Behaviour in Solution

If a block copolymer is synthesised such that the blocks have significantly different affinities for a solvent then the block copolymer will be an amphiphile. Amphiphilic molecules are widely used as detergents as they are able to sequester oils and fats and render them soluble in water. Amphiphilic molecules are also common in nature. The ability of naturally occurring amphiphiles such as phospholipids to form vesicular cells is an essential part of all biological systems.

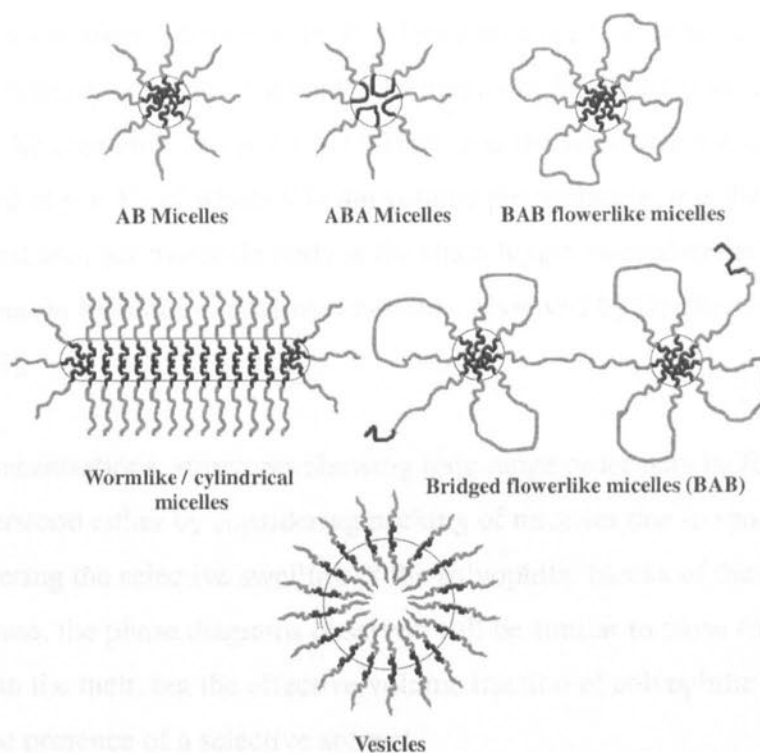


Figure 1.13 – Diagram showing examples of some of the types of micelle which can be formed by diblock and ABA triblock copolymers in a selective solvent. For the purposes of labelling, the A blocks are considered to be the blocks with higher affinity for the solvent and are shown in grey above.

Polyoxyalkylene block copolymers are commonly produced as commercial amphiphiles, both as detergents and in biomimetic systems. This is largely due to the fact that they are highly biocompatible and are therefore essentially non-toxic[30].

In solution at very low concentrations, amphiphiles exist as unimolecular species. At a certain concentration, micellar structures with a ‘solvophobic’ core and a ‘solvophilic’ corona such as those shown in Figure 1.13 will form. This is known as the critical micelle concentration (cmc). The cmc varies with temperature and a solution of fixed concentration will show a critical micelle temperature (cmt). The determined cmc or cmt may also be dependant on the technique used to detect micellization. The cmc decreases with increasing molecular weight of the solvophobic block.

When there is a mismatch between the interfacial area per hydrophile compared to that per hydrophobe, one may observe the formation of bilayered vesicles. This may occur where the condition $\frac{1}{2} < p < 1$ [31]. Here, p is the surfactant packing parameter and is defined as $p = V/al$ where V is the volume per molecule, a is the effective cross-sectional area per molecule and l is the chain length normal to the interface. Vesicle formation by block copolymers has been reviewed by Discher and Eisenberg[32].

At higher concentrations, structures showing long range order may be formed. These may be understood either by considering packing of micelles due to space constraints or by considering the selective swelling of the solvophilic blocks of the copolymer. In the later case, the phase diagrams observed will be similar to those for block copolymers in the melt, but the effective volume fraction of solvophilic block is altered by the presence of a selective solvent.

In this work where the role of the solvent is performed by relatively high molecular weight epoxy resin, the behaviour may be similar to that for block copolymer-homopolymer blends. Theoretical models for the behaviour of microphase separated block copolymers when one block is swelled by the presence of homopolymer have been calculated by Matsen[33], for weakly segregated systems, and by Likhtman and Semenov[34] in the case of strong segregation. Broadly, phase behaviour is expected to be similar to that exhibited in the case of swelling by low molecular weight selective solvents. It is noted, however, that swelling by homopolymer may stabilize additional phases such as the hexagonally perforated lamellar phase and the double diamond phase. These phases, where they have been observed at all in neat block copolymer systems, are believed to be metastable.

1.3 Nanostructured Block Copolymer - Epoxy Thermosets: A Brief Review

The formation of nanostructured systems in cured blends of epoxy resin and diblock copolymer was first reported by Hillmyer *et al.* in 1997[8]. Block copolymers had previously been investigated as epoxy toughening agents, however, no nanoscale structure was observed[35]. Since that initial report, a number of research groups have carried out further investigations into a range of epoxy / block copolymer blend systems. The systems studied to date are summarized in Table 1.1.

1.3.1 Non-reactive Modifiers

1.3.1.1 Studies of morphology & kinetics

In their initial work[8], Hillmyer *et al.* demonstrated the formation of hexagonally packed cylinders with diameters on the order of tens of nanometres. The epoxy system was bisphenol-A diglycidyl ether (BADGE) + phthalic anhydride. Samples containing both PEO-PEP (36 wt.% diblock in epoxy, $\phi_{\text{PEO}}^{\dagger} = 0.52$) and PEO-PEE (25 wt.% diblock, $\phi_{\text{PEO}} = 0.39$) were analysed. Cylinders with a core-shell morphology consisting of non-polar core surrounded by a corona of PEO were observed as shown in Figure 1.14.

In subsequent work[36] the same group carried out a comprehensive analysis involving varying weight fractions of a PEO-PEP diblock ($\phi_{\text{PEO}} = 0.51$, $M_n = 2700$ g/mol) in a system cured with aromatic amine. They obtained a phase diagram similar to that predicted by self-consistent field theory[33] for a mixture of diblock

[†] ϕ_{PEO} is the volume fraction of PEO in the diblock.

Polymer	Abbreviation	Epoxy + Hardener System	Refs
Poly(ethylene oxide)- <i>b</i> -poly(propylene oxide)	PEO-PPO	BADGE + MDA	[37, 38]
Poly(ethylene oxide)- <i>b</i> -poly(butylene oxide)	PEO-PBO	BADGE + PN	[39]
Poly(ethylene oxide)- <i>b</i> -poly(ethyl ethylene)	PEO-PEE	BADGE + PA BADGE + MDA	[8] [36]
Poly(ethylene oxide)- <i>b</i> -poly(ethylene- <i>alt</i> -propylene)	PEO-PEP	BADGE + PA BADGE + MDA BADGE + PN	[8] [36, 40] [41]
Poly(ethylene oxide)- <i>b</i> -poly(propylene oxide)- <i>b</i> -poly(ethylene oxide)	PEO-PPO-PEO	BADGE + MDA	[37, 42-47]
Poly(methyl acrylate- <i>co</i> -glycidyl methacrylate)- <i>b</i> -polyisoprene	P(MA- <i>co</i> -GMA)-PI	PN + MDA BADGE + MDA	[48] [49]
Polybutadiene- <i>b</i> -poly(epoxy-1,4-isoprene- <i>ran</i> -1,4-isoprene)	PB-ePI	BADGE + MDA	[49]
Polystyrene- <i>b</i> -polybutadiene	PS-PB	PPGDGE + MDA	[50]
	star block copolymer	BADGE + MCDEA/DDS	[51, 52]
Poly(ethylene oxide)- <i>b</i> -polyisoprene	PEO-PI	BADGE + MDA	[40, 53]
Poly(ethylene oxide)- <i>b</i> -polybutadiene	PEO-PB	BADGE + MDA	[53]
(Epoxidised polyisoprene)- <i>b</i> -polybutadiene	ePI-PB	BADGE + MDA	[53]
Poly(methyl acrylate- <i>co</i> -glycidyl methacrylate)- <i>b</i> -poly(2-ethylhexyl methacrylate)	P(MA- <i>co</i> -GMA)-PEHMA	BADGE + MDA BADGE (\pm Br) + PN	[53] [41]
Polystyrene- <i>b</i> -polybutadiene- <i>b</i> -poly(methyl methacrylate)	SMB	BADGE + MCDEA/DDS	[54, 55]

Polymer	Abbreviation	Epoxy + Hardener System	Refs
Poly(2-vinylpyridine)- <i>b</i> -polyisoprene	P2VP-PI	PN + HMTA	[56, 57]
Poly(ethylene oxide)- <i>b</i> -poly(ethylene)	PEO-PE	BADGE + MDA	[58]
Poly(ethylene oxide)- <i>b</i> -polystyrene	PEO-PS	BADGE + MOCA	[59]
Poly(ϵ -caprolactone)- <i>b</i> -polybutadiene-poly(ϵ -caprolactone)	PCL-PB-PCL	BADGE + MOCA	[60]
Poly(methyl methacrylate)- <i>b</i> -polystyrene	PMMA-PS	BADGE + MXDA	[61]
		BADGE only	[62]
Poly(methyl methacrylate)- <i>b</i> -polybutadiene	PMMA-PB	BADGE only	[62]
Polystyrene- <i>b</i> -polybutadiene- <i>b</i> -poly(methyl methacrylate)- <i>b</i> -poly(glycidyl methacrylate)	SMBG	BADGE + MCDEA	[63]
Polystyrene- <i>b</i> -polybutadiene- <i>b</i> -poly[(methyl methacrylate)- <i>stat</i> -(methacrylic acid)]	SMBA	BADGE + DDS / MCDEA / MDA	[64]

Table 1.1 – A summary of epoxy-block copolymer blend systems investigated to date. Details of resins and curing agents are given in Table 1.2. Structures of polymer blocks are given in Table 1.3.

Name	Abbreviation	Structure
Bisphenol A diglycidyl ether	BADGE	
Poly(propylene glycol) diglycidyl ether	PPGDGE	
Phenol Novolac	PN	<p>Hardener, R=H Resin, R=</p>
Methylene dianiline	MDA	
4,4'-methylenebis-(3-chloro-2,6-diethylaniline)	MCDEA	
4,4'-diaminodiphenyl sulfone	DDS	
4,4'-methylenebis-(2-chloroaniline)	MOCA	
<i>m</i> -xylenediamine	MXDA	

Table 1.2 – Epoxy resins and curing agents


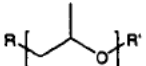
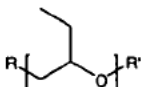
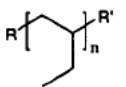
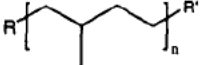
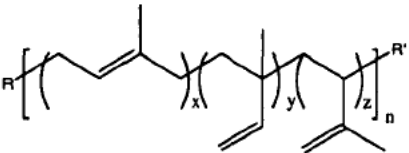
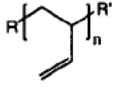
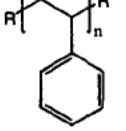
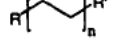
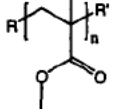
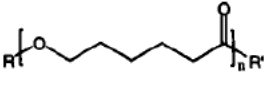
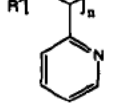

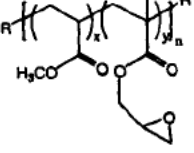
Name	Abbreviation	Structure
Poly(ethylene oxide)	PEO	
Poly(propylene oxide)	PPO	
Poly(butylene oxide)	PBO	
Poly(ethyl ethylene)	PEE	
Poly(ethylene- <i>alt</i> -propylene)	PEP	
Polyisoprene	PI	
Poly(1,4-butadiene)	PB	
Polystyrene	PS	
Polyethylene	PE	
Poly(methyl methacrylate)	PMMA	
Poly(ϵ -caprolactone)	PCL	
Poly(2-vinylpyridine)	P2VP	
Poly(epoxy-1,4-isoprene)	ePI	
Poly(methyl acrylate- <i>co</i> -glycidyl methacrylate)	P(MA- <i>co</i> -GMA)	

Table 1.3 – Block structures of some of the copolymers which have been investigated.

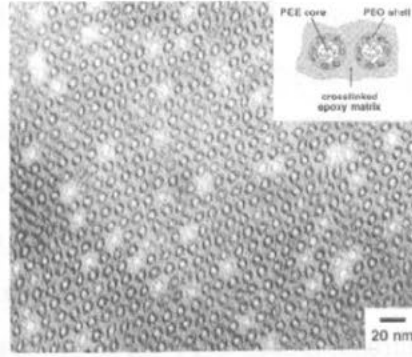


Figure 1.14 – TEM image showing cylinders of PEO-PEE (25 wt.% PEO₃₆PEE₃₉) in an epoxy matrix. The core-shell morphology is clearly visible. Reproduced from Hillmyer *et al.*[8]

with PEO homopolymer. They also observed an increase in d-spacing as epoxy molecular weight was increased. These results were determined to be consistent with swelling (or ‘wetting’) of the PEO block by epoxy resin. Because of the connectivity of the PEO and PEP blocks and the requirements to maintain constant density and minimize chain stretching, this leads to increased interfacial curvature as the concentration of resin is increased and hence to the phase diagram observed in Figure 1.15. Examination of the data showing d-spacing against cure time indicates that swelling continues to occur long after the gel-point. This was attributed to the fact that the gel-point is a property of the bulk sample and does not necessarily coincide with the restriction of local mobility on the nanometre scale.

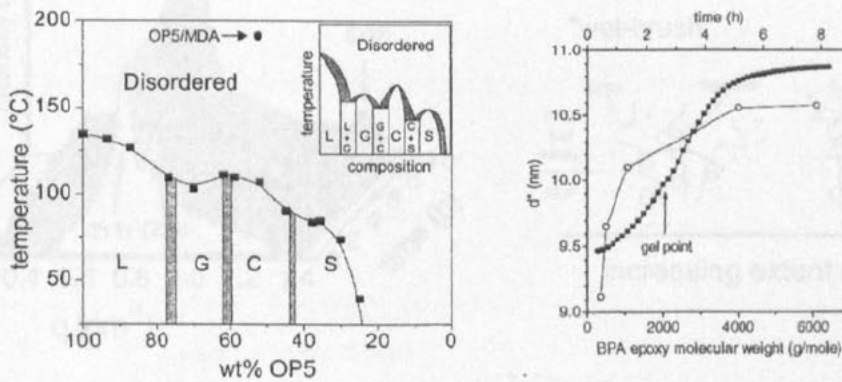


Figure 1.15 – (Left) Phase diagram for a PEO-PEP diblock in epoxy resin, the inset is a suggestion of what the complete diagram may look like (L=Lamellar, G=Gyroid, C=Hexagonally packed cylinders, S=Spheres). (Right) Variation of d-spacing in the 52 wt% diblock system with increasing epoxy molecular weight (open circles) and with cure (filled squares). Adapted from Lipic *et al.* [36].

Time resolved SAXS studies performed during curing indicate that for some compositions, order-order phase transitions occur as the epoxy cross-links. An example is shown in Figure 1.16 wherein a 69 wt% blend of the PEO-PEP diblock in epoxy is shown to undergo a transition from gyroid to lamellar structure as the reaction progresses. To explain this behaviour, it is suggested that the, initially epoxy miscible, PEO block is expelled from the resin as curing progresses. This expulsion leads to a 'drying' or deswelling of the PEO block, leading to a subsequent reduction in interfacial curvature. Consequently, as long as curing has not progressed so far as to kinetically inhibit the phase transition, a morphology with reduced interfacial curvature will be adopted. A similar transition, from spheres to cylinders, was observed in a 35wt% blend – this was seen to occur at 100°C, but not on curing at 60°C. Further evidence for the expulsion of PEO from the resin is provided by the reported observation of a melting endotherm in the DSC trace of the 52wt % sample at a temperature consistent with that of crystalline PEO. Since PEO absorbed in the matrix cannot crystallize, some 'free-PEO' must be present.

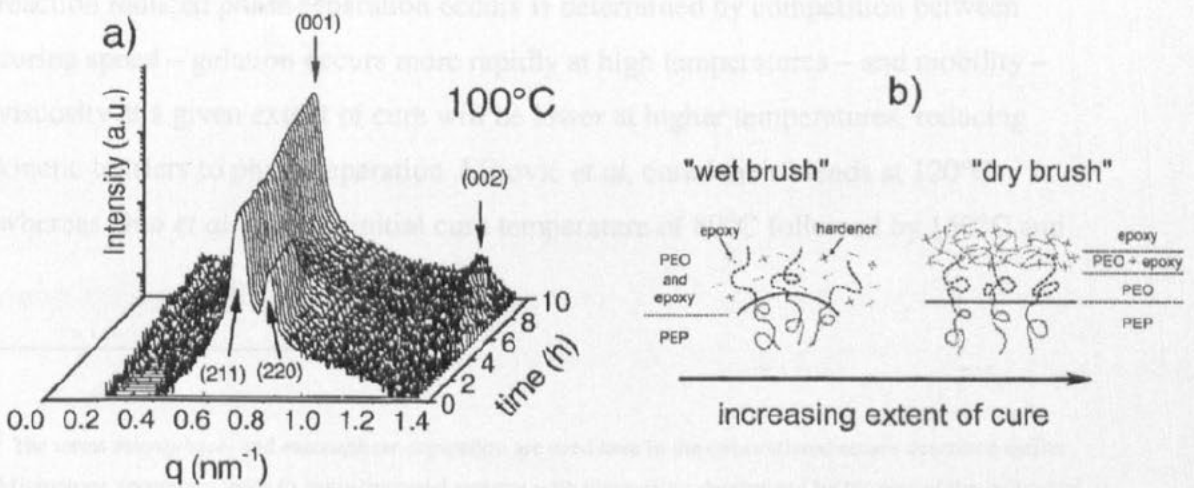


Figure 1.16 – (a) Time resolved SAXS during cure for a PEO-PEP diblock in epoxy (69wt%) showing Gyroid – Lamellar transition. (b) Diagrammatic representation of a possible explanation – expulsion of PEO from epoxy leads to reduced interfacial curvature. Adapted from Lipic *et al.* [36].

Studies with PEO-PPO-PEO triblocks

A number of investigations have been performed using PEO-PPO-PEO triblock copolymers, which are commercially available under the 'Pluronics' trade name. Mijovic *et al.*[37] examined blends of MDA cured BADGE with a PEO-PPO diblock ($M_n = 12000 \text{ g.mol}^{-1}$, 70 wt% PEO) and a PEO-PPO-PEO triblock ($M_n = 4400 \text{ g.mol}^{-1}$, 30 wt% PEO.) Dielectric relaxation spectroscopy was used to monitor changes in mechanical properties during cure. In addition, reaction induced macrophase separation[†] was observed on two different length scales (1 μm and 50 μm) in the triblock system. No visible phase separation occurred in the diblock system, AFM imaging of the cured resin revealed nanostructured systems at some compositions. The difference in solubility between the two block copolymers is most likely due to the difference in PEO content.

Guo *et al.*[42] examined blends of two PEO-PPO-PEO triblocks (30wt% PEO, $M_n = 5800$ and 80wt% PEO, $M_n = 8400$) in DGEBA+ MDA. Microphase separation was observed in all blends from 10-50% triblock for both copolymers. This contrasts with the macrophase separation observed with the 30wt% PEO triblock above. Whether reaction induced phase separation occurs is determined by competition between curing speed – gelation occurs more rapidly at high temperatures – and mobility – viscosity at a given extent of cure will be lower at higher temperatures, reducing kinetic barriers to phase separation. Mijovic *et al.* cured their blends at 120°C whereas Guo *et al.* used an initial cure temperature of 80°C followed by 150°C and

[†] The terms *microphase-* and *macrophase-*separation are used here in the conventional senses described earlier. Microphase separation leads to nanostructured systems with dimensions determined by the size of the individual blocks. The phase boundaries will coincide (approximately) with the inter-block interfaces in the block copolymer. In macrophase separation, separation occurs by nucleation and growth or spinodal decomposition on larger, though not necessarily large, length scales. It is worth noting that the usage of these and similar terms varies between researchers in this field, e.g. the term *microseparated* may be used to describe phase separation on the micron scale.

175°C post-cures. This suggests that, at least for this copolymer, the probability of macrophase separation is determined by kinetic factors.

Up to concentrations of 50wt% in epoxy neither of the copolymers showed melting endotherms by DSC. All samples were optically transparent, therefore the PEO blocks can be assumed to be largely dissolved in the epoxy. Melting exotherms were observed for both copolymers above 60wt% in epoxy. In the case of the 30% PEO system, the samples were opaque, and remained so even after heating. This indicates that macrophase separation had occurred – the opacity is due to the presence of suitably sized separated domains rather than crystallites. In the 80% PEO system, by contrast, the samples were cloudy at room temperature but became transparent when heated. This indicates that the PEO was completely mixed with the epoxy. Note that at 60% block copolymer it is unlikely that the epoxy could every reach complete cure due to dilution by copolymer. Thus it is reasonable to assume that the PEO chains will have the mobility required for melting and crystallization whilst remaining mixed with the epoxy. Crystallisation in these blends was observed by polarized light microscopy. Spherulite size was observed to decrease and crystallization rate was retarded as block copolymer concentration was decreased.

TEM and AFM studies of the cured samples indicated that both block copolymers form structures on the nanometre scale by microphase separation of PPO domains from an epoxy / PEO matrix. In both cases, spherical micelles were formed at low copolymer concentrations (10%). As concentration was increased, PPO domains merged to form first wormlike micelles and then bicontinuous structures. At 20wt% block copolymer both systems show hierarchical nanostructures in AFM phase images. Spherical micelles of diameter ~10nm are dispersed throughout the resin phase which is composed of harder, epoxy-rich, and softer, copolymer-rich, regions on the 100nm scale. An example is shown in Figure 1.17.

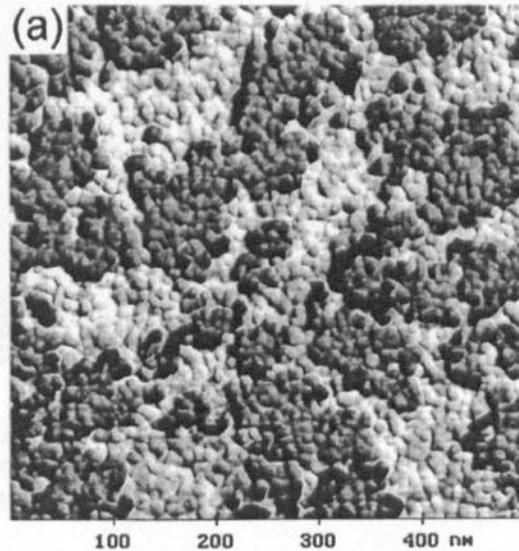


Figure 1.17 – AFM phase image of 20wt% PEO-PPO-PEO (80% PEO) cured in epoxy resin. The lighter areas are harder (epoxy-rich). Adapted from Guo *et al.*[42]

Larrañaga *et al.* have published a number of papers dealing with the kinetics, nanostructure and mechanical properties of a number of PEO-PPO-PEO / BADGE + MDA systems.[44-47]

Curing kinetics of the epoxy system were investigated with increasing amounts of block copolymer additive[47] and with differing volume fractions of PEO in the copolymer[45]. Results from isothermal DSC experiments were fitted to a kinetic model and it was shown that PEO slows the reaction both by acting as a diluent and by interfering with the autocatalytic process. It was suggested that this interference is due to preferential hydrogen bonding between the hydroxyl groups on the resin and the PEO oxygens, thus inhibiting autocatalysis. Reaction rate was found to decrease both with increasing block copolymer content in the resin and with increasing PEO content in the block copolymer.

Structural characterization was performed by AFM and DMTA[44, 46]. At high curing temperatures (140°C), block copolymers with low PEO content were found to macrophase separate from the resin. At lower curing temperature (80°C) microphase separation or homogenous blends were observed (Figure 1.18).

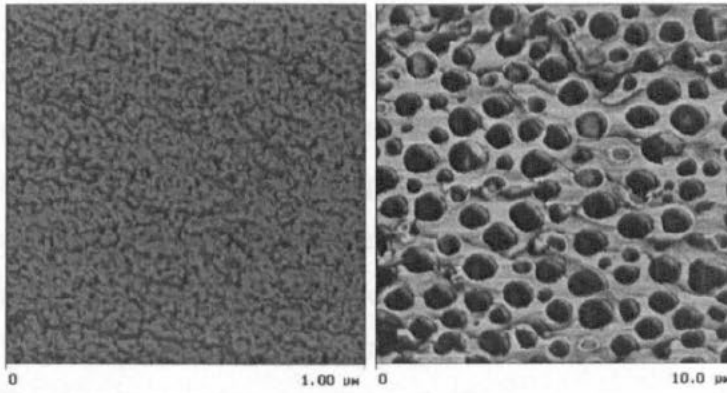


Figure 1.18 – AFM phase images of 30wt% bend of PEO-PPO-PEO ($M_n=2900 \text{ g.mol}^{-1}$ 45wt% PEO) and BADGE / MDA epoxy. Cured at 80°C (left) and 140°C (right) demonstrating microphase and macrophase separation (note different scale bars). Adapted from [46].

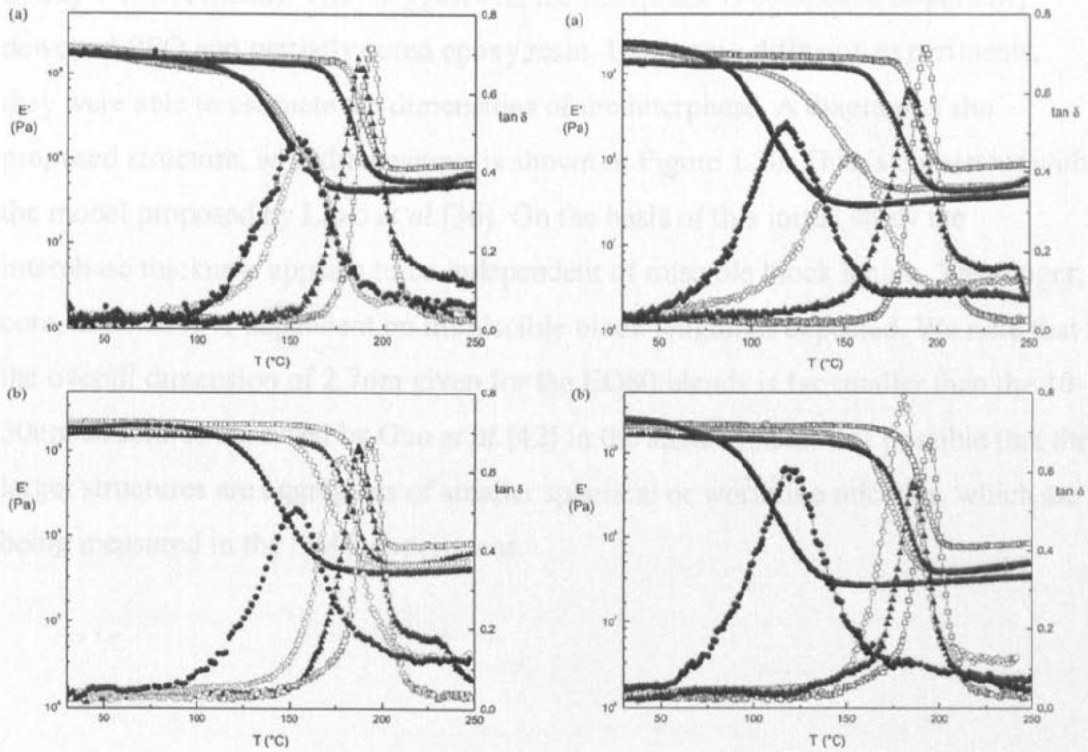


Figure 1.19 – Storage modulus and $\tan \delta$ curves for 10wt% (left) and 20wt% (right) modifier in BADGE / MDA. Cured at 80°C (top) or 140°C (bottom). Open circles are modified with PEO-PPO-PEO (44wt% PEO); filled circles are for PEO modifier, filled triangles for PPO modifier and open squares for the unmodified epoxy. Adapted from [46].

Dynamic mechanical thermal analysis was used to determine the effect on the glass transition temperature of the bulk samples. A 10wt% sample of triblock in epoxy showed no phase separation when cured at 80°C, the observed reduction in T_g was similar to that for 10wt% PEO modified epoxy. When cured at 140°C to induce macrophase separation, its $\tan \delta$ curve more closely resembles that of epoxy cured with PPO, which also macrophase separates. A 20wt% sample of triblock in epoxy, cured at 80°C showing microphase separation has T_g intermediate between the two above cases. The data is reproduced in Figure 1.19.

Sun *et al.* [43] investigated the composition of the interfacial region using magic-angle spinning nuclear magnetic resonance spectroscopy (MAS-NMR). They were able to confirm the presence of an interphase layer in cured 40wt% PEO-PPO-PEO / Epoxy + MDA blends. They suggest that the interphase is composed of partially dewetted PEO and partially cured epoxy resin. Using spin diffusion experiments, they were able to estimate the dimensions of the interphase. A diagram of the proposed structure, with dimensions, is shown in Figure 1.20. This is consistent with the model proposed by Lipic *et al.* [36]. On the basis of this initial study the interphase thickness appears to be independent of miscible block length. The longer, core, dimension is dependent on immiscible block length, as expected. We note that the overall dimension of 2.7nm given for the EO80 blends is far smaller than the 10-30nm structures observed by Guo *et al.* [42] in the same system. It is possible that the larger structures are aggregates of smaller spherical or wormlike micelles, which are being measured in the NMR experiment.

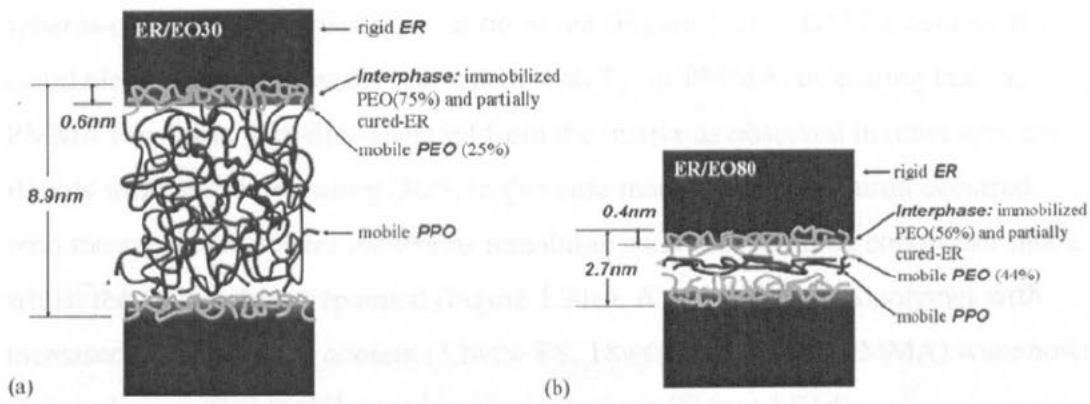


Figure 1.20 – Phase dimensions calculated by spin-diffusion MAS-NMR. EO30 is PEO₂₀PPO₇₀PEO₂₀; EO80 is PEO₇₆PPO₂₉PEO₇₆ (where the subscript indicates the number of repeat units). Adapted from Sun *et al.*[43].

Studies with other block copolymers

Kosonen *et al.* have studied phenolic resin modified with poly(2-vinylpyridine)-*b*-polyisoprene[56, 57]. Through TEM imaging, they observed microphase separation with a spherical morphology from 5-20wt%, cylinders at 30wt% and lamellae at 40wt% ($M_n(\text{P2VP}) = 21000\text{g}\cdot\text{mol}^{-1}$; $M_n(\text{PI}) = 71000\text{g}\cdot\text{mol}^{-1}$). Reducing the size of the miscible P2VP block to match the molecular weight of the resin monomers lead to significant swelling of the P2VP block. Infrared spectroscopy indicated hydrogen bonding between P2VP and the resin which remained present after cure. DSC and dynamical mechanical analysis did not reveal any changes in modulus or glass transition for the modified systems.

Guo *et al.*[50] modified a poly(propylene glycol) type resin with polystyrene-*b*-polybutadiene copolymer. Since neither block was epoxy miscible, macrophase separation was observed in all blends. Isolated domains of copolymer were observed at 5-10wt%, bicontinuous interpenetrating phases were formed for 20-60wt% and at 70wt% and above, domains of resin in a block copolymer matrix were observed.

ABC triblock copolymer blends have been studied by Ritzenthaler *et al.*[54, 55]. A polystyrene-*b*-polybutadiene-*b*-poly(methyl methacrylate) triblock (22%-9%-69% by weight) was studied in MCDEA cured BADGE. An interesting ‘raspberry like’

spheres-on-spheres morphology was observed (Figure 1.21a). DMTA data for the cured blend shows a shoulder coincident with T_g for PMMA, indicating that the PMMA block has partially separated from the matrix as observed in other systems. Blends were also cured using DDS, in this case macrophase separation occurred, with the sphere-on-sphere inclusions remaining stable in the block copolymer phase whilst the epoxy phase separated (Figure 1.21c). A second block copolymer with increased polybutadiene content (12wt% PS, 18wt% PB, 70wt% PMMA) was shown to form 'onion like' multilayered ovular inclusions (Figure 1.21d).

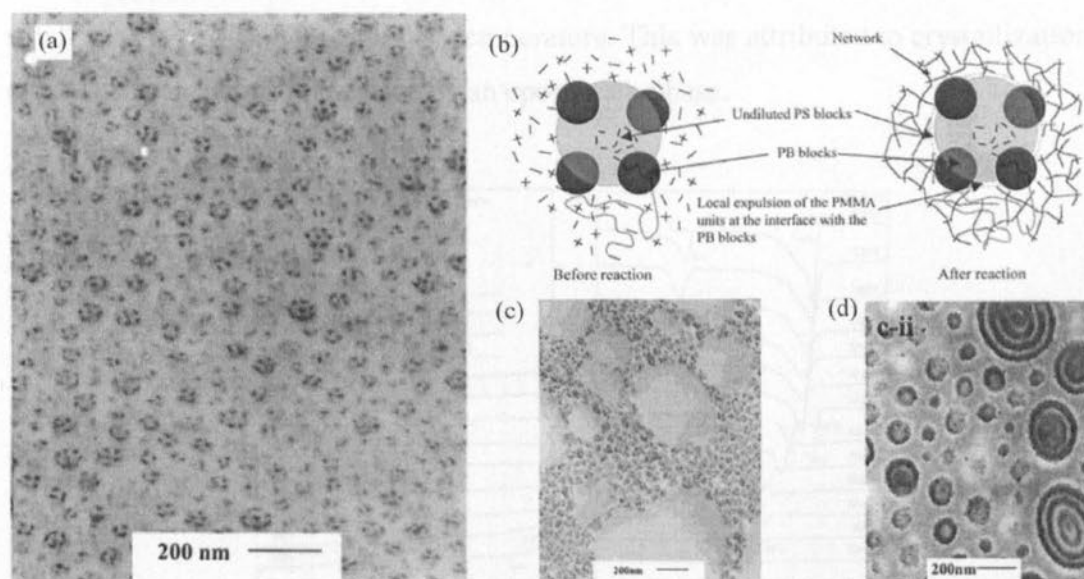


Figure 1.21 – (a) TEM showing 'Raspberry like' morphology in 50wt% of SBM copolymer cured with MCDEA; (b) a schematic representation of the structure. (c) The same system cured with DDS showing macrophase separation whilst maintaining nanoscale morphology. (d) TEM of SBM copolymer with higher B content showing ('onion like' morphology). TEM samples are stained with OSO_4 , PB is darkest, PS is weakly stained, PMMA and the resin are unstained. Adapted from [54, 55]

An investigation into crystallisation in nanoscale domains was performed by Guo *et al.*[58] using a diblock copolymer with a crystallisable immiscible block. A PEO-PE diblock with 50wt% PEO content and M_n of $1400\text{g}\cdot\text{mol}^{-1}$ was used to modify a BADGE + MDA resin. Macrophase separation did not occur in any of the cured blends. 5-30wt% blends of diblock with epoxy show micellar inclusions with increasing packing density. At 40-50wt% the micelles aggregate and merge to form bicontinuous structures. Above 50wt% the samples are volume filled with PE and

PEO crystallites. Melting and crystallization were monitored by DSC and three distinct curing regimes were observed, coinciding with the three morphological regions (Figure 1.22). From 90-70wt% diblock crystallization occurs as in the neat sample, slowing as the concentration of incompletely cured epoxy resin increases. From 5-30wt% crystallization temperature (T_c) is fairly constant due to the PE domains being confined to micelles of similar size across all concentrations. The marked decrease in T_c in these blends is presumably due to physical confinement of the chains and the decreased probability of a homogeneous nucleation site forming within a given time in a very small sample. In the intermediate regime (50%,62%) a small peak was observed at higher temperature. This was attributed to crystallization due to heterogeneous nucleation by an epoxy rich phase.

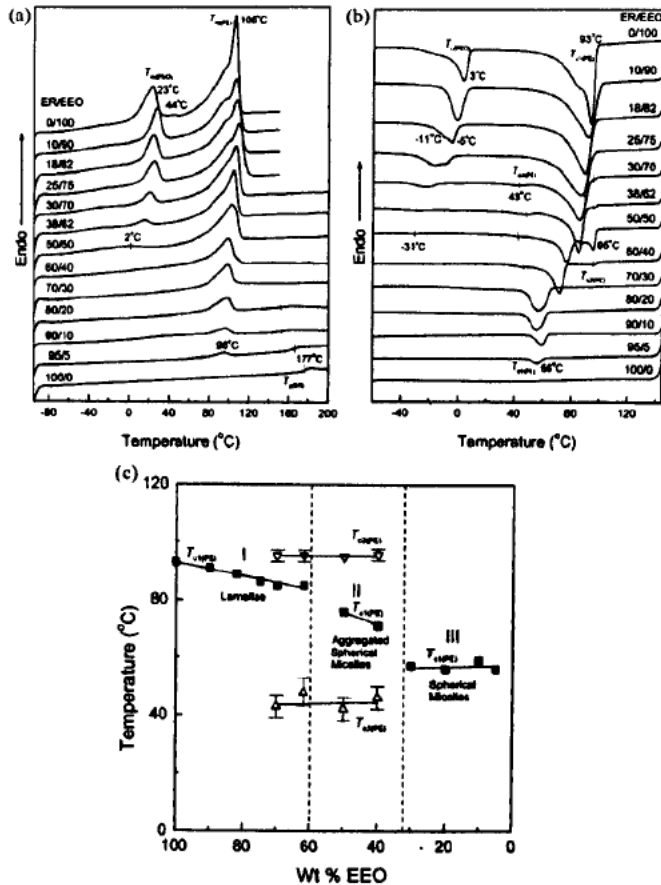


Figure 1.22 – DSC heating (a) and cooling (b) curves for various compositions of cured epoxy resins and PEO-PE diblock. (c) Plot of crystallization temperatures of PE against diblock content showing how the three crystallization regimes coincide with the microscopic structure. Adapted from [58].

1.3.1.2 Reaction Induced Microphase Separation

In the systems described previously, nanoscale structures are formed in solution and ‘fixed’ during cure. Although some systems demonstrate a change of morphology during cure all of the systems have some pre-cure structure. Given that homopolymers can undergo reaction induced macrophase separation as described previously, it is not unreasonable to think that it might be possible to start with a diblock where both blocks are miscible but where one block separates by a reaction induced mechanism during cure. Meng *et al.* have demonstrated this behaviour in two recent papers. Figure 1.23 shows the results from an initial experiment with a poly(ϵ -caprolactone)-*b*-polybutadiene-*b*-poly(ϵ -caprolactone) triblock. The scattering data clearly indicates a lack of structure at the start of cure with a peak having developed by the end of the cure corresponding to the micelles observed in the TEM.

Figure 1.24 shows similar data for a PEO-PS diblock. Structure is present in solution in BADGE but disappears on addition of hardener (Figure 1.24(i)) after cure, multiple order scattering peaks are observed (Figure 1.24 (iii)) and nanostructure is visible by AFM (Figure 1.24 (ii)). In this work, higher concentrations of copolymer were also examined although only pre-cure data is only provided for the 10wt% blend.

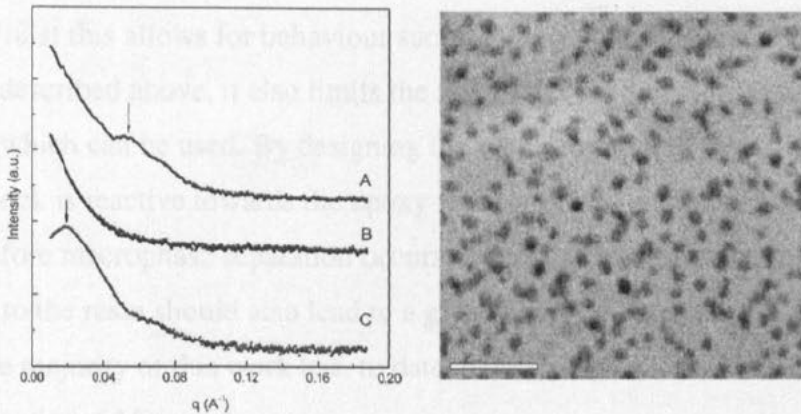


Figure 1.23 – Reaction induced microphase separation in 10wt% PCL-PB-PCL in BADGE + MOCA. [Left] (A) Uncured blend at 25°C; (B) Uncured blend at 150°C (start of cure); (C) Cured thermoset. (Right) TEM image of the cured thermoset; dark spots are OsO₄ stained PB domains, the scale bar is 100nm. Adapted from [60].

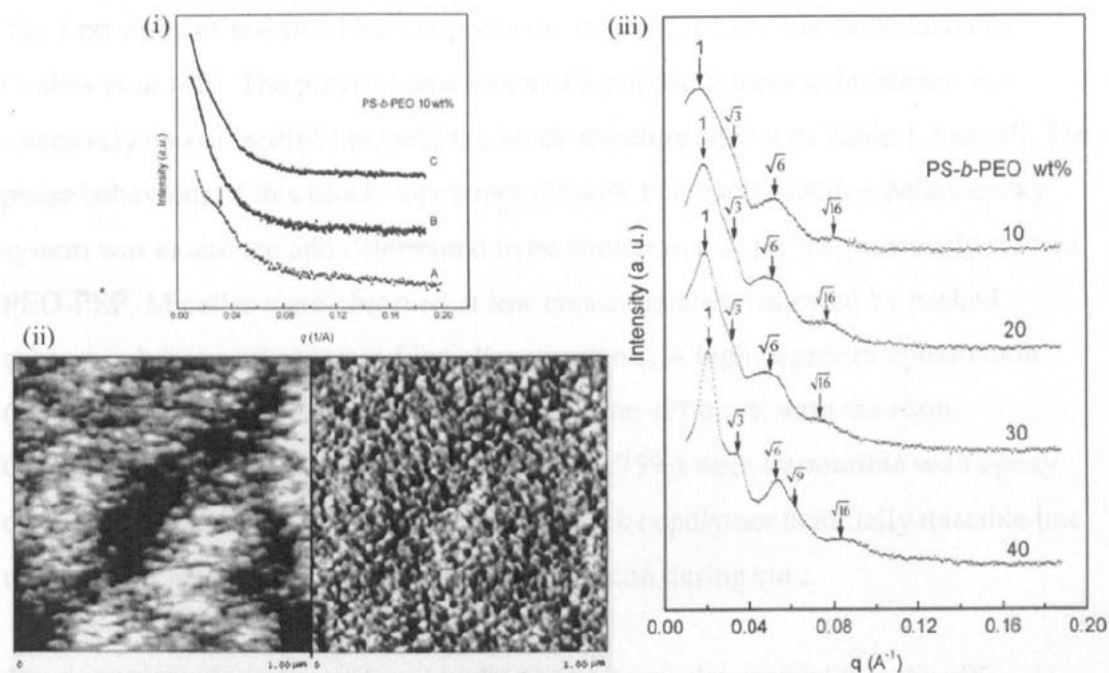


Figure 1.24 – Reaction induced microphase separation in 10wt% PS-PEO diblock in BADGE + MOCA resin. (i) SAXS patterns [A] solution in BADGE at 25°C; [B] BADGE / MOCA / diblock blend at 25°C; [C] blend at 150°C at start of cure. (ii) AFM image (left=height, right=phase) of cured product showing nanostructure. (iii) SAXS patterns of cured products for a number of block copolymer concentrations. Adapted from [59].

1.3.2 Reactive block copolymers

In the work examined so far the formation of microphase separated nanostructures in preference to macrophase separation relies on balancing thermodynamics and kinetics. Whilst this allows for behaviour such as the reaction induced microphase separation described above, it also limits the range of cross-linking agents and curing conditions which can be used. By designing the block copolymer so that the epoxy miscible block is reactive towards the epoxy resin or cross-linker, the structure can be fixed before macrophase separation occurs. Chemically bonding the block copolymer to the resin should also lead to a greater degree of toughening of the epoxy system. The majority of this work has, to date, been carried out in Frank Bates' group at the University of Minnesota.

The first study of reactive block copolymers in epoxy resins was undertaken by Grubbs *et al.*[49]. The polyisoprene block of a polyisoprene-polybutadiene was selectively epoxidised[65] to yield the block structure shown in Table 1.3 as ePI. The phase behaviour of this block copolymer (75wt% PI) in a BADGE + MDA epoxy system was examined and determined to be similar to that for the previously studied PEO-PÉP. Micelles were observed at low concentrations, followed by packed spheres, a hexagonal phase and lamellar structures. A high degree of epoxidation ($\geq 87\%$) was necessary to ensure miscibility of the ePI block with the resin. Copolymers with low degrees of epoxidation ($< 75\%$) were immiscible with epoxy even prior to cure. At 75% epoxidation the block copolymer is initially miscible but undergoes reaction induced macrophase separation during cure.

The curing reaction was analyzed by DSC and it was determined that the ePI epoxides react significantly more slowly than those in the resin. Hence the polyisoprene block remains free to macrophase separate until it is inhibited by the rigidity of the resin, just as for non-reactive block copolymers. The low reactivity of ePI is due to the highly substituted nature of the ePI epoxide, located as it is on the chain backbone. To overcome this problem, poly(methyl acrylate-*co*-glycidyl acrylate)-*b*-polyisoprene copolymers were synthesised. Here, the epoxy group is pendant from the chain. Again, micelles were observed at low concentration and packed more closely as the concentration was increased. DSC analysis revealed a single reaction exotherm, suggesting that the copolymer epoxide has similar reactivity to the BADGE epoxide.

Rebizant *et al.* have investigated versions of the SMB triblocks that were studied by Ritzenthaler as described above. Initially[63] they synthesized an SBMG tetrablock (polystyrene-*b*-polybutadiene-*b*-poly(methyl methacrylate)-*b*-poly(glycidyl methacrylate)). It was determined that the raspberry morphology could be formed and fixed into cured epoxy in the BADGE + DDS system where previously macrophase separation had been observed. It was also determined that as long as the G block is sufficiently short these systems appear to phase separate as SB(MG) triblocks. In later work[64], they examined polystyrene-*b*-polybutadiene-*b*-

poly[(methyl methacrylate)-*stat*-(*tert*-butyl methacrylate)] (SBMT) and the product of hydrolysis of the *tert*-butyl methacrylate block to give a poly[(methyl methacrylate)-*stat*-(methacrylic acid)] block (SBMA triblock). Carboxylic acids are reactive with epoxide groups, as well as with some cross-linking agents. The SBMT triblocks were found to flocculate into visible structures on curing with most hardeners (except MCDEA) whereas the SBMA triblocks maintained their micellar structure (Figure 1.25). The method of hydrolyzing a polyester to give a reactive acid group may offer an advantage over the addition of a glycidyl methacrylate block, which can only be achieved using a limited range of polymerization conditions owing to the reactivity of the monomer. By contrast, polyesters can be synthesised using a range of techniques and made reactive by hydrolysis after polymerization.

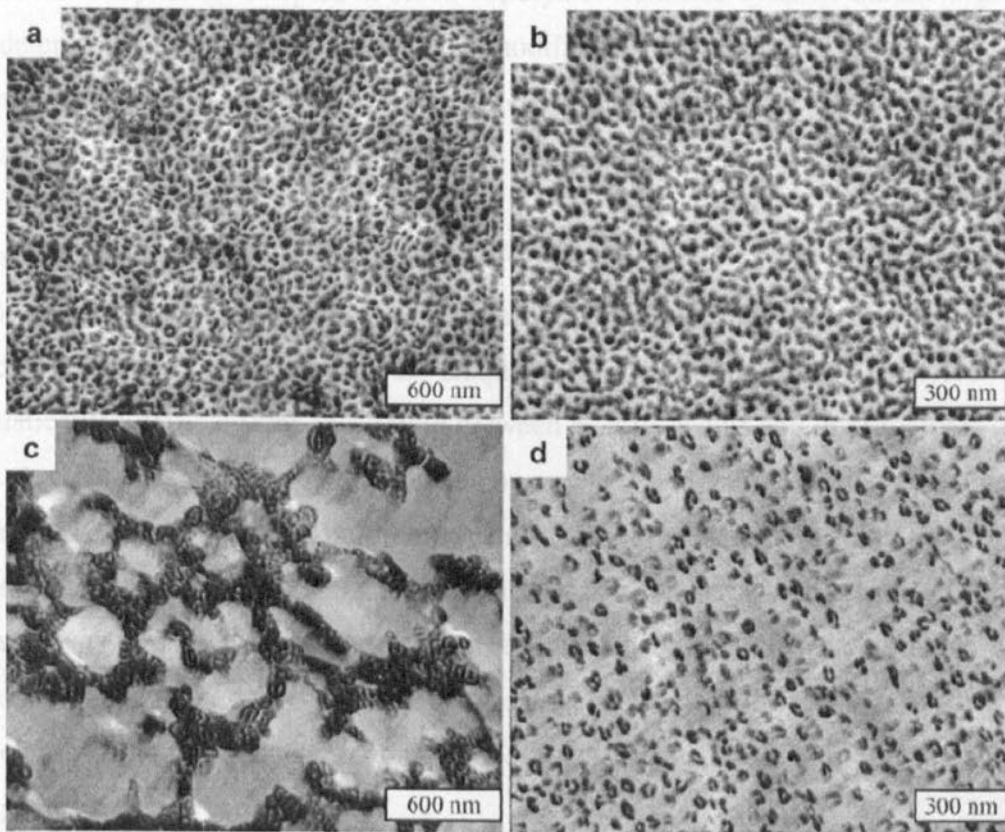


Figure 1.25 – TEM images of SBMT (left) and equivalent SBMA (right) triblock copolymers at 30wt% in BADGE + DDS before (top) and after (bottom) cure at 135°C showing the effect of reactive groups in the epoxy miscible block. Reproduced from Rebizant *et al.*[64]

1.3.3 Fracture toughening

Epoxy resins cured using aromatic cross-linking agents usually have high glass transition temperatures. Whilst this is a desirable property for many applications, it also means that unmodified cured resins can be extremely brittle. Traditionally, toughening is achieved using rubbery modifiers which are either thoroughly immiscible with the epoxy or undergo reaction induced macrophase separation [66-70]. The level of toughening achieved and the effect on the mechanical properties of the cured resin are dependant on the curing conditions. It has been suggested that since the morphology adopted in block-copolymer modified systems should largely be determined by the composition of the modifier, these systems may give reproducible levels of toughening over a much wider range of curing conditions. Again, much of this work has been carried out in the Bates group.

Dean *et al.*[40] studied the effect of PEO-PEP block copolymers at low concentration on a BADGE + MDA system. Spherical micelles were found to improve fracture toughness, (K_{Ic} , see chapter 2 for a definition) by 25-35%. No statistically significant link was found between micelle radius and improvement in K_{Ic} . A vesicular morphology formed was by one of the copolymers and was found to increase K_{Ic} by 45% even at half the concentration of the micelle forming systems. It was suggested that the resin inside the vesicle acts as a separated microparticle in a similar way to phase separated modifiers. Because the bulk of the modifying particle actually consists of epoxy with only the vesicle walls containing block copolymer, much lower modifier concentrations are required to achieve a similar degree of toughening.

It is worth noting that several studies report fracture toughness in terms of the strain energy release rate, G_c :

$$G_c = \frac{K_{Ic}^2}{E} (1 - \nu^2) \quad (1.15)$$

where E is the Young's modulus and ν the Poisson's ratio of the sample. The Poisson's ratio is taken to be constant for all samples in a given set. Since variation in E is generally undesirable it is best recorded separately from fracture toughness. Hence discussion here is limited to changes K_{Ic} only.

In a further paper[53] non-reactive PEO-PB copolymers are compared to ePI-PB and polymers with a reactive P(MA-co-GMA) epoxy miscible block. These form nanoscale structures which are chemically bonded into the resin before and after gelation of the epoxy resin respectively. Again, vesicles were found to be best at improving fracture mechanics (quoted as improvement in G_c only). Non-reactive vesicles were inferior to the vesicles in which the ePI block was 'stitched' to the resin after gelation. In turn, superior toughness was achieved using P(MA-co-GMA) based diblocks which were 'stitched' to the resin before gelation had occurred. Samples were prepared by dissolving resin, hardener and copolymer in a common solvent then removing the solvent by evaporation. The size of vesicles formed was found to depend on the concentration of the mixture in the solvent and on the time between dissolution and evaporation. More concentrated solutions with longer equilibration times produced larger vesicles. This suggests that the vesicles were formed in solution prior to solvent removal, the probability of two small vesicles coalescing to form a larger one increases with concentration and time.

Seemingly conflicting results were obtained in a study using PEO-PEP and reactive block copolymers in partially brominated BADGE resins cured with phenol novolac[41]. Spherical micelles were found to give significantly greater improvements in toughness than vesicles. Even greater enhancement was found when wormlike micelles were formed ($\sim 4\times$ improvement in K_{Ic} ; $\sim 3\times$ with spherical micelles). The relative improvement in toughness was found to increase as brominated epoxy content increased (increased bromination leads to a more brittle resin in the absence of toughening agent). The glass transition temperature of these

systems was also found to increase in the systems containing spherical and wormlike micelles. This is the opposite of what one would normally expect and has not been fully explained, though it was suggested that the presence of PEO may enhance the cross-linking in some way.

Wu, Thio & Bates observed similar behaviour when they studied PEO-PBO diblock copolymers in non-brominated BADGE + phenol novolac[39]. Again, wormlike micelles were found to provide the greatest improvement in K_{Ic} ($\sim 4\times$) followed by spherical micelles ($\sim 2.5\times$) and vesicles ($\sim 1.8\times$). The glass transition was again seen to rise after modification, with the greatest increase for the wormlike morphology. It is suggested that the toughening observed with micelles may be due to cavitation processes. With worm-like micelles, SEM indicates that worms bridging the crack are 'pulled-out', also there is evidence for nanometre scale crack deflection leading to the detachment of thin flakes of epoxy from the fracture surface. They speculate that the increase in T_g may be due to localised concentration fluctuations of epoxy and hardener when blended with diblock, leading to a modified network structure.

Very recently, Thio, Wu and Bates have reported the behaviour of poly(ethylene oxide)-*b*-poly(hexylene oxide) (PEO-PHO) diblocks in phenol novolac cured BADGE [71]. The highly non-polar PHO block is immiscible with BADGE even at low molecular weights. Wormlike micelles were generated by mixing a vesicle forming diblock (9 wt% PEO) and a spherical micelle forming diblock (44 wt% PEO). Here the wormlike morphology was again found to give the best improvement in K_{Ic} ($\sim 6\times$), but vesicles were found to give greater improvements than spherical micelles ($\sim 3.5\times$ and $\sim 1.75\times$ respectively). Again there appears to be some correlation between T_g and the improvement in K_{Ic} .

Ritzenthaler[55] and Rebizant[64] have reported maximum K_{Ic} improvements of around $2\times$ by particles forming the 'spheres-on-spheres' morphology described above.

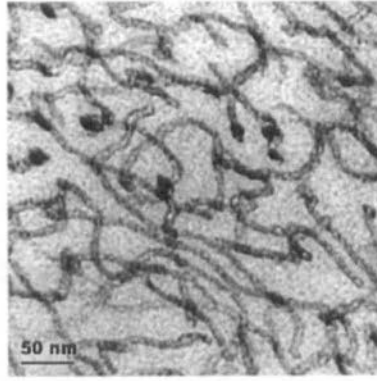


Figure 1.26 – TEM image showing wormlike micelles of PEO-PHO in a BADGE + PN system. Stained with RuO_4 . Reproduced from [71].

1.4 Aims

A number of studies detailed above have examined the structures formed by block copolymers in epoxy resins and the subsequent effect on the mechanical properties of the cured resin. Although diblocks and ABA triblocks with epoxy miscible end groups have been studied, to date no work has been published regarding the behaviour of ABA triblocks having an epoxy miscible midblock and immiscible end blocks. Also although Thio and Bates have examined PEO-PBO diblocks at low concentration, no study appears to have been performed at higher block copolymer loadings. The author is aware of a patent application, published as this work was in progress [72] where the use of PEO-PBO-PEO triblocks as epoxy modifiers is claimed, however experimental results provided therein are limited to the PEO-PBO and PEO-PHO diblock systems described above.

The aim following work therefore is to examine the behaviour of epoxy resin-block copolymer systems where the block copolymers are PBO-PEO-PBO and PEO-PBO-PEO triblocks.

2 Materials and Methods

2.1 Materials

Except where otherwise stated, all materials were used as received without further purification.

2.1.1 Epoxy Resin

The epoxy resin used in this work was the diglycidyl ether of bisphenol-A, hereafter referred to as BADGE (Bisphenol-A, Diglycidyl Ether). BADGE is the major resin component in many commercial epoxy systems. Dow chemicals estimates that almost a million metric tonnes of BADGE was produced globally in 2003 [73].

BADGE is synthesised industrially by the reaction of bisphenol-A with epichlorohydrin, a reaction scheme is presented in Figure 2.1.

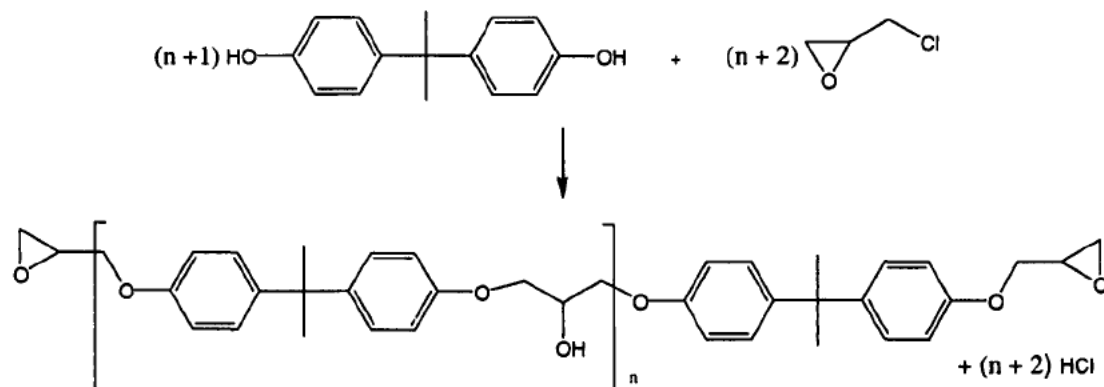


Figure 2.1 – Reaction scheme showing the reaction of Bisphenol-A and epichlorohydrin to produce BADGE.

This reaction produces a mixture of BADGE oligomers of varying length (typically $n = 0$ to $n = 40$). In order to ensure stoichiometric balance of resin to hardener it is necessary to determine how many epoxide groups are present per unit mass in any given batch of epoxy resin.

2.1.1.1 · Determination of epoxide-equivalent weight

The epoxide equivalent weight (EEW) is defined as the mass, in grams, of resin containing one mole of epoxide groups. Thus, for difunctional epoxy oligomers, the EEW is equal to half of the number average molecular weight.

BADGE was purchased from Sigma-Aldrich Ltd. and was labelled as having an EEW in the range 172-176 $\text{g}\cdot\text{mol}^{-1}$. A sample of material was analysed using the method described by King [74]. Hydrochloric acid undergoes nucleophilic addition to epoxide groups in a stoichiometric manner. Thus if a quantity of epoxy resin is reacted with an excess of HCl, the EEW can be calculated by determining how much of the HCl remains after the reaction is complete.

1.25 ml of concentrated aqueous HCl was added to 98.75 ml of dioxane to produce a 0.015 $\text{mol}\cdot\text{l}^{-1}$ solution. Portions of around 120 mg of BADGE were dissolved in 10.0 ml of this solution and stirred at room temperature for ten minutes. To the reaction was added 10 ml of ethanol containing two drops of 1% phenolphthalein solution. The resulting mixture was titrated with 0.025 $\text{mol}\cdot\text{l}^{-1}$ standard sodium hydroxide solution, until a faint pink endpoint was observed. The epoxide equivalent weight was then calculated using Equation (2.1) where W_E is the mass of epoxy resin used; C_{NaOH} is the concentration of sodium hydroxide solution; and V_E and V_B are, respectively, the titre volumes required to neutralize a sample containing resin and a 'blank' sample of HCl / dioxane with which no resin has been reacted.

$$EEW = \frac{W_E}{C_{\text{NaOH}}(V_B - V_E)} \quad (2.1)$$

Averaging over seven experiments, the EEW of the resin was determined to be $168.5 \pm 6.40 \text{ g.mol}^{-1}$.

2.1.2 Cross-linking Agent

Diethyltoluenediamine (DETDA) was a gift from Lonza Group Limited, Basel, Switzerland. The product, marketed as 'Lonzacure 80', is an 80:20 mixture of the 2,4- and 2,6-isomers as shown in Figure 2.2.

DETDA was stored at -20°C when not in use so as to prevent oxidation.

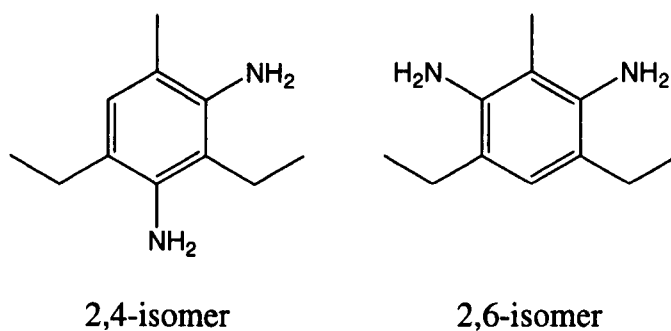


Figure 2.2 – The structure of diethyltoluenediamine (DETDA)

2.1.3 Block Copolymers

A series of block copolymers of ethylene oxide and 1,2-butylene oxide were used in this study. For succinctness, the structures of these polymers are abbreviated using the symbols E_m to represent a poly(ethylene oxide) block of degree of polymerization m and B_n to represent a poly(1,2-butylene oxide) block of degree of polymerization n .

The structure of BEB and EBE triblocks is shown in Figure 2.3

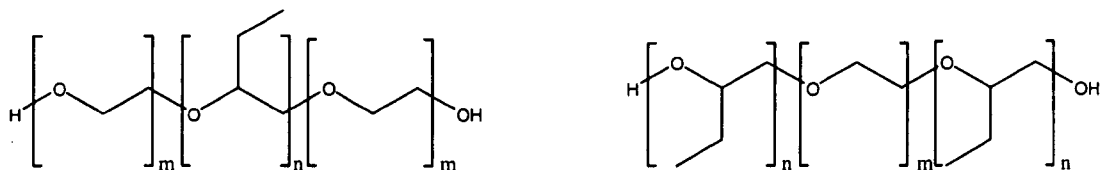


Figure 2.3 – The structure of $E_m B_n E_m$ and $B_n E_m B_n$ triblock copolymers

2.1.3.1 Block copolymer bulk properties

The block copolymers were previously synthesised and characterised by Shaomin Mai, Chiraphon Chaibundit and Withawat Minvanish at the University of Manchester. Oxyanionic polymerisation was used, experimental details are given elsewhere[75-77].

The bulk properties of these materials have been studied extensively[75-84]. A summary of some relevant properties of the block copolymers used in this study is given in Table 2.1.

The copolymers have low polydispersities, as measured by gel-permeation chromatography. In the case of EB and BEB polymers (M_w/M_n) < 1.05, whilst for the EBE samples, (M_w/M_n) < 1.2 [75-77].

The number average molar mass, M_n , was determined by NMR measurements. Overall chain volume can be compared using r_v , the volume of the block copolymer relative to a single E-block segment. For an $E_m B_n$ diblock:

$$r_v = m + n(v_B / v_E) \quad (2.2)$$

where (v_B / v_E) is the ratio of volumes occupied by a B-block and an E-block. For liquid PEO and PBO (v_B / v_E) is 1.89. [85]

Polymer	$M_n / \text{g.mol}^{-1}$	r_v	ϕ_E	$d_{\text{solid}} / \text{\AA}$	Melt Morphology	$d_{\text{melt}} / \text{\AA}$	$T_{\text{ODT}} / ^\circ\text{C}$
B ₂₀ E ₁₄₁ B ₂₀	9100	217	0.65	140	Dis	-	-
B ₁₇ E ₂₀₁ B ₁₇	11300	265	0.76	139	Dis	-	-
B ₃₄ E ₉₃ B ₃₄	9000	222	0.42	138	Gyr	122	79
B ₂₅ E ₂₁₀ B ₂₅	12800	305	0.69	151	Lam	117	50(T_{DOT}) [*]
B ₃₇ E ₁₅₀ B ₃₇	11900	290	0.52	164	Lam	121	143
B ₄₄ E ₁₂₇ B ₄₄	11900	293	0.43	150	Hex [†]	125	129
B ₆₄ E ₇₅ B ₆₄	12500	397	0.24	134	BCC	111	86
E ₉₁ B ₅₆ E ₉₁	12000	288	0.63	149	Lam	130	142
E ₉₀ B ₈₂ E ₉₀	13800	335	0.54	152	Lam	131	204
E ₄₃ B ₁₀₀ E ₄₃	11000	275	0.31	143	Hex	126	148
E ₁₂₆ B ₅₁ E ₁₂₆	14800	352	0.73	166	Lam	129	105
E ₁₁₅ B ₁₀₂	12500	310	0.37	252	Hex	177	225
E ₁₃₆ B ₁₈	7300	170	0.80		Dis	-	-

^{*} No ODT temperature is available for B₂₅E₂₁₀B₂₅ so the disorder to order transition (DOT) temperature is given.

[†] B₄₄E₁₂₇B₄₄ shows a Hex → Gyr transition at 70°C. The ODT given is for the Gyr → Dis transition.

Table 2.1 – Block copolymers used in this work with some relevant bulk properties: number average molecular weight, M_n ; Copolymer volume relative to one E-block segment, r_v ; Volume fraction of E-block, ϕ_E ; Typical d-spacing in the solid after slow cooling (lamellar morphology due to E-block crystallisation), d_{solid} ; morphology observed in the melt at 70°C (*Dis* – disordered, *BCC* – body centred cubic packed spheres, *Lam* – lamellar, *Hex* – hexagonally packed cylinders.); d-spacing at 70°C, d_{melt} ; order-disorder transition temperature observed by SAXS, T_{ODT} . Data from refs [83, 86].

The volume fraction of E-block, ϕ_E is calculated as:

$$\phi_E = \frac{m}{m + n(v_B/v_E)} \quad (2.3)$$

The poly(ethylene oxide) block in EB copolymers is known to crystallize on solidification [75, 78, 81, 82]. Hence EB copolymers tend to adopt a lamellar morphology in the solid phase with layers of crystalline E-block alternating with amorphous layers composed of the B-block and the non-crystalline parts of the

E-block. The B-block is not crystallisable due to steric hindrance from its pendant ethyl groups, which have atactic stereochemistry. Figure 2.4 shows an example of SAXS data for a BEB triblock which shows a clear variation in morphology and d-spacing between the solid and melt phases. The improved sharpness of the peaks in the melt phase indicates stronger ordering in this phase compared with the solid. The transition to a disordered melt (broad, weak peak) is also shown, T_{ODT} data was previously obtained by monitoring this transition using time-resolved SAXS [83, 86].

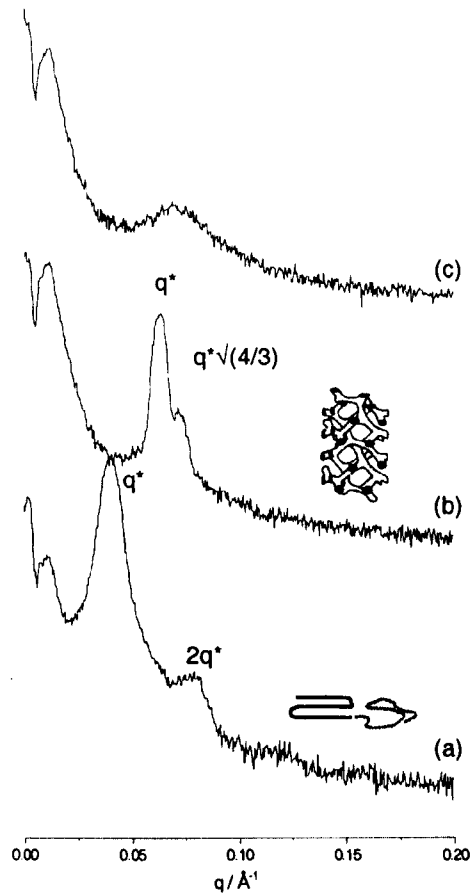


Figure 2.4 – SAXS patterns for neat block copolymer $B_{34}E_{93}B_{34}$. (a) 25°C solid after slow cooling, showing lamellar morphology due to crystallisation of the E-block. (b) 70°C melt showing gyroid morphology. (c) 150°C disordered melt. The vertical axis indicates arbitrary intensity on a \log_{10} scale.

2.1.4 Preparation of Block Copolymer / Epoxy Blends

2.1.4.1 Blending of components

Because of the difficulty involved in accurately matching the stoichiometry of BADGE and DETDA when preparing small samples, BADGE and DETDA were premixed in larger quantities and stored at -20°C to inhibit reaction until required. The mixture was monitored by FTIR to ensure no reaction occurred whilst in storage. Representative spectra are shown in Figure 2.5.

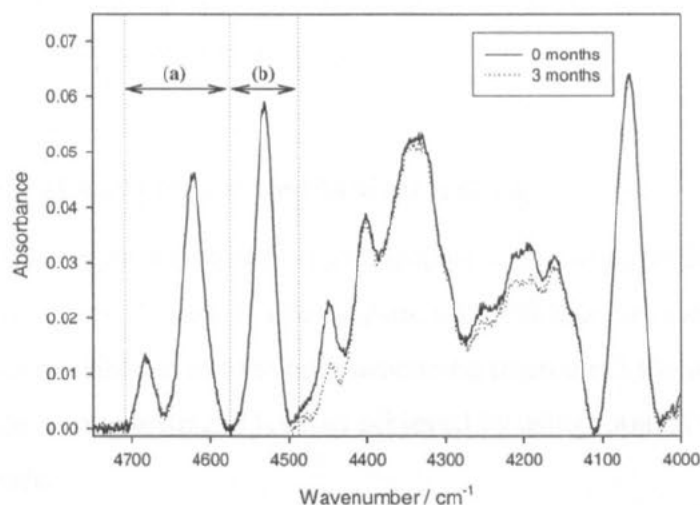


Figure 2.5 – FTIR spectra of BADGE / DETDA immediately after mixing and after 3 months stored at -20°C . Spectra are normalized against the integral of region (a). Region (b) is the epoxide stretch and bend and demonstrates that the epoxide remains unreacted.

Typically, 10.0g (59.35 mmol) of BADGE was weighed into a flask, along with 2.645g (14.84 mmol) of DETDA 50 ml of acetone was added and the mixture was stirred until homogenous. The solvent was removed by rotary evaporation and the resulting mixture was decanted into vials for storage.

In a typical preparation of a block copolymer / epoxy blend, 24.82mg of $\text{B}_{25}\text{E}_{210}\text{B}_{25}$ was weighed into a vial; to this was added 502.3mg of BADGE / DETDA as prepared above. 1 ml of acetone was added, and the mixture was stirred until all components had dissolved. For samples containing up to 30wt% block copolymer, the acetone was usually removed immediately on a rotary evaporator. Higher

concentration samples were prone to bumping and solvent was generally allowed to evaporate overnight before the sample was placed under vacuum to ensure complete removal of acetone.

2.1.4.2 Curing of samples for SAXS / TEM

Samples for TEM were cured in size 0 gelatin capsules (Agar Scientific) at 75°C for at least 72 hours, and then post-cured at 180°C for two hours to ensure complete cross-linking. After curing part of the sample was cut away (using a razor blade or a hacksaw depending on consistency) for use in SAXS experiments. The remainder of the sample was available for microtoming.

2.1.4.3 Curing of samples for mechanical testing

Mechanical testing requires precisely sized samples with sharply defined edges. In the case of brittle materials such as epoxy resin, it is desirable to avoid machining the sample wherever possible so as to avoid introducing microcracks which may cause premature failure during testing. This was achieved by using moulds formed with a silicone elastomer.

A template consisting of a 3 × 4 grid of cuboid protrusions (25mm long × 6mm wide × 3mm high) on a flat surface was milled from a block of aluminium. Silastic 145 silicone elastomer prepolymer (Dow Corning) was mixed in a 10:1 mass ratio with its corresponding catalyst. The mixture was poured onto the template, left to stand for one hour to allow air bubbles to escape then cured in an oven at 75°C for at least 12 hours. The manufacturers recommended curing time at elevated temperature is significantly shorter (~4 hours). However, it was found that moulds cured according to that schedule would bind irreversibly to epoxy resin. This problem was solved by longer mould curing time. It is assumed that the bonding occurred between epoxy resin and unreacted silicone in the less well cured moulds.

In order to ensure no residual low boiling impurities which might form bubbles in the samples were present uncured blends of epoxy / block copolymer were placed under vacuum at 60°C for 20 minutes. Immediately after removal from the rotary evaporator or vacuum oven, samples were poured carefully into the mould, with care taken not to introduce bubbles. The mould was placed into an oven preheated to 75°C and samples were cured for at least 72 hours followed by a two hour post-cure at 180°C.

On removal from the mould, well formed samples of roughly 25mm × 6mm × 3mm were produced. Final finishing of the top surface was performed with fine grain silicon carbide abrasive paper.

2.1.4.4 Curing of samples for optical microscopy

Samples suitable for transmission optical microscopy were produced by placing a drop of epoxy / block copolymer blend on a microscope slide, covering with a 22mm diameter circular cover slip and compressing to form an optically translucent film. As with other samples, curing was at 75°C for at least 72 hours followed by a two hour post-cure at 180°C.

2.2 Experimental Techniques

2.2.1 Optical Microscopy

Optical micrographs were obtained using an Olympus BX-50 optical microscope equipped with a JVC TK-C1381 colour video camera attached *via* a U-CMAD-2 camera mount. The microscope was equipped with a linear polarizer below the sample stage and analyzer above the objective so that polarized light microscopy could be performed.

The resolution of microscopy is limited by diffraction to around half the wavelength of the incident radiation. In optical microscopy this corresponds to a limit of around 250nm in the best case. Therefore, it is not possible to resolve structure on the nanoscale with a light microscope. It is, however, possible to infer the presence of certain types of nanoscopic structure from features which can be observed in an optical micrograph.

2.2.1.1 Birefringence

The refractive index of a medium is defined as $n = c/v$; where c is the speed of light in a vacuum and v is the phase velocity (i.e. the velocity of propagation of wave crests) of the radiation in the medium. In 'birefringent' materials, refractive index varies depending on the direction of propagation of the light within the material. In a beam of linearly polarized light where the direction of polarization is at 45° to a pair of axes, the light can be considered to have components travelling directly along each axis. (A vector of magnitude A at 45° to the axes can be represented as two vectors, each of magnitude $A\sqrt{2}$, travelling along orthogonal axes.) In birefringent materials, the component along one axis will be slowed relative to the component along the other axis. Thus, on leaving the material, the two components will be out of phase, this leads to a rotation of the plane of the polarised light and, in some cases, coloured interference patterns.

Birefringence is best observed by placing the sample between crossed polarizers, such that only the parts of the material which rotate the plane of polarized light are visible.

Birefringence may occur where an anisotropic phase (such as rods or lamellae) with one refractive index is present within a matrix with a different refractive index. For maximum effect, the d-spacing should be about one twentieth of the wavelength of the incident light [87]. Birefringence also occurs in regions, such as crystallites, where inter-atomic bonds are strongly aligned. Light travelling parallel to the axis of

alignment interacts more strongly with the bonding electrons and so is slowed to a greater degree than light travelling orthogonal to the axis.

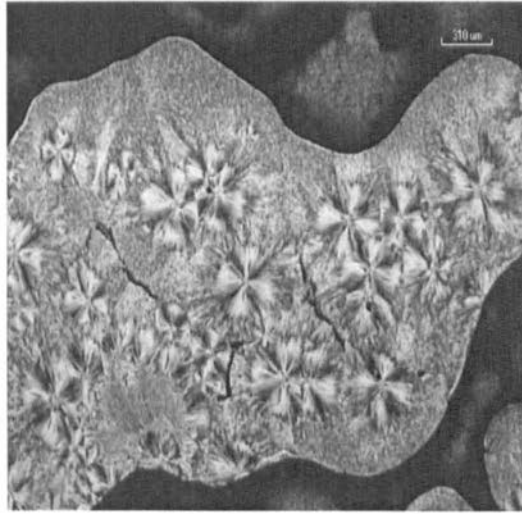


Figure 2.6 – Crossed-polar optical micrograph showing birefringence in a sample of solid $B_{20}E_{141}B_{20}$

2.2.2 Transmission Electron Microscopy (TEM)

TEM allows us to utilize the wave-like properties of an electron beam to overcome the optical diffraction limit and is therefore an excellent tool for directly imaging nanoscale structures.

A stream of electrons is created by, for example, thermionic emission, accelerated through a high voltage and focused into a beam and onto the sample using electromagnetic lenses. After the beam passes through the sample, another series of lenses focus the emerging beam to produce a magnified real space image. This image may be projected onto a phosphor coated screen, for direct viewing by the operator, or recorded by a camera. All of this occurs under high vacuum to minimize scattering of the electrons by air.

The wavelength of an electron travelling at relativistic speeds is given by[88]:

$$\lambda = \frac{h}{\sqrt{2m_0eV\left(1 + \frac{eV}{2m_0c^2}\right)}} \quad (2.1)$$

Where h is Planck's constant (6.626×10^{-34} N.m.s); m_0 is the rest mass of an electron (9.109×10^{-31} kg); e is the charge on an electron (1.602×10^{-19} C); V is the voltage of the accelerating field and c is the speed of light in a vacuum (2.998×10^8 m/s).

Hence, for accelerating field of 100kV, the wavelength of the electron beam is 3.70pm. The diffraction limit is no longer a problem! Image quality is instead limited by issues such as sample thickness (electrons are scattered so strongly that all but the thinnest samples will simply block the beam) and contrast.

Contrast in TEM is dependant on a number of factors including the thickness of the sample and the atomic mass of the constituent atoms[88]. Electrons in the beam are scattered through electrostatic interaction with protons and electrons in the atoms of the sample. Hence heavier elements scatter electrons more strongly. As polymers are generally composed only of lighter elements, it is necessary to selectively stain the sample with a heavy metal in order to provide contrast.

Samples were microtomed to produce specimens of thickness <100nm using a Reichert ultramicrotome equipped with a diamond knife. Specimens were floated onto Nickel grids. Specimens were stained in the vapour of a 0.5% aqueous solution of Ruthenium Tetraoxide (PolySciences Europe) at room temperature for 40 minutes. Trent *et al.*[89] have previously demonstrated that RuO_4 is capable of staining a wide variety of polymers including polyethers.

Images were acquired on a Philips CM100 TEM operating with an accelerating voltage of 80kV at magnifications of between 50k \times and 105k \times . Images were recorded onto 8cm \times 10cm photographic plates (Kodak EM) and developed using Ilford PQ universal developer at 20 $^\circ$ C for 5 minutes. Digital image files were obtained using an Epson flatbed scanner with a transparency adapter.

2.2.3 Scanning Electron Microscopy (SEM)

As in TEM, the scanning electron microscope relies on electromagnetic lenses to focus a beam of electrons so that small features can be observed. However whereas in TEM the image is formed by transmitted electrons which have been scattered through a shallow angle, in SEM it is electrons which have been backscattered that are detected: In practice, this means that SEM is a surface imaging technique. As in TEM contrast is observed between regions of the sample where the constituent atoms have significantly differing atomic numbers but, again, this effect is negligible in simple polymeric samples. Importantly, surface topography also contributes to contrast. An electron scattered from the bottom of a depression is more likely to re-enter some part of the sample, and thus fail to reach the detector, than one scattered from the top of a peak.

The surface of electrically insulating polymer samples can become charged in the SEM, causing the deflection of the electron beam. To prevent this, samples must be coated with an electrically conductive surface layer prior to imaging.

Samples used had been fractured in the mechanical property testing experiments describe later. A small piece containing the fracture surface was cut from the bulk of the sample using a hacksaw and mounted onto an aluminium stub using Silver-DAG conductive adhesive. A thin conductive layer of gold was deposited over the surface in an EMSCOPE SC500 sputter coater. Scanning electron micrographs were obtained using a Camscan Mk.2 scanning electron microscope with an accelerating field of 5kV.

2.2.4 Fourier Transform Infra-Red Spectroscopy (FTIR)

Electromagnetic radiation in the infrared region has photon energies on the order of those associated with bending and stretching of covalent bonds between atoms. Hence the pattern of specific wavelengths absorbed from a beam of infrared radiation can provide information on which functional groups are present in a sample. [87, 90] The area under a functional group's absorption peak is proportional to the relative concentration of that group. Thus IR spectroscopy can be used to monitor reaction kinetics by tracking changes in the concentration of a reacting group over time. To compensate for changes in the intensity between individual spectra in a series, it is also necessary to normalize against a reference peak from a group which is not involved in the reaction.

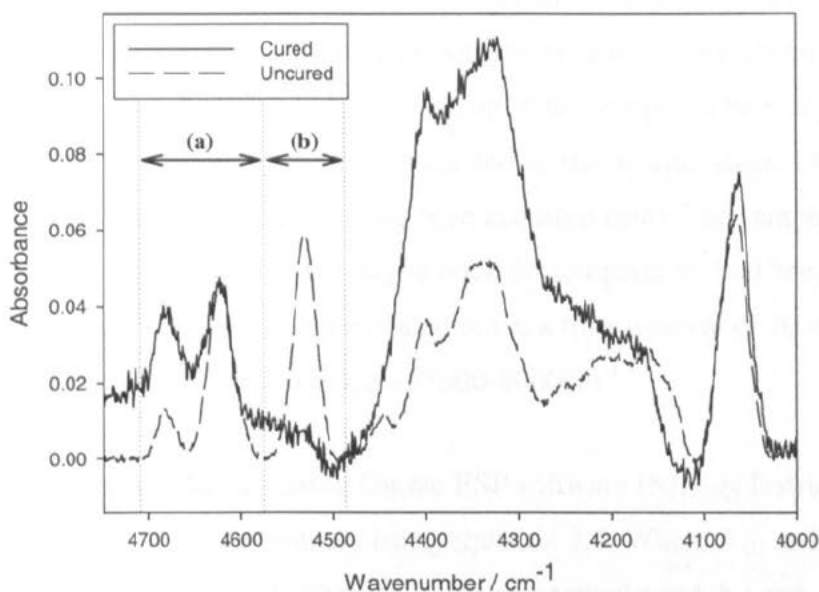


Figure 2.7 – FTIR spectra of a stoichiometric BADGE / DETDA mixture before and after curing. Reaction kinetics was followed by normalizing a time series of spectra against the integral of region (a) and monitoring the disappearance of peak (b).

Mijović *et al.* have shown that spectroscopy in the near-infrared region provides reliable results for kinetic studies in epoxy / amine systems[91, 92]. By using a non-crosslinking model system composed of a monofunctional epoxide and a difunctional aromatic amine they were able to compare results obtained from FTIR to those from an analysis by high performance liquid chromatography (HPLC). They

conclude that the best results can be obtained by normalizing against the aromatic C-H stretching vibrations found around 4670-4620 cm^{-1} and monitoring the disappearance of the peak around 4530 cm^{-1} which they attribute to stretching and bending in the epoxide ring. Figure 2.7 shows the changes observed in the spectrum – the increase in intensity in the 4450-4100 cm^{-1} is due to contributions from absorption interactions of hydroxyl groups formed during the reaction. A marked reduction in signal-to-noise ratio is observed during curing, indicating reduced signal amplitude at the detector. This may be due limited freedom of movement of the bonds in the cured resin.

Spectra were acquired on a Perkin-Elmer SpectrumOne FTIR spectrometer equipped with a KBr beamsplitter and Lithium Tantalide detector. A purpose built electronically controlled heating stage, with a hole to allow passage of the beam, was fitted in the sample chamber. 0.5mm thick potassium bromide discs were pressed from spectroscopic grade KBr (Aldrich). A drop of the sample to be analysed was sandwiched between two KBr discs and mounted on the heating stage. (A background spectrum of the discs having been acquired first). The sample was heated rapidly to 75°C and data acquisition begun once the temperature had been reached. Spectra (an average over 4 scans) were acquired at a time interval of 20 minutes, with a resolution of 1 cm^{-1} over a range of 5000-4000 cm^{-1} .

Time-series data was analysed using Omnic ESP software (Nicolet Instrument Corp). Extent of reaction, p , was determined using equation 2.5. Where $A_{e,0}$ and $A_{r,0}$ are the initial areas of the epoxide and reference peaks respectively and $A_{e,t}$ and $A_{r,t}$ are the corresponding areas at time t .

$$p_t = 1 - \left[\frac{A_{e,t} A_{r,0}}{A_{e,0} A_{r,t}} \right] \quad (2.5)$$

2.2.5 Differential Scanning Calorimetry (DSC)

DSC can be used to observe changes in the thermal properties of a material, such as the change in heat capacity which accompanies a polymer's glass transition and exothermic or endothermic processes such as crystallization and melting.

The power-compensated DSC apparatus consists of two small sample chambers, each with its own heating element. One of these chambers will contain the sample, usually sealed into a small pan. The other chamber contains a reference, such as a sealed empty pan.

The chambers are heated or cooled at a controlled rate. The control system of the instrument alters the power to each heater so that the temperatures of the two chambers do not diverge from each other. If an endothermic event, such as melting, occurs in the sample then it will be necessary to supply additional power to the sample heater in order to maintain its temperature. Likewise, during an endothermic event, such as crystallization, power input to the sample heater can be reduced (or power to the reference heater increased). Thus, if the difference in power applied to the heaters is plotted against temperature, endotherms and exotherms can be observed as peaks and troughs in the plot.

In the absence of thermal transitions, the slope of the plot is related to the heat capacity of the sample. Events such as the glass transition are accompanied by a change in the heat capacity, which appears as a 'step' in the DSC plot.

Experiments were carried out using a Perkin-Elmer DSC-7 system equipped with a CCA-5 controlled cooling system for experiments at sub-ambient temperature. The equipment was calibrated using Zn and Sn reference samples. 10-20mg of sample was weighed into an aluminium sample pan and sealed. The reference pan was empty. Heating and cooling ramps were performed at 20°C / min. All samples were run at least twice with a five minute hold at high temperature after the first run to eliminate any thermal history.

2.2.6 Small Angle X-Ray Scattering (SAXS)

X-ray scattering techniques can provide structural information on length scales from the positions of individual atoms in crystals to structures of a hundred nanometres or so in size, given the correct experimental setup. Since scattering angle is inversely related to feature size, scattering at small angles ($<3^\circ$) is useful for probing features in the nanometre range.

Extensive details on SAXS theory and applications are available elsewhere[93, 94]. The detailed application of small angle scattering to block copolymer systems has recently been reviewed by Hamley and Castelletto[95].

Contrast in X-Ray scattering occurs due to periodic fluctuations in electron density. A totally homogenous medium will show no scattering. The electric field of an incident beam of radiation will interact with the electric field (electrons and protons) of a scattering centre. Energy is absorbed from the incident beam during polarization and then re-emitted as relaxation takes place. Whereas the incident beam is strongly directed, scattered radiation is emitted over all available directions. In Figure 2.8, we imagine the radiation emitted from two scattering centres on different planes of a periodic lattice.

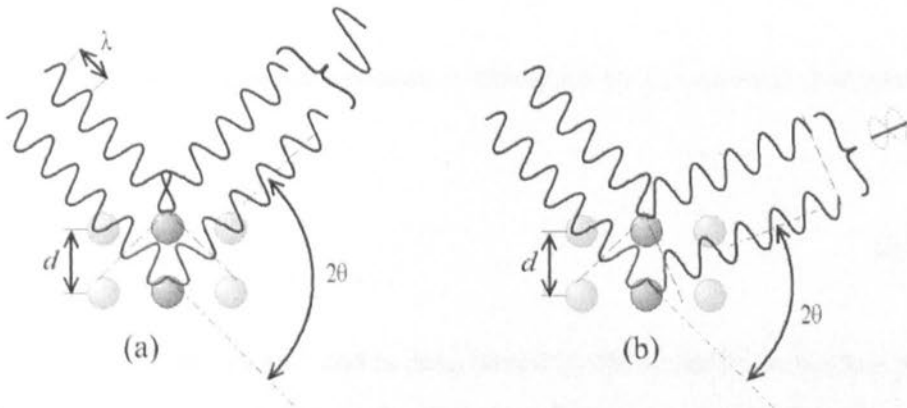


Figure 2.8 – Bragg diffraction in a regular lattice. The incident beam is coming from the left. The scattered beam depicted in (a) interferes constructively and will produce a Bragg peak. In (b) radiation is scattered so that destructive interference occurs - no signal will reach the detector at this angle. Adapted from image by Christophe Dang Ngoc Chan [96].

At some angles the scattered radiation from the different centres will be in phase and will interfere constructively – this radiation will reach the detector and appear in the scattering pattern. At other angles, the radiation will be out of phase, destructive interference will occur and no signal will be detected. The relationship between the lattice spacing and the positions of observed scattering maxima is given by Bragg's Law:

$$n\lambda = 2d \sin \theta \quad (2.6)$$

Where λ is the wavelength of the incident radiation, d is the spacing between planes of the lattice (this quantity is often referred to as 'd-spacing'), θ is half of the angle between the incident and scattered radiation and n is an integer.

Small angle scattering data are usually presented with the scattering angle given in terms of the 'scattering vector', q :

$$q = \frac{4\pi \sin \theta}{\lambda} \quad (2.7)$$

In this form, data acquired using radiation of different wavelengths can still be directly compared.

The complete scattering intensity pattern is described by a combination of two factors:

$$I(q) = S(q)P(q)N\langle\eta^2\rangle \quad (2.8)$$

Where $P(q)$ is the 'form factor' and is determined by the shape of individual particles (such as spherical micelles); $S(q)$ is the 'structure factor' and is determined by long range order such as packing of micelles onto a lattice; N is the number of scattering centres and η is the scattering contrast.

Unfortunately, it is not possible to determine a real space structure directly from a scattering pattern with no additional knowledge of the system. This is because only the intensity of the scattering pattern is known, not its amplitude. Thus one cannot extract information about the phase of the scattered radiation and cannot extract a complete, 3-dimensional, picture of the sample. In any event, even aligned structures observed in SAS may only show periodicity over short distances. Averaging over all orientations of domains within the scattering volume - that part of the sample which is both illuminated by the incident beam and observed by the detector - may mean that only a single dimension of information is available. Therefore, if a complete analysis of the SAXS pattern is desired, one must predict a possible 3d structure, derive a model and fit the data to it. The data may well provide a good fit to more than one model, so information from other techniques is often required to confirm the validity of any new model.

Models for a number of commonly occurring situations have been developed and are described in the literature[95]. For example the form factor describing a sphere is given by Equation (2.9) and a graphical example given in Figure 2.9:

$$P(q) = \left\{ \frac{3}{(qR)^3} [\sin(qR) - qR \cos(qR)] \right\}^2 \quad (2.9)$$

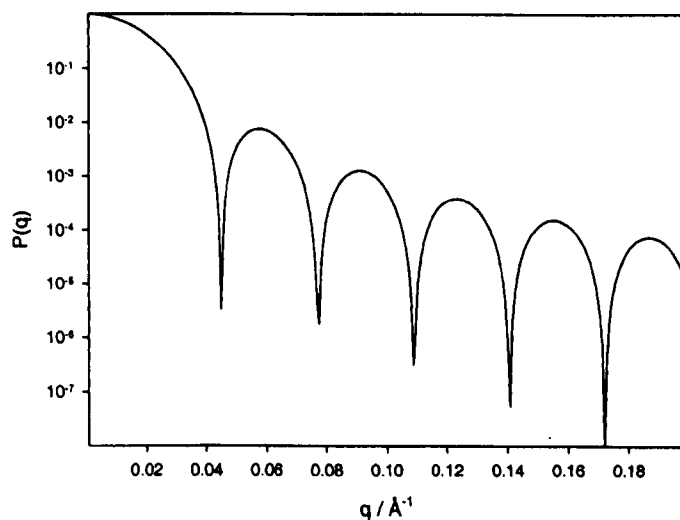


Figure 2.9 – Predicted form factor for a sphere of radius 10nm

Fortunately, it is still possible to extract useful information from a SAXS pattern without additional modelling. One common method for determining block copolymer morphology with SAXS is to compare the positions of the higher order Bragg peaks to that of the first order peak. The position of the first order peak is denoted as q^* . A list of values of q/q^* for known morphologies is presented in Table 2.2.

By combining equations (2.6) and (2.7), we can use the position of the q^* peak to determine the d-spacing:

$$d = \frac{2\pi}{q^*} \quad (2.10)$$

Structure	q/q^*
Lam	1, 2, 3, 4, 5, 6,...
Hex	1, $\sqrt{3}$, $\sqrt{4}$, $\sqrt{7}$, $\sqrt{9}$, $\sqrt{12}$,...
BCC	1, $\sqrt{2}$, $\sqrt{3}$, $\sqrt{4}$, $\sqrt{5}$, $\sqrt{6}$,...
FCC	1, $\sqrt{4/3}$, $\sqrt{8/3}$, $\sqrt{11/3}$, $\sqrt{12/3}$, $\sqrt{16/3}$,...
Gyr	1, $\sqrt{4/3}$, $\sqrt{7/3}$, $\sqrt{8/3}$, $\sqrt{10/3}$, $\sqrt{11/3}$,...

Table 2.2 – Peak positions of Bragg peaks for some known block copolymer morphologies. Accompanying figure from Ref [95].

In strongly ordered samples, several higher order peaks may be seen. As the sample becomes less well ordered, high order peaks will become less visible and the peaks will become more broad. Notice the difference between the sharp, strong ordered peaks and the broad, weaker disordered peak in the figure in Table 2.2.

NanoStar Data

The bulk of the SAXS data presented herein was collected on a NanoStar laboratory scale SAXS instrument (Bruker AXS). The system consists of a copper based sealed X-Ray tube coupled to a multilayered Goebel mirror which acts as a monochromator as well as parallelizing the beam. This isolates a beam of Cu-K α radiation with a wavelength of 1.54Å. All flight tubes are kept under vacuum. A 750 μ m pinhole at 270mm from the source eliminates most of the divergence. The second, beam defining, pinhole is at 400mm from the source, diameter 400 μ m. A third pinhole just before the sample chamber eliminates scattering from the previous pinhole. The sample is mounted on a motorised translation stage in an evacuable chamber. After passing through the sample, the scattered beam enters a second flight tube leading to the HiStar 1024 \times 1024 pixel area detector. The system is equipped with a semi-transparent beamstop. Data intensity can be normalised against the integral of the direct beam signal, allowing data taken at different times to be compared.

The q-axis was initially calibrated using silver behenate as a reference. Typically, scans were collected for two hours, corrected for detector response and a background subtracted where necessary. Data not showing orientation was integrated using Bruker SAXS software to produce 1d plots from the 2d data.

The Daresbury SRS

X-Rays are weakly scattered. Because laboratory X-Ray equipment cannot produce a collimated beam at high flux, data must be collected over an extended period of time to obtain an acceptable signal-to-noise ratio. Some samples simply do not scatter sufficiently strongly to be observed on laboratory scale instruments.

In the Synchrotron Radiation Source (SRS) electrons are accelerated then injected into a 'storage ring'. In the storage ring, radiofrequency fields are used further accelerate the electrons until they are moving at close to the speed of light. The same fields are then used to maintain the speed of the electrons and electromagnets are used to keep them moving in a circular path. As their motion is forced to deviate from a linear path, electrons travelling at relativistic speeds emit 'synchrotron radiation'[97]. This is high intensity broadband radiation which includes components in the X-Ray region. If a tube is set on the correct tangent to the ring, very bright, collimated light of X-Ray wavelengths will be emitted into it. This light can be monochromated and passed to a sample station in the user accessible 'hutch'.

Synchrotron radiation experiments were performed on station 6.2 at the Daresbury SRS. The technical details of this station are described in depth elsewhere [98-100]. The camera length was set at 3.5m the wavelength was set at 1.40Å. The detector system was a 1-dimensional RAPID2 detector[101] with 1024 pixels. Calibration of the q-axis was performed using wet rat tail collagen. Frames were collected for 30 seconds. Data analysis was performed using standard techniques with the CCP13 software suite.

2.2.7 Small Angle Light Scattering (SALS)

The theoretical basis of SALS is similar to that for SAXS. The major differences the longer wavelength of visible light - meaning that larger structures are observed – and the fact that contrast in SALS occurs due to differences in refractive index rather than electron density. Light scattering has many applications which are detailed elsewhere [94]. In the current work, we are concerned only with Bragg Law type scattering (Equation 2.6)

The SALS system was constructed by Yoshiyuki Ishii and is described in full elsewhere [102]. Briefly, the beam is emitted from a 20mW He-Ne laser operating at 633nm. The beam is collimated by a 100µm pinhole and scattering is removed by an

adjustable iris diaphragm. The beam then passes into the sample stage, a Linkam THMS-600, which has a hole for passage of the beam and can provide programmable controlled heating and cooling. The beam is scattered onto a flashed opal diffuser, with a small central opaque beamstop to prevent the direct beam overloading the detector. An image of the pattern as projected onto the diffuser is captured by a Princeton Instruments SITe 512×512 pixel CCD detector fitted with a 50mm $f/1.8$ lens. The distance between the stage and the diffuser can easily be altered to change the range of detection. Diffraction gratings with line spacings of $5\mu\text{m}$ and $1.667\mu\text{m}$ were used to calibrate the d-spacing axis. After data capture with the manufacturer's software, analysis was performed using the Fit-2D package originally developed for analysis of data from the ESRF synchrotron light source[103, 104].

2.2.8 Mechanical Testing

2.2.8.1 Fracture toughness testing

Fracture toughness testing was carried out using a method derived from ASTM D5045-99[105]. A schematic of the equipment used is given in Figure 2.10. The testing machine was an EnduraTEC ELF3200 from Bose-Electroforce operating in three-point bend configuration. Samples were prepared as described above and finished using abrasive paper so that the sides were flat and parallel. Samples had approximate length (l) of 25mm, width (W) of 6mm and thickness (B) of 3mm. A pre-crack was produced by first cutting a wide notch of length approximately 1mm into the edge of the bar using a hacksaw, then using a razor blade to extend a fine notch into the sample. The total length from the edge of the sample to the tip of the crack is defined as the crack length (a).

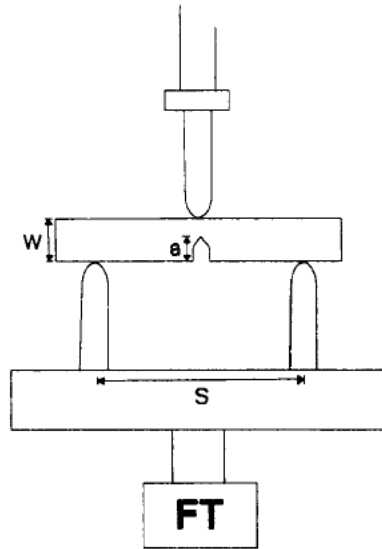


Figure 2.10 – Schematic diagram of the 3-point bend apparatus used in fracture toughness and flexural strength tests. *FT* is the force transducer; *S* is the span between the centres of the supports; The sample has width *W*, thickness *B* (into the plane of the paper – not shown) and, in the case of fracture toughness samples an initial crack of length *a*.

The sample was placed onto supports, separated by a span (*S*) of around 20mm, as shown. *S*, *W* & *B* were measured for each sample using Vernier callipers with a resolution of 0.01mm. The sample was brought into contact with the upper ‘nose’, and then the nose was brought down at a crosshead rate of 0.01mm / s. The transmitted force was measured by a force transducer with maximum load 450N. The force-displacement curve was recorded by a computerised data acquisition system. After the sample had broken, the crack length (*a*) was measured using optical microscopy.

For each sample the critical stress intensity factor, K_{Ic} , was calculated using:

$$K_{Ic} = \left(\frac{P_Q}{B\sqrt{W}} \right) f(x) \quad (2.11)$$

Where P_Q is the load at breaking and $f(x)$ is a factor which accounts for differences in the initial crack length. It can be calculated using the equation derived by Strawley[106]:

$$f(x) = 3 \left(\frac{S}{W} \right) \sqrt{x} \frac{[1.99 - x(1-x)(2.15 - 3.93x + 2.7x^2)]}{(1+2x)(1-x)^{3/2}} \quad (2.12)$$

Where $x = a / W$.

2.2.8.2 Flexural strength testing

Flexural strength tests based on ASTM D790-99[107] were performed using the same apparatus as described in section 2.2.8.1 above. The sample preparation was similar, but no notch or pre-crack was cut. Samples were placed on the apparatus such that the face, rather than the edge, of the block was in contact with the supports (i.e. rotated 90° around the long axis relative to the fracture toughness method).

Again, the nose was lowered into the sample at a rate of 0.01mm / s and the force-displacement curve was recorded.

The flexural stress (σ_f), that is the maximum stress in the outer surface of the test specimen, can be calculated for any point on the force-displacement curve using:

$$\sigma_f = \frac{3PS}{2WB^2} \quad (2.13)$$

Where P is the load and S , W and B are the span, width and thickness of the sample as before. The modulus of elasticity, that is the ratio of stress to strain within the elastic limit can be calculated by drawing a tangent to the steepest initial straight line portion of the load-displacement curve then using:

$$E_B = \frac{S^3 m}{4WB^3} \quad (2.14)$$

Where m is the gradient of the tangent.

2.2.8.3 Dynamic mechanical analysis (DMA)

If a force is applied to a viscoelastic material, then the material will undergo deformation. It is usual to express the applied force as a stress, $\sigma = F/A$, where F is the applied force and A is the area over which it acts. The deformation is expressed as a strain, $\varepsilon = \delta\ell / \ell$, where ℓ is the undeformed length and $\delta\ell$ is the magnitude of the deformation.

If a sinusoidal stress of sufficiently small amplitude is applied to a viscoelastic material then the strain on the material will also follow a sinusoidal pattern. However, the strain curve will lag behind the stress imposed by some phase angle, δ .

By measuring the amplitudes of the stress and strain and the phase angle, it is possible to determine a complex tensile modulus, E^* :

$$E^* = E' + iE'' \quad (2.15)$$

E' is the (tensile) storage modulus and is related to the in-phase component of the response and E'' is the (tensile) loss modulus and is related to the out-of-phase component of the response.

Conceptually, the storage modulus comes from the behaviour of the elastic part of the sample within which energy is stored. The loss modulus describes the behaviour of the viscous part of the sample which dissipates energy.

The properties E' , E'' and δ together describe the stiffness and damping properties of a material.

Experiments were carried out on a VA2000 Viscoanalyser from Metravib RDS. Samples were prepared as previously described and fixed into the machine using mechanical clamps. The sample was heated to 40°C and measurements taken over a range of frequencies from 0.1-100 Hz. A strain amplitude of 0.03% was used, having previously determined that this was within the linear response region for the material.

2.2.8.4 Gel-point determination

In the same way as application of a sinusoidal tensile load to viscoelastic solids is used to measure their tensile modulus above, so the application of a sinusoidal shear stress can be used to determine the shear modulus of viscoelastic liquids. As for the tensile case, the complex shear modulus G^* is composed of the shear storage modulus G' and the shear loss modulus G'' .

As an epoxy system goes from a molecular mixture to cross-linked solid, the rheological response will change dramatically. Initially, the mixture is a free flowing liquid and both moduli are low in magnitude. As reaction occurs, the liquid will become more viscous, thus the loss modulus will increase as more of the applied energy is dissipated. The magnitude of the storage modulus depends on the storage of energy by reversible deformation of a network structure. Thus it remains low until sufficiently large network structures have formed. As the network increases in size, the storage modulus also increases. Eventually the storage and loss moduli will cross, this is the gel point[108].

Experiments were performed on a Rheometrics RDA-II Dynamic Analyzer. Disposable parallel plates of diameter 40mm were machined from aluminium. Freshly prepared uncured epoxy / block copolymer mixture was deposited onto the lower plate and the upper plate was brought down until a gap size of approx 1mm was obtained. The sample was heated to 75°C and measurements were recorded every minute until sufficient cross-linking had occurred to prevent oscillation of the plates. The plates were set to oscillate at a frequency of 1rad / s with 0.2% strain amplitude.

3 Results and Discussion

3.1 Preliminary experiments

3.1.1 BADGE-PBO Cloud Point Curve

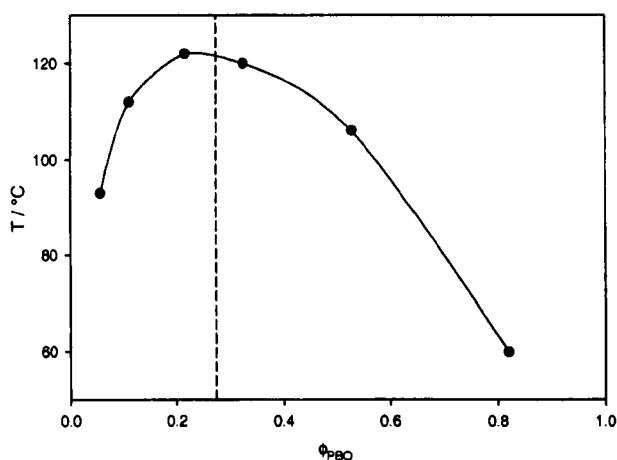


Figure 3.1 – The cloud point curve of PBO ($M_n = 2000 \text{ g.mol}^{-1}$) in BADGE. The dashed line indicates the value of ϕ_c calculated from Flory-Huggins theory.

The cloud point curve for mixtures of poly(1,2-butylene oxide) (PBO) and BADGE was determined using optical microscopy. PBO of $M_n \approx 2000 \text{ g.mol}^{-1}$ (Aldrich) was thoroughly mixed with BADGE at various concentrations. The molecular weight of the PBO sample corresponds to a degree of polymerization, $N \approx 28$. In each case, two initially transparent liquids produced a white, opaque, mixture. A drop of each mixture was pressed between two glass cover slips and heated to 150°C using a Linkam THMS-600 microscope hot stage. At this temperature, all mixtures were transparent and appeared homogenous when viewed under the microscope. Each sample was then cooled at a controlled rate of 2°C per minute; the cloud point was recorded as the temperature at which phase separation (in the form of spherical nuclei) was first observed.

From the results presented in Figure 3.1 It can clearly be seen that the PBO-BADGE system exhibits UCST type behaviour.

The location of the critical composition, ϕ_c , and the value of the Flory-Huggins parameter at that point, can be calculated using the following equations, derived from Flory-Huggins theory[109]:

$$\phi_c = \frac{1}{1 + \left(\frac{N_A v_A}{N_B v_B} \right)^{1/2}} \quad (3.1)$$

$$\chi_c = \frac{1}{2N_A} \left[1 + \left(\frac{N_A v_A}{N_B v_B} \right)^{1/2} \right]^2 \quad (3.2)$$

Here, N_A and N_B are the degrees of polymerization of the two components, and v_A and v_B are the volumes occupied by the respective monomers. The bulk densities of PBO and BADGE at 25°C were measured by pyknometry and found to be 0.97g.cm⁻³ and 1.16 g.cm⁻³ respectively. Thus the monomer volumes can be calculated to be $v_{PBO} = 123 \text{ \AA}^3$ and $v_{BADGE} = 488 \text{ \AA}^3$.

Substitution into equations 3.1 and 3.2 leads to a predicted $\phi_c = 0.274$, which can be seen to be in good agreement with the maximum in the cloud point curve. The calculated value of $\chi_c = 0.240$.

The behaviour of poly(ethylene oxide) (PEO) in BADGE systems cured with aromatic amines has been investigated by Sixun *et al.*[110]. The system was found to be homogenous at all concentrations and to remain mixed throughout cure.

3.1.2 Determination of the gel point

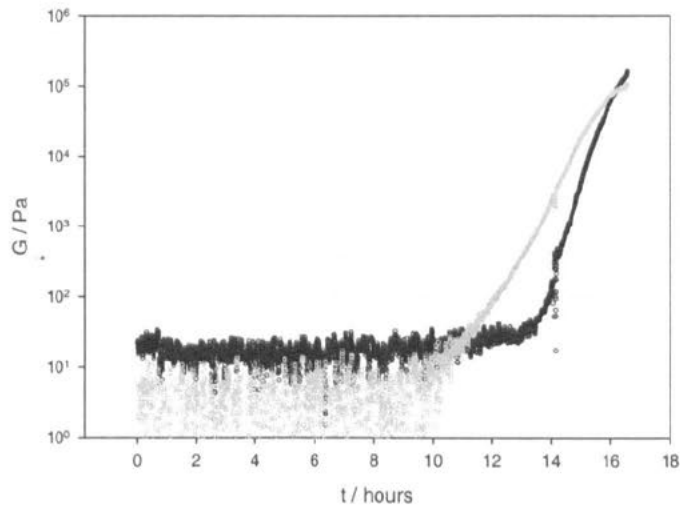


Figure 3.2 – Storage modulus, G' , (black circles) and loss modulus, G'' , (grey circles) during cure of BADGE + DETDA system at 75°C.

The gel point of the unmodified BADGE + DETDA system was determined by rheometry as described earlier. The crossover of G' and G'' can be seen in Figure 3.2 to occur after 16.2 hours. Correlation with FTIR data obtained for the unmodified system, given below, indicates an extent of reaction at the gel point of approximately 0.53. This is in good agreement with the theoretical value of 0.58 determined using the Flory-Stockmayer theory.

3.1.3 Bridging behaviour in BEB triblocks

Bridging between micelles in solution has been observed in aqueous solutions of BEB triblocks with relatively long hydrophilic blocks and relatively short hydrophobic blocks [111-114]. If this behaviour can be replicated in epoxy systems, it might serve to improve the mechanical properties of the cured resin.

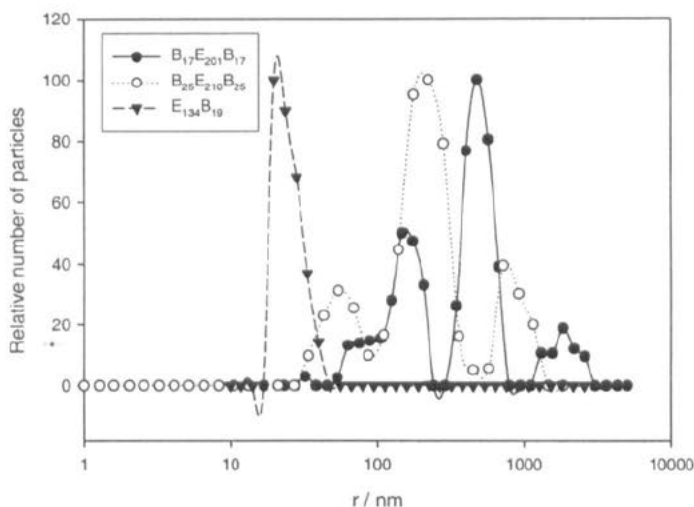


Figure 3.3 – Particle size distributions in 5wt% aqueous solutions of some block copolymers.

To confirm that some of the BEB triblocks used here are capable of bridging behaviour, the particle size distribution of 5wt% aqueous solutions was measured. Solutions were stirred for 4 weeks (dissolution of BEB triblocks in water is a slow process). The particle size distribution was determined using dynamic light scattering. If a beam of light is shone into a solution containing small particles, the particles will scatter some of that light. By measuring the intensity of light scattered at right-angles to the incident beam over time, we can monitor fluctuations caused by Brownian motion of the particles. Since larger particles move more slowly than smaller ones, an estimate of the size distribution can be extracted from the data[115].

Measurements were performed using a Brookhaven BI-9000AT light scattering system equipped with a laser of wavelength 532nm and output power 125mW. Intensity average particle diameters were determined by using a non-negative least squares algorithm to fit the data to the Stokes-Einstein equation for near monodisperse, non-interacting hard spheres.

The resulting data is presented in Figure 3.3. The diblock $E_{136}B_{18}$ was included as a non-bridging control sample. It can clearly be seen that the BEB triblocks form large structures where the simple diblock does not, suggesting that bridging does indeed occur.

3.2 Observations during sample curing

3.2.1 Reaction Kinetics

Reaction kinetics of the system modified with $E_{115}B_{102}$ were investigated at the chosen curing temperature of 75°C using FTIR spectroscopy. The extent of reaction as a function of time was determined using the procedure described earlier and the results are presented in Figure 3.4.

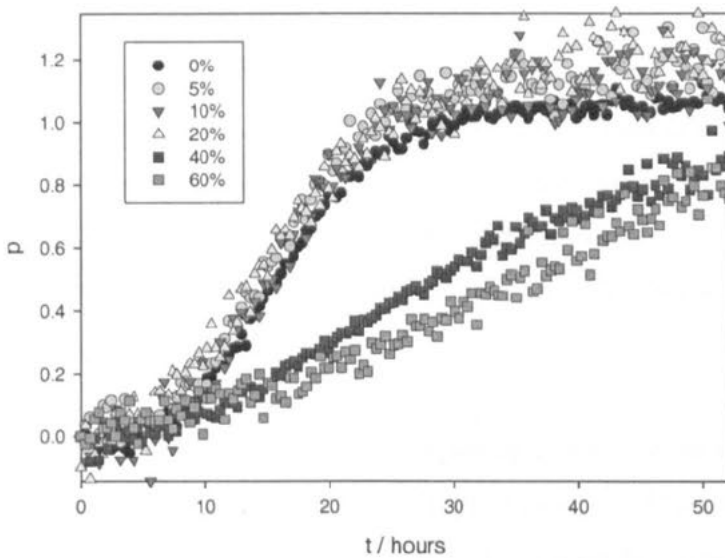


Figure 3.4 – Extent of reaction, p , over time as determined by FTIR spectroscopy for various concentrations of $E_{115}B_{102}$ in BADGE + DETDA. Concentrations are given in weight percent of modifier.

Larrañaga *et al.* have examined in detail the cure kinetics of MDA cured BADGE modified with PEO-PPO-PEO triblocks[45, 47]. They found that significant retardation occurs with the addition of modifier, even at relatively low concentration (10wt%). They attributed this to a combination of effects, the first being the dilution of the epoxy system by block copolymer. Secondly, they suggest that hydrogen bonding occurs from the hydroxyl groups on the epoxy backbone to oxygen atoms in the block copolymer. This interaction leads to reduced hydrogen bonding between the hydroxyl groups and oxygen atoms in unopened epoxide rings, thus interfering

with the autocatalytic step of the reaction. They proposed a model to account for these effects and successfully fitted it to data acquired from isothermal DSC experiments.

As can be seen, no such retardation was observed at low concentrations in this system. This is unlikely to be due to the substitution of PPO with PBO since they are chemically extremely similar. It may be due to differences in cure mechanisms between DETDA and MDA cured systems, but again, this is unlikely as they are chemically similar and Ishii and Ryan have shown that the BADGE + DETDA system fits the autocatalytic model[16]. A similar plot is shown in Figure 3.5, a smoothed set of p versus t data from FTIR measurements on the unmodified system was used to generate the data. The plot is linear up to the gel point in agreement with the autocatalytic model. The data from the FTIR measurements is in agreement with that of Ishii so there seems to be little reason to doubt the measurement technique. A final possible reason for the disagreement is that the low temperature and cure rate in this study may mask any differences in cure mechanism at lower modifier concentrations.

In an attempt to clarify this result, a control experiment was performed wherein the cure of an epoxy system modified with 10wt% PEO (Aldrich, $M_n = 4600\text{g}\cdot\text{mol}^{-1}$) was monitored by FTIR. Results are shown in Figure 3.6. These data suggest that the rate of reaction is indeed reduced in the presence of PEO homopolymer but that this effect is not observed in a micelle forming system.

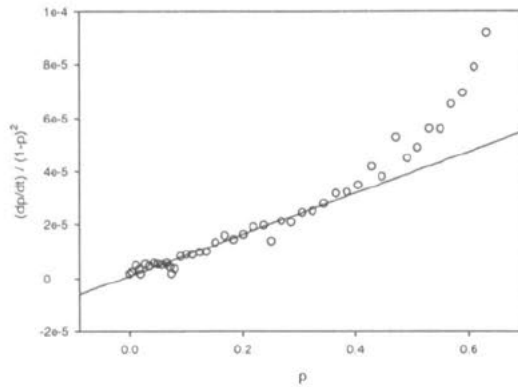


Figure 3.5 – Fit demonstrating the agreement between data acquired by FTIR for the unmodified BADGE + DETDA system and the autocatalytic model. The data shown for the unmodified system in Figure 3.4 was smoothed using a moving mean with a window size of nine data points and the differential determined numerically.

One possible explanation for the observed behaviour would be as follows. In the PEO modified epoxy, and in copolymer modified systems where the modifier remains soluble at low concentration, the PEO is distributed homogeneously throughout the matrix. Therefore its interaction with the resin will be maximized. In a micelle forming system, the PEO is localized in the coronae of the micelles. Thus there will be significant volumes of resin which have no interaction with PEO. Even where micelles are present, geometrical constraints imposed by their spherical nature will limit interaction between PEO and the matrix. Thus, the degree of retardation caused by the PEO will be reduced.

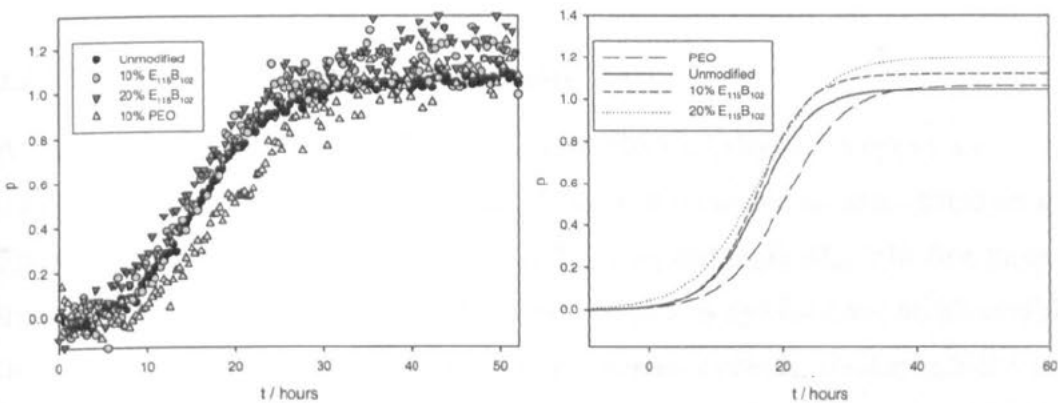


Figure 3.6 – Extent of reaction profiles for unmodified epoxy resin, resin modified with 10wt% PEO and resin modified with a micelle forming block-copolymer. Three parameter sigmoidal functions have been fitted to the raw data (left) and are presented here (right) to simplify visualization of trends.

Returning to the data in Figure 3.4, the dramatic decrease in reaction rate between 20wt% and 40wt% might be explained by the transition of the system from a 'solution' of micelles in epoxy to an ordered gel like system where the resin is acting as a swelling agent. In this later system, where there is significant interpenetration of resin and PEO, the increased viscosity and steric hindrance caused by interpenetration would significantly decrease the reaction rate.

It should be noted that, at the cure temperature at which their kinetics experiments were conducted, two of the three triblock copolymers investigated by Larrañaga *et al.* undergo macrophase separation[44, 46]. The third triblock copolymer appears to show microphase separation in AFM phase images, but the precise nature of any microphase separated domains has not been determined. In contrast, E₁₁₅B₁₀₂ is known to form micellar structures under the conditions used in this experiment - supporting data are presented later.

The results presented here suggest that cure kinetics in micelle forming systems may be an interesting topic for further research. However, significant optimization of the experimental methodology is required so as to reduce noise and increase the limit of detection such that definitive conclusions may be drawn.

3.2.2 Visual Observations

3.2.2.1 Visual observations in solution

At room temperature, most 5-20% solutions of block copolymer in epoxy are transparent, with no observable differences between them and an unmodified sample. The exceptions are B₃₇E₁₅₀B₃₇, B₄₄E₁₂₇B₄₄, E₁₁₅B₁₀₂ and B₆₅E₇₅B₆₅. The first three of these show varying degrees of turbidity when viewed by eye but have no observable features when viewed under a microscope. In aqueous systems, similar turbidity is normally attributed to flocculation of nanometre size particles to form aggregates which are large enough to scatter visible light. B₆₅E₇₅B₆₅ on the other hand shows macrophase separation from the uncured resin. The sample is completely opaque

when viewed by eye. Examination of a sample pressed between two cover slips by optical microscopy reveals phase separated spherical domains on the order of $10\mu\text{m}$ in size. An optical micrograph is shown in Figure 3.7.

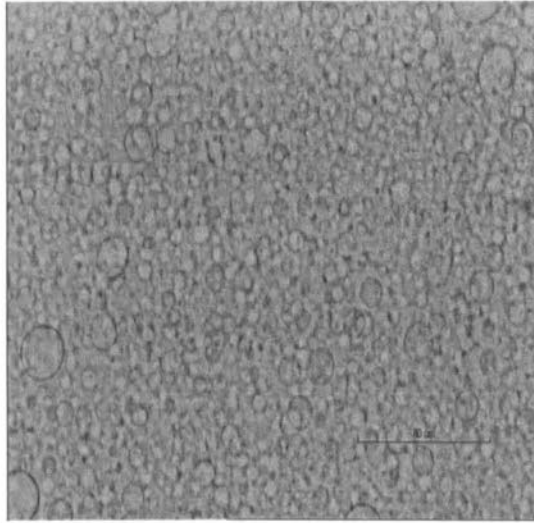


Figure 3.7 – Optical micrograph of solution of $\text{B}_{64}\text{E}_{75}\text{B}_{64}$ in BADGE + DETDA at 25°C prior to cure. Phase separation on the $10\mu\text{m}$ scale can be seen clearly

Solutions are generally free flowing up to around 30wt%; by 40wt% they are more gel like and will only flow at elevated temperatures, if at all. The gel like samples are translucent at room temperature but become transparent above the melting point of PEO, indicating that PEO and epoxy are mixed.

3.2.2.2 Visual observations of the cured samples

After curing, samples were examined by eye for evidence of phase separation. The findings are summarized in Table 3.1. Several samples are cloudy at low concentrations but have no structure visible under the optical microscope. Again, this is believed to be due to the formation of aggregates of a number of nanometre scale particles forming structures that can scatter visible light.

wt% / Polymer	5%	10%	20%	30%	40%	50%	60%
E ₁₁₅ B ₁₀₂	Grey	Grey	White	White	White	Grey	Grey
B ₆₄ E ₇₅ B ₆₄	Black	Black	Grey	X	Grey	X	Grey
B ₄₄ E ₁₂₇ B ₄₄	Black	Black	White	X	White	X	Grey
B ₃₄ E ₉₃ B ₃₄	Grey	Grey	White	White	White	X	Black
B ₃₇ E ₁₅₀ B ₃₇	Grey	Grey	White	X	White	X	Grey
B ₂₀ E ₁₄₁ B ₂₀	White	White	White	White	White	Black	X
B ₂₅ E ₂₁₀ B ₂₅	Grey	Grey	Grey	Grey	White	X	Grey
B ₁₇ E ₂₀₁ B ₁₇	Grey	Grey	Grey	Grey	White	X	Black
E ₄₃ B ₁₀₀ E ₄₃	White	White	White	X	Grey	X	Grey
E ₉₀ B ₈₂ E ₉₀	White	White	White	X	White	X	Black
E ₉₁ B ₅₆ E ₉₁	White	White	White	X	White	X	Grey
E ₁₂₆ B ₅₁ E ₁₂₆	White	White	White	X	White	X	Black

Table 3.1 – A summary of visual observations of cured resins. White boxes represent transparent samples. Black boxes indicate completely opaque samples. Grey boxes indicate turbid (low concentration) or translucent (high concentration) samples. The presence of an X indicates that no sample was produced at that composition.

Low concentration samples of two of the BEB triblocks are completely opaque due to the presence of phase separated domains on the micron scale. In B₆₄E₇₅B₆₄ the phase separated domains observed in solution are also seen to be present in the cured sample. Further examination by polarized optical microscopy (Figure 3.8) shows that each domain appears to be composed of a single spherulite. The spherulites are not observed in the uncured blend and no crystallization is observed in the neat block copolymer at room temperature.

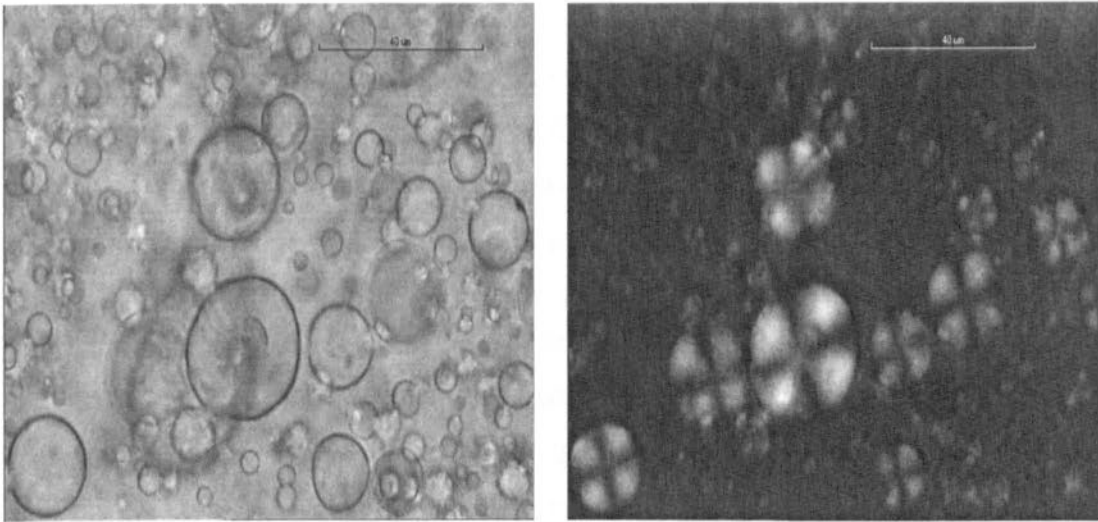


Figure 3.8 – Optical micrographs from a cured sample of 5% $B_{65}E_{75}B_{65}$ in BADGE + DETDA after cooling to 25°C. The left hand image is a simple transmission micrograph. The right hand image is from the same sample between crossed polarizers showing birefringence, presumably from PEO spherulites.

It has been shown that the lack of crystallinity at room temperature in $B_{65}E_{75}B_{65}$ is due to its BCC structure[116]. In microphase separated systems, crystallization can occur in one of two ways. ‘Confined crystallization’ occurs when a block crystallizes without a change in morphology of the system. By contrast in ‘breakout crystallization’, the underlying morphology is destroyed and crystallization proceeds to form a lamellar morphology as described earlier (with the lamellae possibly further ordered into spherulites). The crystallization temperature, T_c , tends to be significantly lower in cases of confined crystallization than in those where breakout occurs. This is because, whereas in breakout crystallization a single nucleation event can initiate a crystallization process which propagates throughout the sample, in confined crystallization, one nucleation event is required per separated domain). It has been shown that, whereas breakout crystallization is initiated by a heterogeneous nucleation process, confined crystallization proceeds in a manner consistent with homogenous nucleation. The shear number density of domains in a typical microphase separated sample ($\sim 10^{17}$ domains / cm^{-3} for a BCC morphology) means that the probability of sufficient impurities being present to heterogeneously nucleate each domain is very negligible. T_c for bulk $B_{65}E_{75}B_{65}$ has been shown to be -21.0 °C compared to values in the region of 10-30 °C in less confined geometries[116].

Confined crystallization is favoured in cases where systems are strongly segregated so that there is a significant energy barrier to the breakout process, which requires the system to pass through a 'mixed' phase as it arranges itself into the crystalline morphology. Also, morphologies where propagation is restricted in all three dimensions, such as BCC, are more likely to display confined crystallization.

Time resolved microscopy during cure of the 5wt% $B_{65}E_{75}B_{65}$ system at 75°C shows that, on heating, the block copolymer dissolves to form a homogenous solution. Phase separation occurs by nucleation and growth with no evidence of crystallization until the gel point is reached, whereupon crystallization, as indicated by the appearance of 'Maltese cross' birefringence patterns, occurs rapidly in all of the macrophase separated domains. As the phase separation progresses, the volume fraction of PBO in the minor phase will increase. Thus any microstructure within the minor phase will progress from spheres of PBO in a PEO/epoxy matrix and is unlikely to reach the stage of confined PEO spheres in a PBO matrix and the system is free to undergo breakout crystallization once the PEO is expelled from the resin. It is interesting that crystallization occurs at such a high temperature, indeed after curing is complete, the sample can be heated to >200°C without loss of birefringence. This may be due to confinement of the crystalline domains by cured epoxy.

Low concentrations of $B_{44}E_{127}B_{44}$ are transparent in solution but become opaque on curing. The optical micrograph of a cured sample presented in Figure 3.9 reveals an interpenetrating network structure on the micron scale. This suggests that reaction induced phase separation has occurred by spinodal decomposition with vitrification taking place prior to coalescence of the domains.

Some samples become translucent, or even opaque, at higher concentrations. In all cases except that of 60% $B_{34}E_{93}B_{34}$, the sample becomes increasingly transparent as it is heated above the melting temperature of PEO. This suggests that the change in optical properties is due to the crystallization of PEO blocks in these samples. The

60% $B_{34}E_{93}B_{34}$ sample does not change appearance on heating, this is attributed to macrophase separation of the block copolymer from the resin.

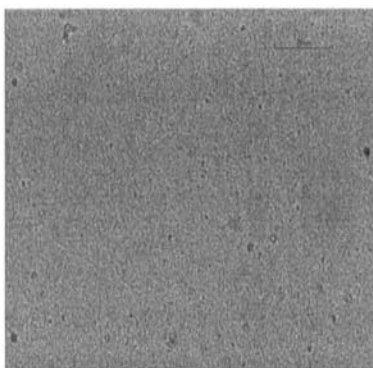


Figure 3.9 – Optical micrograph showing phase separation in a cured sample containing 5% $B_{44}E_{127}B_{44}$. The pattern formed is probably due to reaction induced phase separation by spinodal decomposition.

The mechanical properties of the samples can also be seen to vary as the concentration of modifier is increased. From 5-30% modifier, the cured samples are hard, glassy solids which require the use of a hacksaw to cut. No softening is observed on heating to 75°C. In contrast, above 30wt%, the samples are noticeably softer, as evidenced by the fact that they can be smoothly cut in two with a razor blade. On heating, these samples become increasingly rubbery. This behaviour can be attributed to incomplete curing of the epoxy resin because of dilution and steric hindrance by PEO, which we believe to be intermixed with the resin. Incomplete curing will lead to a lower crosslink density and a more elastic product. Crystallization of the PEO lends some further rigidity to the sample, when the PEO is melted the sample becomes rubbery.

The two BEB samples that show macrophase separation at low concentrations were found to be less mechanically robust than other samples of similar concentration. They exhibited a tendency to crumble when cut.

3.3 Microstructure of Cured Samples

3.3.1 Effect of concentration

Cured samples of epoxy resin containing different block copolymers at a variety of concentrations were studied by small-angle x-ray scattering (SAXS). The results for each system studied are presented below. Unless otherwise stated, all samples in this, and later experiments were cured at 75°C and post-cured at 180°C as described earlier. All SAXS patterns were obtained at room-temperature unless otherwise stated.

3.3.1.1 E₁₁₅B₁₀₂

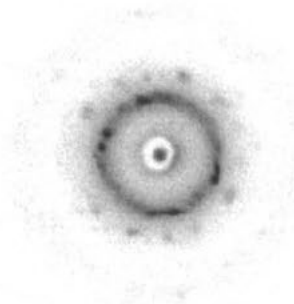
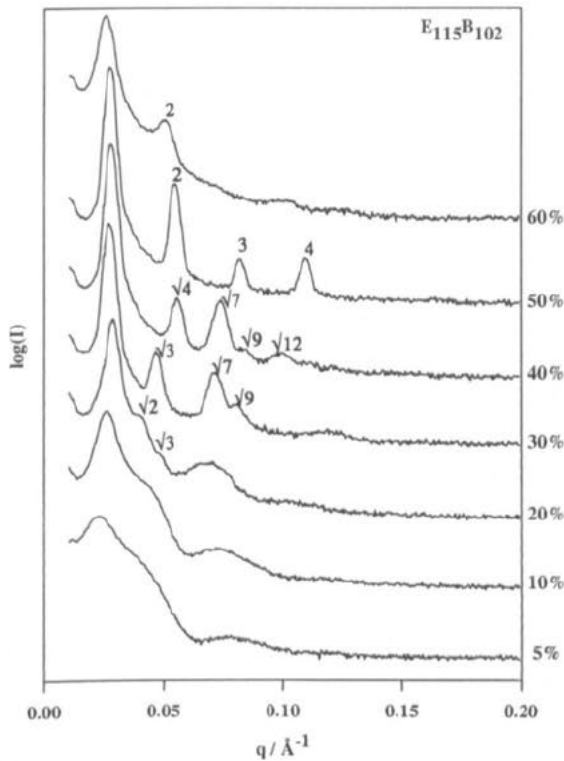


Figure 3.10 – SAXS patterns for cured samples of E₁₁₅B₁₀₂ at various concentrations in epoxy resin. The right hand image shows the two-dimensional scattering pattern from an aligned 20wt% sample – demonstrating reflections from a BCC lattice.

This diblock copolymer was chosen for investigation because its behaviour in aqueous solution has previously been investigated by Battaglia and Ryan [117, 118]. In that work, the polymer was slowly taken up into solution from a film deposited on the inner surface of a vial. SAXS patterns for solutions over a range of concentrations are reproduced in Figure 3.11. The water swells the hydrophilic PEO blocks until the point of maximum swelling, known as the full hydration distance, is reached. Further addition of water after this point causes lamellae to detach from the surface of the swollen gel. Once in solution, the lamellae fold to form vesicles in order to isolate the hydrophobic PBO blocks from the solvent. At higher concentrations (10wt%), these vesicles are seen to pack into a hexagonal structure and, with a further increase in concentration (30wt%), a 'sponge phase' consisting of partially coalesced vesicles. At concentrations of 60% and above, a lamellar gel phase is observed.

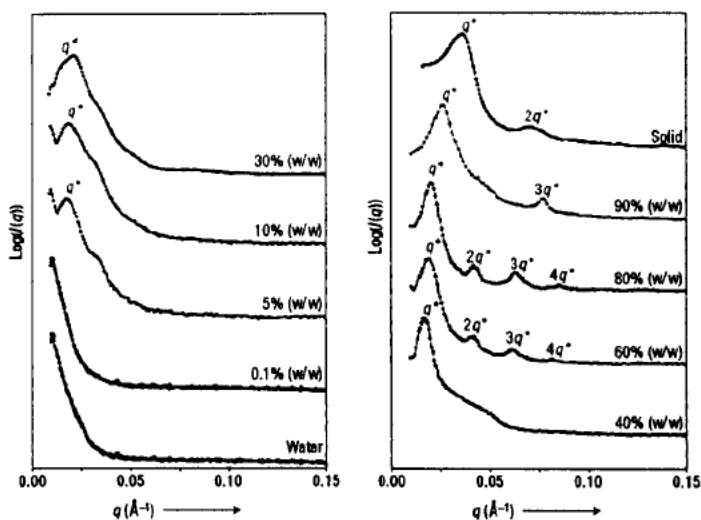


Figure 3.11 – One-dimensional SAXS patterns for various concentrations of $E_{115}B_{102}$ in aqueous solution. Adapted from ref. [118].

Behaviour in the epoxy system is seen to be somewhat different. This may well, at least in part, be due to differences in the method of sample preparation. In the aqueous system, the final concentration is approached by dilution of a locally concentrated domain. The viscosity of epoxy resin necessitates the formation of a dilute solution in a solvent which is good for both resin and modifier and attainment

of the final concentration through removal of the solvent. In order to mimic the aqueous experiment, it would be necessary to find a solvent which was common to epoxy resin and PEO but a non-solvent for PBO.

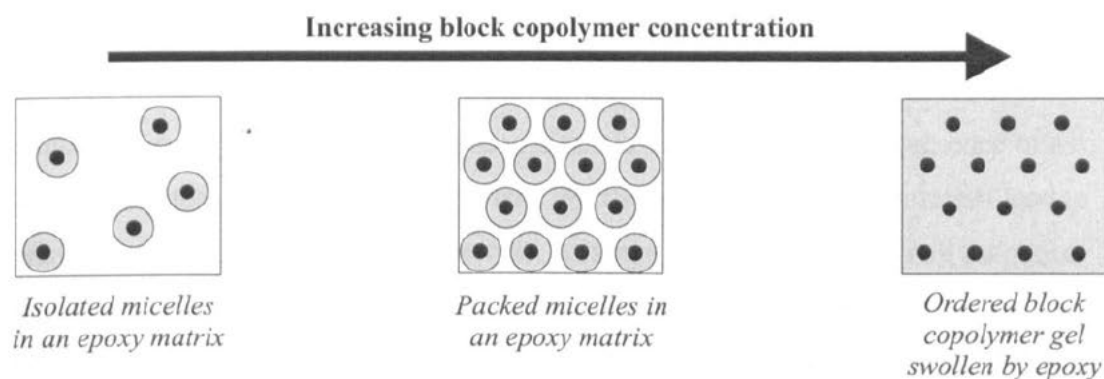


Figure 3.12 – Structure development from dilute micellar solution to swollen gel in an epoxy resin-block copolymer system. The black regions represent epoxy immiscible PBO cores. The white region is epoxy resin containing no block copolymer and the grey regions contain a mixture of epoxy and PEO

Contrast in the SAXS experiments is assumed to arise only from contrast between PBO and its surroundings. Since PEO is miscible with epoxy resin, it is assumed to be contrast matched to the matrix.

In the epoxy based system, the SAXS data and TEM analysis show that interacting micellar structures are formed at 5-10wt%. These data are presented and discussed in detail in Section 3.3.2.

At 20wt% the presence of a body-centred cubic (BCC) structure is indicated by the characteristic $q^* : q^*\sqrt{2} : q^*\sqrt{3}$ peaks in the scattering pattern. The pattern appears to be a convolution of BCC scattering with micellar scattering, suggesting that it derives from packed spherical micelles.

Figure 3.10 shows a two-dimensional scattering pattern obtained after shear-aligning a 20wt% sample. Uncured samples were sandwiched between two mica windows using an M3 washer as a spacer. Oscillatory shear was applied by sliding one piece of mica back and forth whilst keeping the rest of the sample stationary. The sheared

samples were then cured as normal. The SAXS pattern was obtained with the shear gradient axis parallel to the beam and the shear axis aligned vertically. The spots visible in the pattern serve to demonstrate a highly ordered packed structure.

Figure 3.12 shows a possible scheme for development of structure at relatively low concentrations. Somewhere below 5wt% micelles may exist in isolation. As the concentration is increased, they begin to interact, as indicated by the presence of a structure factor peak in the SAXS pattern. Further increases in concentration lead to packing of micelles into a BCC structure. At some point the micelles will merge so that all volume not occupied by the immiscible core will consist of epoxy miscible chains swollen by the resin. This can be considered to be a transition from a solution of micelles in the epoxy matrix to a block copolymer gel with the miscible blocks swollen by the epoxy.

As the concentration of block copolymer is further increased, the degree of swelling of PEO will decrease because there will be less resin per unit mass of PEO. This will lead to a reduction in the degree of curvature at the PEO-PBO interface and, coupled with the need to accommodate a greater volume fraction of epoxy immiscible PBO, will eventually lead to a change in morphology. This is most clearly observed between 20wt% and 30wt%, where a transition from BCC to hexagonally packed cylinders occurs, and between 40wt% and 50wt%, where the transition from a hexagonal to a lamellar morphology (with its characteristic peaks at integral multiples of q^*) is observed.

At 30wt% and 40wt% the patterns are consistent with the $q^* : q^*\sqrt{3} : q^*\sqrt{4} : q^*\sqrt{7}$ pattern expected of a hexagonally packed cylinder morphology. However, at 30wt% the peak expected at $q^*\sqrt{4}$ is absent whilst at 40wt%, the peak expected at $q^*\sqrt{3}$ is not detected. This can be attributed to the presence of minima in the form factor of the cylinders coincident with the expected structure factor peaks. Since the observed intensity is proportional to the product of the structure- and form-factors, this may result in no structure factor peak being observed. Movement of the form-factor minimum from $q^*\sqrt{4}$ to $q^*\sqrt{3}$ was attributed to an increase in the diameter of the

cylinders due to the need to accommodate a greater volume of PBO as the concentration of block copolymer is increased.

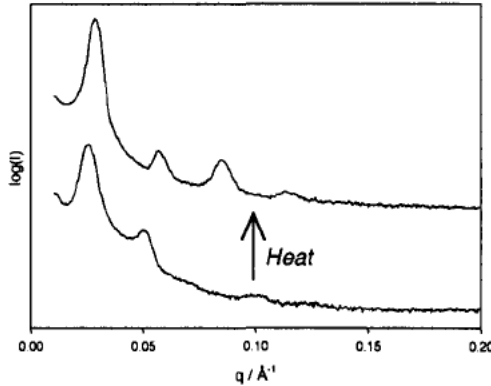


Figure 3.13 – Effect of heating from room temperature to 75°C on the scattering pattern obtained from a 60wt% sample of E₁₁₅B₁₀₂ in cured in epoxy.

The absence of higher order reflections at 60wt% when compared with 50wt% together with an increase in peak breadth indicates a reduction in the degree of long range order. This can be attributed to ‘drying’ of the PEO as there is no longer sufficient epoxy resin present to appreciably swell all of the PEO. On heating the sample to 75°C, well above the melting point of PEO, more reflections become visible (Figure 3.13). Crystallization of unswollen PEO causes a reduction in long range order. However, some of the PEO must still be swollen by the epoxy in order to have been locked into the lamellar morphology – the neat block copolymer shows a hexagonal phase in the melt at this temperature.

The crystallization can be observed using crossed polarizers on an optical microscope as shown in Figure 3.14. A distorted ‘Maltese cross’ structure is observed for the 60wt% sample, indicative of crystallization of the PEO. Note that, unlike the behaviour of B₆₅E₇₅B₆₅ described above, macrophase separation is not observed, the crystallisation occurs whilst maintaining miscibility. The 40wt% sample also shows birefringence, this is attributed to alignment, over macroscopic length scales, of the cylindrical domains within the hexagonal structure. No birefringence is observed in cured samples containing E₁₁₅B₁₀₂ at the other concentrations examined.

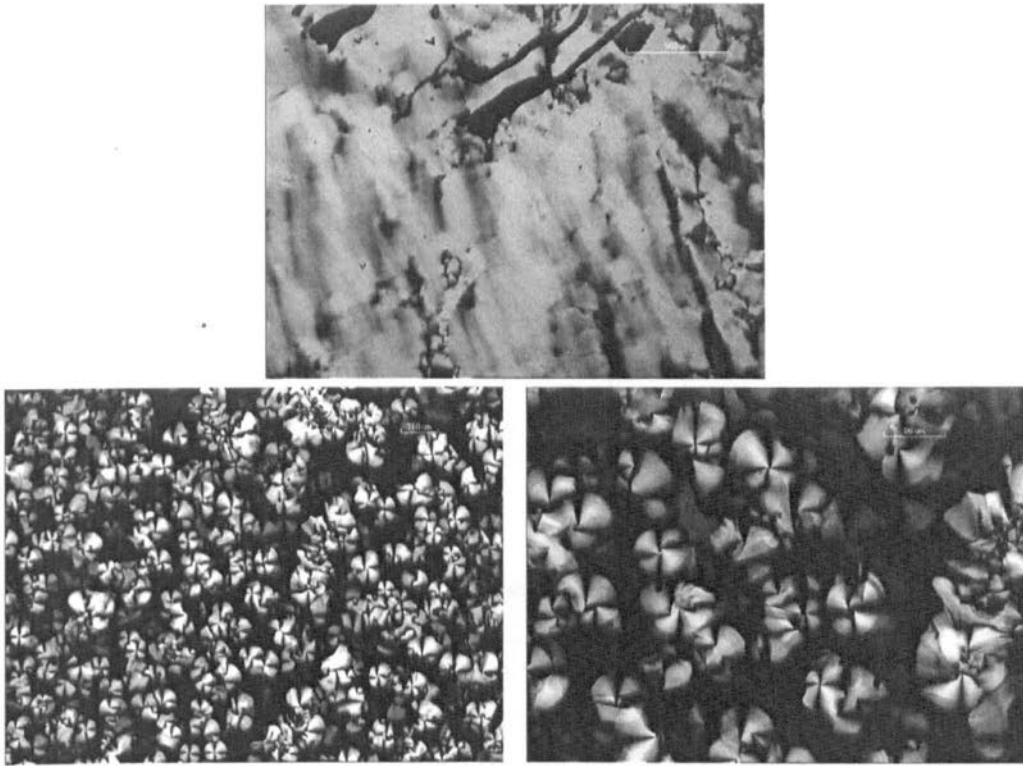


Figure 3.14 – Crossed-polar optical micrographs from thin samples of $E_{115}B_{102}$ in epoxy resin cured between two cover slips. (Top) 40wt% sample showing birefringence. The black areas are voids within the sample. (Bottom) 60wt% sample at two different magnifications showing distorted ‘Maltese cross’ pattern associated with crystallization of PEO.

3.3.1.2 $E_{43}B_{100}E_{43}$

SAXS patterns for a concentration series of $E_{43}B_{100}E_{43}$ in BADGE + DETDA are shown in Figure 3.15. It is clear that, in this case, interacting micellar structures are present up to 20wt%. By 40wt%, the effect of packing and reduced surface curvature has caused the system to adopt a hexagonal structure. The same effects lead to a lamellar morphology being observed by 60wt%. There is a noticeable shift in the q^* peak to higher q , i.e. shorter d-spacing, as the concentration of block copolymer is increased. This is probably due to a reduction in swelling of the PEO blocks as the concentration of resin is reduced. This behaviour is not clearly observed in $E_{115}B_{102}$ above, however, this may simply be due to the resolution of the X-ray detector. The resolution available at a given point on the detector goes as $1/q$ (i.e. the resolution is uniform in reciprocal space). Hence, at low values q , a significant change in d-spacing is required in order to produce a detectable shift in a peak position in

reciprocal space. Since the $E_{115}B_{102}$ system has its principal scattering peak at lower q than that of $E_{43}B_{100}E_{43}$ the change in its d-spacing may not be detectable.

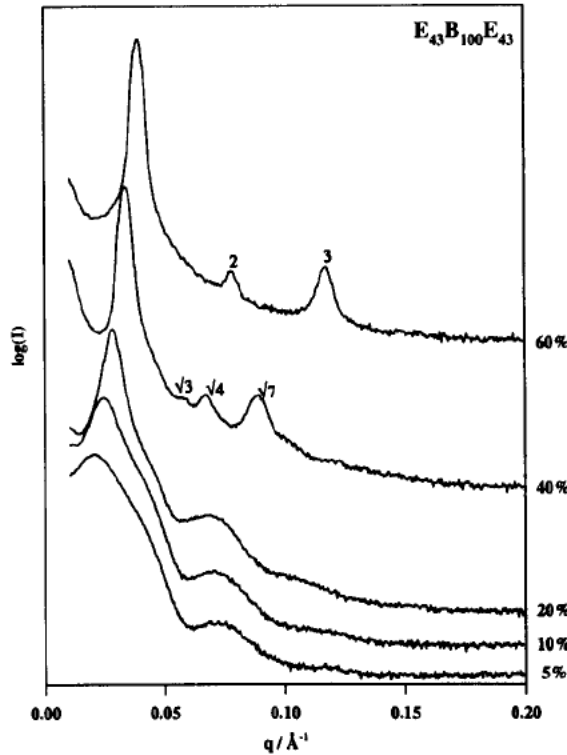


Figure 3.15 – SAXS patterns for various concentrations of $E_{43}B_{100}E_{43}$ cured in epoxy resin.

3.3.1.3 $E_{90}B_{82}E_{90}$

The behaviour of the $E_{90}B_{82}E_{90}$ system, as shown in Figure 3.1, is similar to that observed for the samples above. Again, a transition from micelles to BCC to hexagonally packed cylinders and on to lamellae is observed and again, the q^* peak is observed to move to higher q as the concentration of swelling agent is reduced. Interestingly, crossed-polar optical microscopy of a 60wt% sample reveals large (mm scale) structures, which are assumed to be block-copolymer rich regions. The sample appears transparent to the eye and no features are visible under the microscope without the use of polarizers. An example micrograph is shown in Figure 3.17.

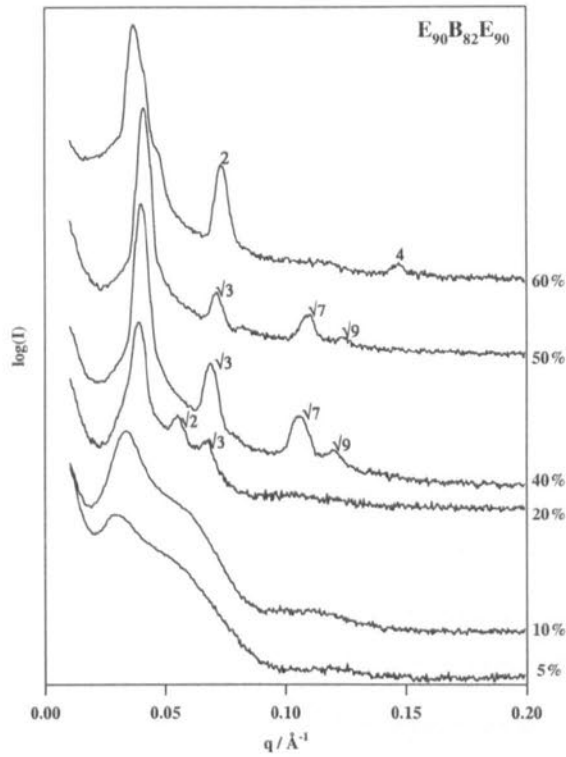


Figure 3.16 – SAXS patterns for a concentration series of $E_{90}B_{82}E_{90}$ in cured BADGE + DETDA.

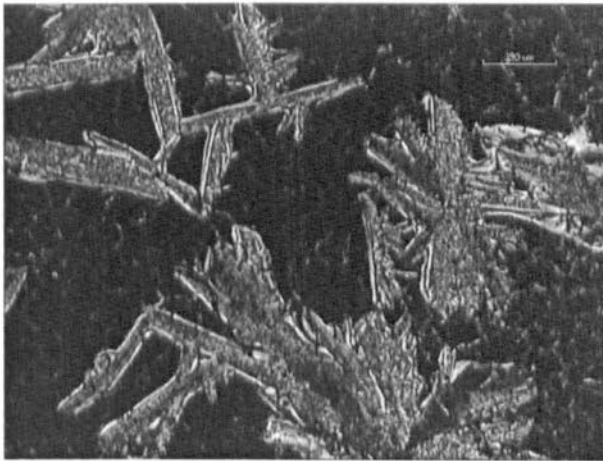


Figure 3.17 – Crossed-polar optical micrograph of cured sample containing 60wt% $E_{90}B_{82}E_{90}$.

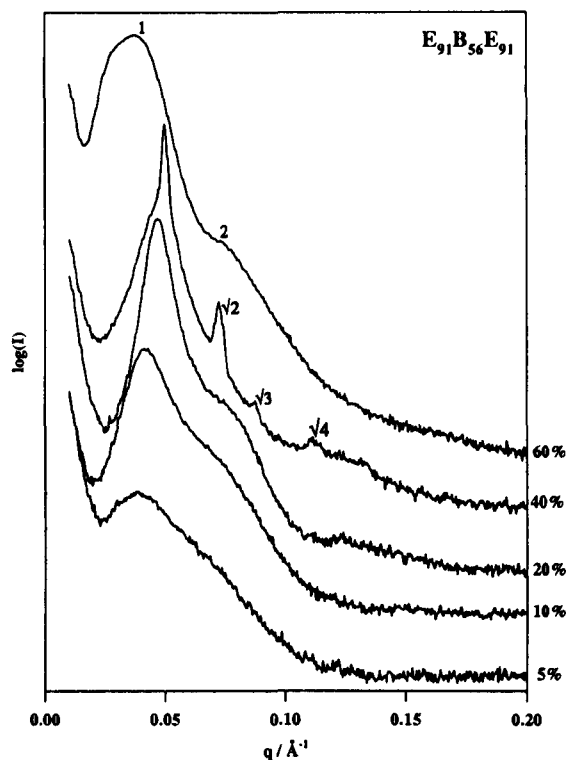
3.3.1.4 E₉₁B₅₆E₉₁

Figure 3.18 - SAXS patterns for a concentration series of E₉₁B₅₆E₉₁ in cured in BADGE + DETDA.

The SAXS patterns for E₉₁B₅₆E₉₁ are far less clear than for other EBE triblock based systems. At 40wt% a BCC structure is clearly formed although the underlying ‘lump’ at low q suggests some semi-crystalline polymer is present in the system, or possibly that loosely ordered micelles and the BCC structure co-exist at this concentration.

Given that a BCC structure is formed at 40%, it is assumed that the patterns at 5-20wt% are due to micellar scattering. The broadening of the signals when compared to other micelle forming systems is thought to be due to increased polydispersity in the size of the micelles (a polydispersity of just 10% in the size of micelles leads to a completely smoothed scattering pattern[7]). This might be due to the comparatively low PBO content of this system ($\phi_E = 0.63$) leading to a reduced tendency to microphase separate from the epoxy. Incomplete microphase separation leads to polydispersity in the separated phases. However, this tendency is not observed with triblock having an even lower volume fraction of PBO, as described below. By 60wt% a lamellar system with significant polydispersity in its d -spacing (as indicated by the broad peaks) has formed. A significant shift in d -spacing is observed between

40wt% (126Å) and 60wt% (168Å), this may be driven by crystallization of the PEO blocks. Crossed optical micrographs suggest that, by 60wt%, the system is structured into lamellae on the macroscopic scale. Figure 3.19 shows this organization clearly, d-spacings can be seen to be on the order of microns and the lamellae are further organized into randomly oriented domains tens of microns in size. Again, no structure is observed in this sample without the use of polarized light.



Figure 3.19 – Crossed polar optical micrograph of 60wt% $E_{91}B_{56}E_{91}$ in cured epoxy.

3.3.1.5 $E_{126}B_{51}E_{126}$

The structures exhibited by $E_{126}B_{51}E_{126}$ in epoxy follow the same pattern through micelles, BCC and hexagonal packed cylinders until lamellae are formed around 50wt%. The most interesting result from this system is the apparent presence of non-lamellar structure at 60wt%. The lamellar structure tends to indicate a midpoint in the phase diagram of an AB diblock copolymer, with structures where A is the minor component forming at lower values of ϕ_A and structures where A is the major component forming at higher values. Thus it seems reasonable to think that the structure observed at 60wt% $E_{126}B_{51}E_{126}$ is phase-inverted with respect to the structures observed at <50wt%. Unfortunately, this explanation does not fit well with the structure of the polymer.

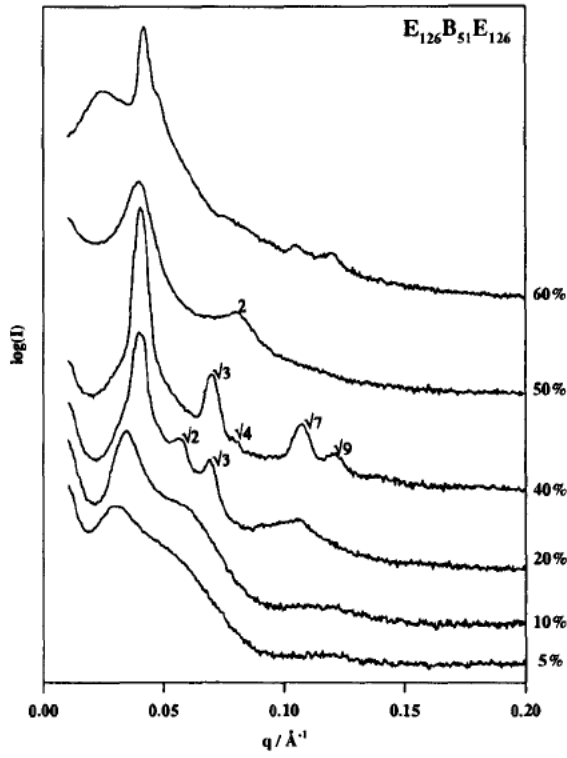


Figure 3.20 - SAXS patterns for a concentration series of $E_{126}B_{51}E_{126}$ in cured BADGE + DETDA.

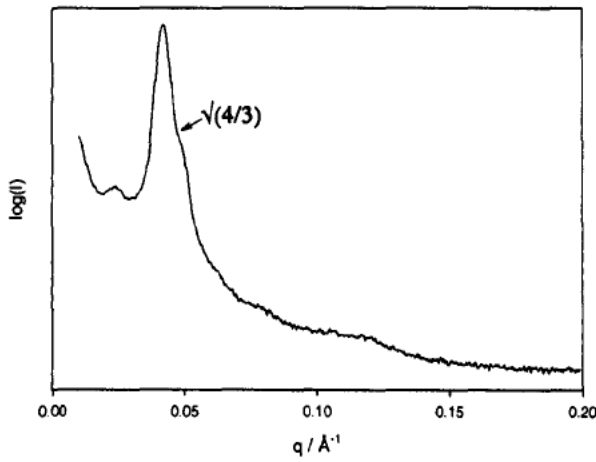


Figure 3.21 - SAXS pattern for 60wt% $E_{126}B_{51}E_{126}$ at 70°C.

Neat $E_{126}B_{51}E_{126}$ has a lamellar structure in the melt at 70°C . Since epoxy resin swells the PEO block, it can only serve to increase the effective volume fraction of PEO. As PEO is already the major component ($\phi_E = 0.73$), the structures observed at lower block copolymer concentrations in epoxy resin must have PBO as the minor component. There is no reason to think that this system should ever go beyond the equilibrium melt structure of lamellae as the epoxy content is decreased. The peak at low q might be indicative of semi-crystalline PEO. Perhaps the epoxy matrix is saturated with PEO prior to cure and expels some PEO during cure. This would lead to some semi crystalline, expelled regions, and some regions where the concentration of triblock in epoxy is $<60\text{wt}\%$. These might then be of sufficiently low concentration to form a gyroid phase with PBO as the minor component. It is noted that, on heating, signal remains at low q ($q = 0.0242 \text{ \AA}^{-1}$; $d = 260 \text{ \AA}$). It is unclear why this peak arises, being far lower in q than that for the unmodified block copolymer ($d = 129 \text{ \AA}$).

3.3.1.6 $B_{64}E_{75}B_{64}$

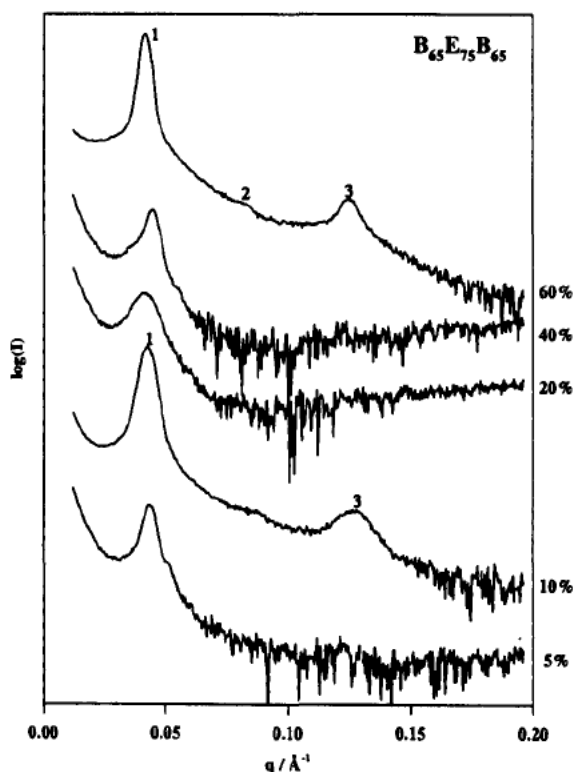


Figure 3.22 – SAXS patterns for a concentration series of $B_{64}E_{75}B_{64}$ in cured in BADGE + DETDA

$B_{64}E_{75}B_{64}$ is not completely miscible with BADGE + DETDA at room temperature and demonstrates a macrophase separated structure at 5wt% and 10wt% after curing, as described previously. Although the samples at 20wt% and above appear completely mixed, only the 60wt% sample shows any discernable structure, that of lamellae with alternating blocks of equal length (this is indicated by the lack of even numbered reflections due to coincidence with form factor minima).

The structure of the 5wt% and 10wt% samples does not change appreciably on heating to 70°C. If the block copolymer was completely phase separated from the resin, it would be expected to adopt its normal melt morphology which, at this temperature, is a BCC array of PEO spheres in a PBO matrix. Since this does not occur, it seems reasonable to assume that the macrophase separated structure consists of block copolymer rich domains interspersed with block copolymer poor domains. Some miscibility of PEO with the resin must be maintained. The structures observed at 10wt% and 60 wt% are very similar. It is possible that the signal observed from the 10wt% sample arises only from the block copolymer rich domains which might, locally, have a similar concentration of block copolymer to that of the 60wt% sample.

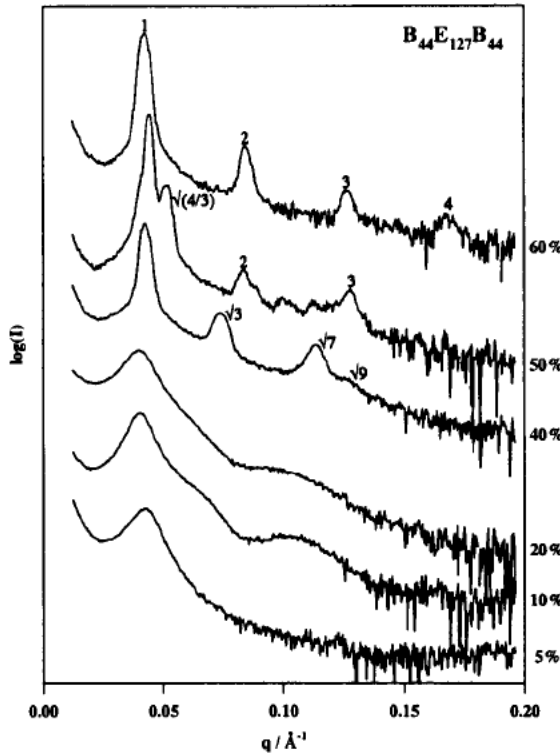
3.3.1.7 $B_{44}E_{127}B_{44}$ 

Figure 3.23 – SAXS patterns for a concentration series of $B_{44}E_{127}B_{44}$ cured in BADGE + DETDA.

Similar behaviour is observed in $B_{44}E_{127}B_{44}$ systems as was observed in the various EBE systems described above. At 60wt% a lamellar morphology is observed, the pattern at 50wt% is representative of a lamellar phase in transition to the gyroid phase. By 40wt% hexagonally packed cylinders are observed and at lower concentrations, a micellar morphology appears to be adopted. As shown earlier, at 5wt% and 10wt% this system undergoes reaction-induced phase separation during cure. The scattering pattern for the 10wt% sample suggests that micelles are present at this concentration. Again, it appears that the sample is macrophase separated into domains of high and low block copolymer concentration, rather than into separate domains of block copolymer and epoxy resin.

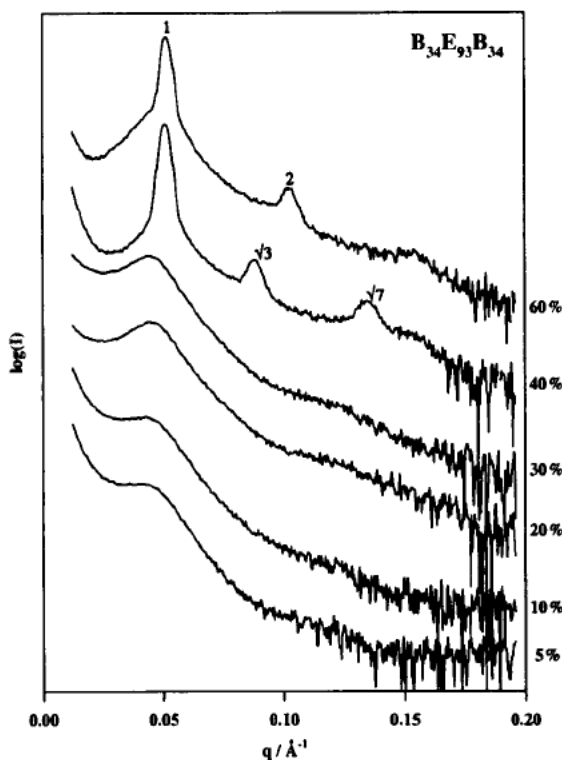
3.3.1.8 B₃₄E₉₃B₃₄

Figure 3.24 – SAXS patterns for a concentration series of B₃₄E₉₃B₃₄ in BADGE + DETDA.

This block copolymer has the same ϕ_E as B₄₄E₁₂₇B₄₄ above but has a significantly lower molecular weight [$M_n(\text{B}_{44}\text{E}_{127}\text{B}_{44}) = 11.9 \text{ kg}\cdot\text{mol}^{-1}$], $M_n(\text{B}_{34}\text{E}_{93}\text{B}_{34}) = 9.0 \text{ kg}\cdot\text{mol}^{-1}$). As a consequence microphase separation is not clearly observed until the formation of hexagonally packed cylinders at 40wt%. Since optical turbidity and diffuse scattering peaks are observed in lower concentration samples, this suggests that partial microphase separation occurs in these samples but that the domains are not sufficiently well defined so as to produce a useful scattering pattern. TEM analysis of the 5wt% sample presented later (Figure 3.31) indicates the presence of clusters of micelles. Thus these peaks may indicate liquid-like order with insufficient long-range order or too much polydispersity to allow the form-factor to be resolved.

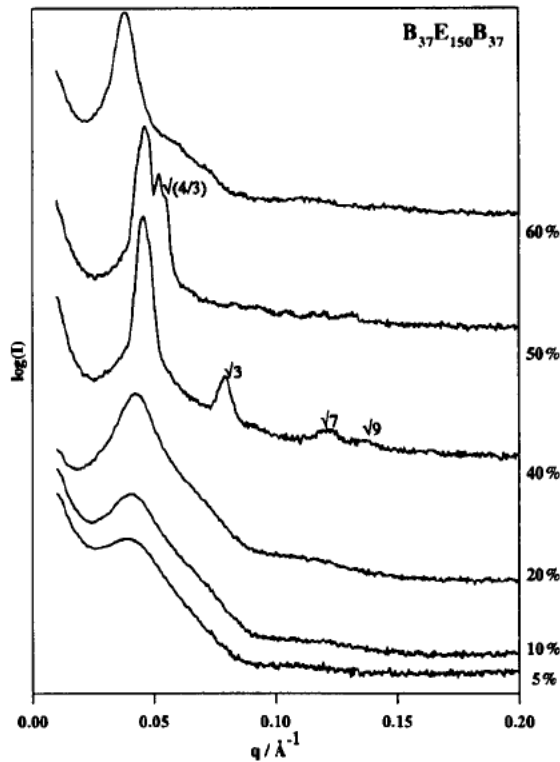
3.3.1.9 $B_{37}E_{150}B_{37}$ 

Figure 3.25 – SAXS patterns for a concentration series of $B_{37}E_{150}B_{37}$ cured in BADGE + DETDA

Systems containing $B_{37}E_{150}B_{37}$ (which has greater ϕE than the previous polymer but a higher molecular weight.) again appear to form micelles at up to 20wt%. The breadth of the peaks again indicates greater polydispersity than in the EBE based systems. A hexagonal phase is exhibited at 40wt% transitioning to a gyroid phase by 50wt%. At 60wt% the range over which order is maintained apparently drops significantly as only the primary scattering peak is observed clearly, although there are some weak, broad peaks at higher q which might be indicative of coexisting structures. Optical microscopy reveals the presence of spherulites, presumably any nanoscale order is confined to domains within the spherulites. Heating the sample to 100°C makes no difference to the structure observed under optical microscopy or the scattering pattern.

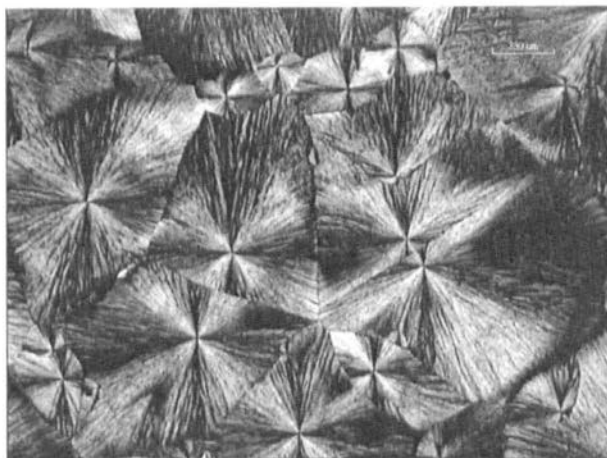


Figure 3.26 – Crossed-polar optical micrograph of a sample of 60wt% $B_{37}E_{150}B_{37}$ cured in BADGE + DETDA.

3.3.1.10 $B_{20}E_{141}B_{20}$, $B_{25}E_{210}B_{25}$ and $B_{17}E_{201}B_{17}$

The scattering patterns for those BEB triblocks having $\phi_E > 0.6$ which have been examined are presented in Figure 3.27. Broad peaks, which develop as the concentration is increased, indicate that some sort of order is developing on the nanometre scale. However the scattering patterns are only useful in determining the structure at 60wt% where peaks at q^* and $2q^*$, typical of a lamellar morphology, are observed in all cases. This peak broadening is attributed to incomplete microphase separation leading to structures which, where they have any long range order, are highly polydisperse.

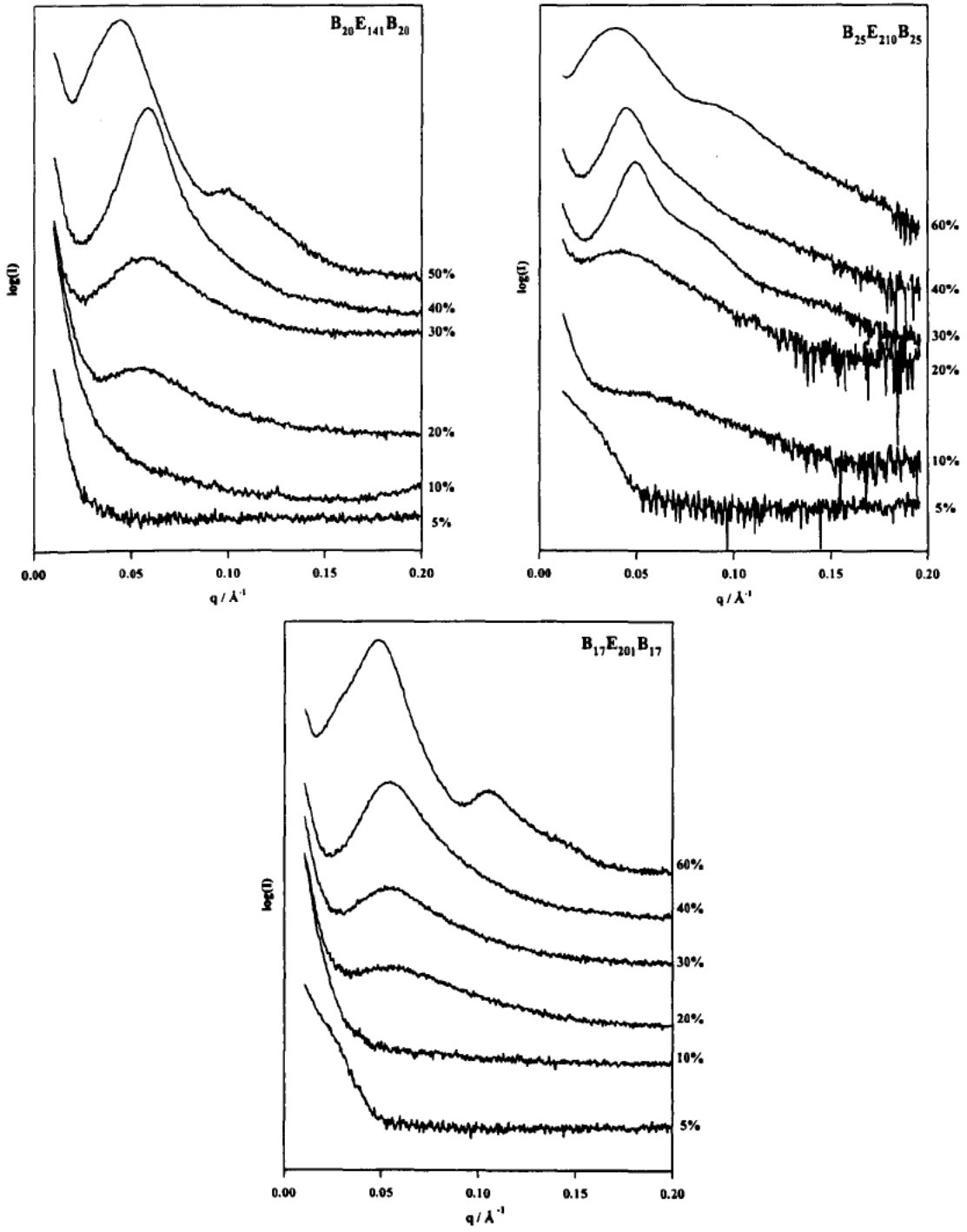


Figure 3.27 – SAXS patterns for concentration series of $B_{20}E_{141}B_{20}$, $B_{25}E_{210}B_{25}$ and $B_{17}E_{201}B_{17}$ cured in BADGE + DETDA.

3.3.1.11 Effect of the curing temperature

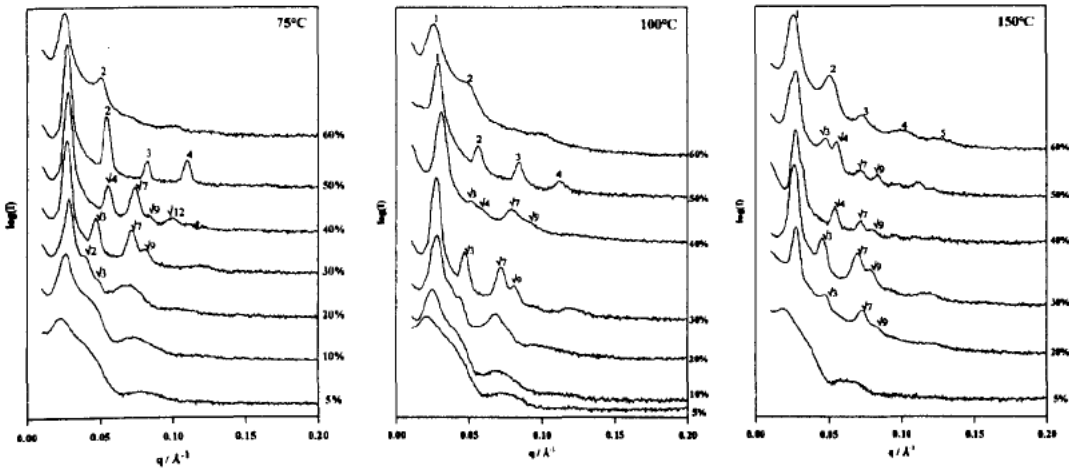


Figure 3.28 – SAXS patterns obtained for concentration series of $E_{115}B_{102}$ in BADGE + DETDA cured at different temperatures.

In order to determine the influence of curing temperature on the morphologies observed, samples of epoxy resin containing $E_{115}B_{102}$ were cured at elevated temperatures of 100°C and 150°C followed by a 180°C postcure as before. The SAXS patterns obtained are shown in Figure 3.28. The 100°C series essentially shows the same structures as the 75°C series, with slightly broadened peaks and different patterns for the Hex phase peaks at 30 & 40wt% with concentration. Again, this can be attributed to the relative positions of peaks in the structure factor of the hexagonal array and minima in the form factor of its component cylindrical rods. The measured ratios of peak position in the 20wt% sample are a poor fit to any common structure, however visually it appears very similar to the 75°C sample and so is assumed to be a BCC structure.

At 150°C the BCC phase at 20wt% has become a hexagonal phase and this is maintained, with variations in the pattern as the relative volume fractions of the components change, until a lamellar phase is formed at 60wt%. This observation suggests that PEO blocks are even more preferentially swollen by epoxy than PBO at higher curing temperatures. This means that the effective volume fraction of the

(PEO+Epoxy) phase will be higher at elevated temperatures for any given concentration.

3.3.1.12 Summary and general comments

A summary of the morphologies observed in this section is presented in Table 3.2. It can be seen that those systems which show microphase separation tend to follow the familiar series of transitions observed in block copolymers and their aqueous solutions (Micelles \rightarrow body-centred cubic \rightarrow hexagonally-packed cylinders \rightarrow [gyroid] \rightarrow lamellae). The epoxy resin swells the PEO block, thus increasing its volume fraction and altering the morphology. At low copolymer concentration structures will, therefore, consist of a PEO minor phase with a (PEO + Epoxy) major phase.

Polymer	ϕ_E	$M_n / \text{g.mol}^{-1}$	5%	10%	20%	30%	40%	50%	60%
E ₁₁₅ B ₁₀₂	0.37	12500	M	M	B-218	H-221	H-221	L-220	L-242
E ₄₃ B ₁₀₀ E ₄₃	0.31	11000	M	M	M	-	H-184	-	L-158
E ₉₀ B ₈₂ E ₉₀	0.54	13800	M	M	B-157	-	H-153	H-151	L-168
E ₉₁ B ₅₆ E ₉₁	0.63	12000	U(M)	M	M	-	H-184		L-157
E ₁₂₆ B ₅₁ E ₁₂₆	0.73	14800	M	M	B-156	-	H-153	L-156	G-157
B ₆₄ E ₇₅ B ₆₄	0.24	12500	U-146	L-146	U-146	-	U-139	-	L-147
B ₄₄ E ₁₂₇ B ₄₄	0.43	11900	U(M)	M	M	-	H-145	G+L-140	L-148
B ₃₄ E ₉₃ B ₃₄	0.42	9000	M	U(M)	U(M)	U(M)	H-123	-	L-121
B ₃₇ E ₁₅₀ B ₃₇	0.52	11900	U(M)	M	M	-	H-135	G-135	U-162
B ₂₀ E ₁₄₁ B ₂₀	0.65	9100	X	X	U	U	U-106	L-140	-
B ₂₅ E ₂₁₀ B ₂₅	0.69	12800	U	U	U	U-125	U-140	-	L-160
B ₁₇ E ₂₀₁ B ₁₇	0.76	11300	U	X	U	U	U-115	-	L-125

Table 3.2 -A summary of the morphologies adopted by varying concentrations (wt%) of block copolymer in epoxy after curing at 75°C. ϕ_E is the volume fraction of E block in the 'dry' block copolymer; M_n is the number average molecular weight of the block copolymer. Morphologies are denoted as *M* – micelles; *B* – BCC packed micelles / spheres; *H* – Hexagonally packed cylinders; *G* – gyroid; *L* – Lamellar; *X* – no scattering observed; *U* – Undefined (scattering observed but no clear pattern discernable). Numbers indicate the position of the primary scattering peak (in Å). Structure attributions in parentheses are tentative.

The BEB triblocks examined seem to be less prone to microphase separation than the EBE triblocks. Scattering patterns suggest that often, either no microphase separation occurs or that the phase separation is incomplete, leading to polydisperse systems as indicated by broad signals in the SAXS pattern. There are a number of possible reasons for this. The propensity for microphase separation appears to be related to the molecular weight of the PBO block, in addition to its volume fraction (this is suggested by the fact that $B_{44}E_{127}B_{44}$ microphase separates, where $B_{34}E_{93}B_{34}$ does not). This is likely to be because low molecular weight PBO is partially soluble in the epoxy resin at the curing temperature. Although the total mass of PBO present in the BEB triblocks is similar to the EBE equivalents, in the BEB triblocks each of the two smaller blocks will be more highly soluble in the resin.

The behaviour of $E_{91}B_{56}E_{91}$ as compared to $E_{126}B_{51}E_{126}$, where the later shows a greater tendency to microphase separate despite having a similar sized B-block and a lower volume fraction of PBO, suggests that the total molecular weight of the block copolymer is also significant. The BEB triblocks used have, on average, slightly lower molecular weights than their EBE counterparts.

Finally, if at low concentrations, the BEB systems do form bridged micellar structures as suggested in the introduction, these may not remain stable during cure. Bates *et al.*[8, 39, 40] have suggested that PEO is partially expelled from the resin during cure. This behaviour has not been directly observed during the present work, however, no special effort was made to detect it. (If such expulsion did occur in micellar systems, one might expect scattering contrast to arise both between PBO & PEO and between the expelled PEO & the matrix. In this case one would observe SAXS patterns typical of a core-shell structure, rather than the simple spherical particle scattering that arises, as shown below.) In order for a bridging PEO block to be expelled from the resin, one or both ends must be pulled from their respective micelle centres, disrupting the structure of the network.

The tendency of a given block copolymer to microphase separate at a given concentration seems, as might be expected, to follow the patterns observed in the study of critical micelle concentrations in solution in a non-reactive solvent which is selective for one block[7, 30]. (i) The tendency to microphase separate at a given concentration increases with increasing length of the solvent immiscible block. (ii) Increasing total molar mass at constant composition of the block copolymer increases the tendency to microphase separate. EBE and BEB triblocks have been observed to have higher critical micelle concentrations than their diblock counterparts[119, 120]. This is attributed to the entropic penalty associated with the folding of the triblock and the necessity for the blocks to be arranged in space such that both inter-block interfaces are located at the surface of the same sphere. BEB triblocks were noted to have critical micelle concentrations significantly greater than those of EBE triblocks, but no definitive reason for this has been determined.

One last observation which is best dealt with here concerns optical microscopy of those triblock containing samples which, at 40wt%, form structures composed of hexagonally packed cylinders. Sample crossed-polar optical micrographs for $B_{37}E_{150}B_{37}$ and $E_{43}B_{100}E_{43}$ are shown in Figure 3.29 but very similar patterns are also observed in $E_{90}B_{82}E_{90}$, $B_{44}E_{127}B_{44}$ and $E_{126}B_{51}E_{126}$.

The birefringence is due to alignment of the cylinders. (the samples were aligned before curing by sliding the top cover slip back-and-forth over the bottom one). This 'fan type' structure is commonly observed in hexagonally ordered systems[121] .

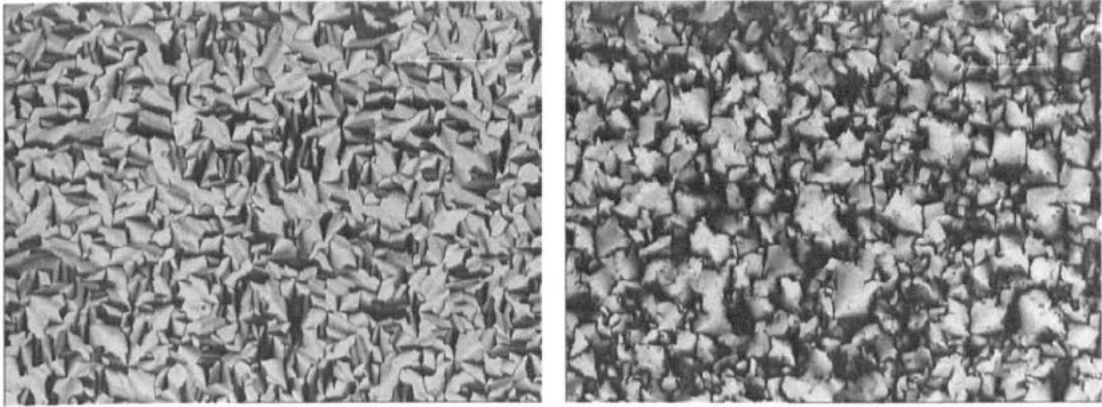


Figure 3.29 – Crossed-polar optical micrographs of cured samples of 40wt% B₃₇E₁₅₀B₃₇ (left) and E₄₃B₁₀₀E₄₃ (right), showing a 'leaf-pile' type structure.

3.3.2 The Micellar Regime

3.3.2.1 The Rayleigh-Percus-Yevick model

The scattering patterns observed at low concentrations in several of the above samples can be attributed to interacting spherical micelles. The undulations in the signal at moderate q -values arise, in part, from scattering by the core of the micelle which can be represented by the standard Rayleigh form factor for scattering from monodisperse spheres[94]:

$$P(q, r_c) = \left[\frac{4\pi r_c^3}{3} \right]^2 \left\{ \frac{3[\sin(qr_c) - qr_c \cos(qr_c)]}{(qr_c)^3} \right\}^2 \quad (3.3)$$

where r_c is the radius of the micelle core.

The peak at lower q arises from interaction between micelles and requires the addition of a structure factor to the scattering model. The Percus-Yevick model approximates the correlation between two hard spheres[122]. It can be evaluated as follows:

$$S(q, r_{hs}, \phi_{hs}) = \frac{1}{\left(1 + \frac{24\phi_{hs} f(A)}{A}\right)} \quad (3.4)$$

where ϕ_{hs} is the effective volume fraction of hard spheres; $A = 2qr_{hs}$; r_{hs} is the radius of the interacting hard spheres and $f(A)$ is a function defined in equations 3.5 & 3.6.

$$f(A) = \frac{\alpha}{A^2}(\sin A - A \cos A) + \frac{\beta}{A^3}[2A \sin A + (2 - A^2)\cos A - 2] + \frac{\gamma}{A^5}\{-A^4 \cos A + 4[(3A^2 - 6)\cos A + (A^3 - 6A)\sin A + 6]\} \quad (3.5)$$

$$\alpha = \frac{(1 + 2\phi_{hs})^2}{(1 - \phi_{hs})^4} \quad \beta = \frac{-6\phi_{hs} \left(1 + \frac{\phi_{hs}}{2}\right)^2}{(1 - \phi_{hs})^4} \quad \gamma = \frac{\phi_{hs} (1 + 2\phi_{hs})^2}{2(1 - \phi_{hs})^4} \quad (3.6)$$

The combined Rayleigh-Percus-Yevick (RPY) model has been successfully applied to interacting block copolymer micelles in a range of situations including melts[123], aqueous solutions[124] and cured epoxy resin systems[40].

3.3.2.2 Micelle parameters from SAXS data

Data obtained from SAXS experiments on low concentration samples were analyzed using the RPY model. The raw data from each experiment was normalized using the semi-transparent beamstop signal for NanoStar data and the back-ion chamber for data from the Daresbury SRS. A background pattern was obtained from an unmodified epoxy sample which had been cured under the same conditions as the modified samples. The normalized background was subtracted from each pattern before fitting of the model.

As applied here, the model assumes a system containing monodisperse micelles. In practice some polydispersity in micelle size is inevitable. Optimum parameters for fitting were therefore determined by eye, taking into account that polydispersity of

the micelle radii will lead to broader, shallower minima than are predicted for the ideal case.

Examples of corrected scattering patterns are shown, together with lines demonstrating the fitting, in Figure 3.30. A summary of the optimum fitting parameters for all samples which were successfully fitted is given in Table 3.3.

Polymer	wt%	$r_c /$ nm	$r_{hs} /$ nm	ϕ_{hs}	Polymer	wt%	$r_c /$ nm	$r_{hs} /$ nm	ϕ_{hs}
E ₁₁₅ B ₁₀₂	5	6.8	12.8	0.21	E ₁₂₆ B ₅₁ E ₁₂₆	5	4.5	10.0	0.26
E ₁₁₅ B ₁₀₂	10	7.6	12.5	0.42	E ₁₂₆ B ₅₁ E ₁₂₆	10	4.8	9.5	0.40
E ₄₃ B ₁₀₀ E ₄₃	5	7.9	13.0	0.20	B ₄₄ E ₁₂₇ B ₄₄	10	5.5	8.2	0.42
E ₄₃ B ₁₀₀ E ₄₃	10	8.1	12.0	0.30	B ₄₄ E ₁₂₇ B ₄₄	20	5.5	7.9	0.37
E ₄₃ B ₁₀₀ E ₄₃	20	8.5	11.8	0.47					
E ₉₀ B ₈₂ E ₉₀	5	4.5	10.0	0.22	B ₃₇ E ₁₅₀ B ₃₇	5	4.7	6.8	0.22
E ₉₀ B ₈₂ E ₉₀	10	5.0	9.5	0.38	B ₃₇ E ₁₅₀ B ₃₇	10	4.7	7.3	0.30
					B ₃₇ E ₁₅₀ B ₃₇	20	4.7	7.5	0.40
E ₉₁ B ₅₆ E ₉₁	10	3.7	7.4	0.34					
E ₉₁ B ₅₆ E ₉₁	20	4.1	7.3	0.47					

Table 3.3 – Summary of parameters obtained from Rayleigh-Percus-Yevick fits to SAXS data for low concentration samples. r_c is the radius of the micelle core; r_{hs} is the effective interaction radius based on a hard-sphere model; ϕ_{hs} is the effective volume fraction occupied by the interacting hard-spheres.

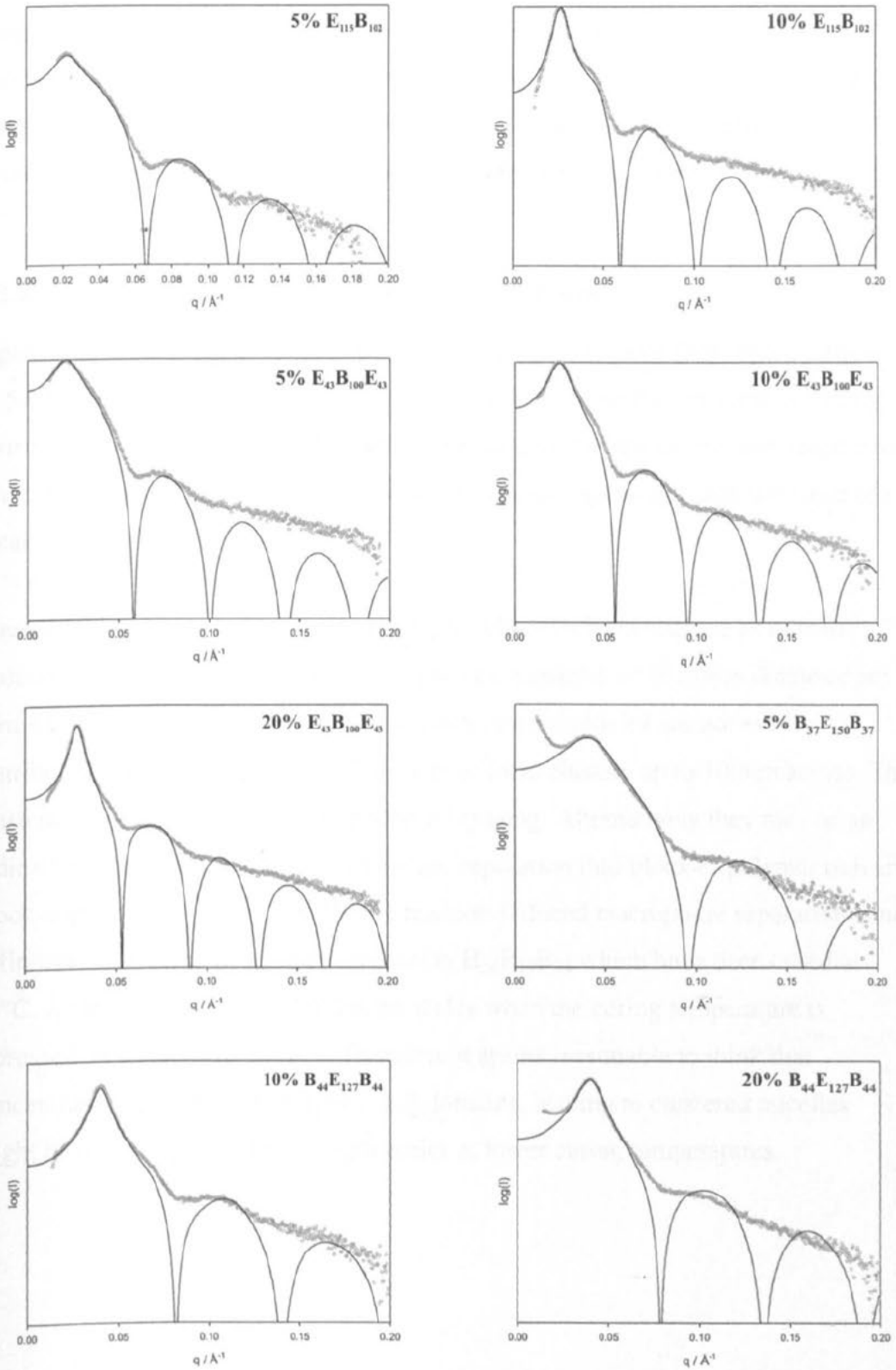


Figure 3.30 – Corrected SAXS patterns (grey circles) and corresponding Rayleigh-Percus-Yevick fits (black lines) for some of the samples analyzed.

Because the above data come from manual fits, and because of the lack of sharp peaks in the data, some degree of imprecision is unavoidable. From observation during fitting, the parameters represent a 'best-fit' within an uncertainty of ± 3 in the last digit. Measurements of duplicate samples and scattering from various locations in the same sample produced identical parameters within this uncertainty.

3.3.2.3 TEM – Confirmation of micellar structure

Figure 3.31 shows transmission electron micrographs obtained from cured samples of 5wt% $E_{115}B_{102}$ and $B_{34}E_{93}B_{34}$. The former clearly shows the presence of evenly distributed spherical particles throughout the sample. The mean diameter taken over ten of the larger particles is 14.3nm, which is in good agreement with the value of r_c obtained from SAXS ($2r_c = 13.6\text{nm}$).

Whereas the SAXS patterns for $B_{34}E_{93}B_{34}$ provide no clear evidence of micellar structure, the TEM results suggest that spherical particles of 10-20nm diameter are formed. However, unlike the previous sample, these particles are not evenly distributed in space. Instead they flocculate to form clusters up to 100nm across. The clusters may be the result of inter-micellar bridging. Alternatively they may be an indication of the beginnings of macrophase separation into block-copolymer rich and block-copolymer poor regions. Whilst reaction-induced macrophase separation is not definitively observed in samples containing $B_{34}E_{93}B_{34}$ which have been cured at 75°C, it clearly occurs at visible length scales when the curing temperature is increased, as demonstrated later. Therefore it seems reasonable to think that concentration into block-copolymer rich domains, leading to clustered micelles might be occurring on shorter length scales at lower curing temperatures.

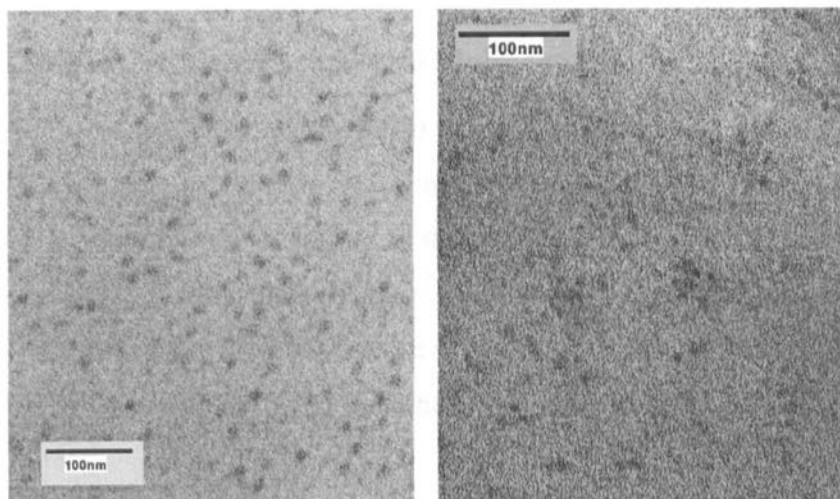


Figure 3.31 – Transmission electron micrographs of sections cut from cured samples containing 5wt% of $E_{115}B_{102}$ (left) and $B_{34}E_{93}B_{34}$ (right). The darkest areas are assumed to be PBO, stained in RuO_4 vapour.

When comparing information obtained by TEM to that from SAXS, it is important to note that TEM images very small volumes of material whereas SAXS signals are averaged over a comparatively large volume. In this work the volume observed by SAXS is $\sim 10^{10}$ times greater than that shown in the above images. Care has been taken to obtain TEM images which, on the basis of observations before image capture, appear to be representative of the sample as a whole.

The pattern visible in the background of the above images is also seen in unmodified epoxy resin. This type of pattern is commonly seen in TEM images of cured epoxy resin. It is probably due to alternating regions of more and less highly cross-linked epoxy resin. The less highly cross-linked resin will be more heavily stained by RuO_4 .

3.3.2.4 Variation of micelle size with block-length

A number of theories have been developed to predict how micelle size scales with the length of the copolymer blocks. A recent review can be found in the monograph by Hamley[7]. These may be expressed in terms of r_c or of the association number, here written as N_w , which denotes the average number of copolymer chains per micelle. If we assume that the micelle core is composed solely of PBO chains and that they have only liquid like order then these two quantities are related through Equation 3.7[30].

$$\frac{4\pi r_c^3}{3} = nN_w v_B \quad \text{where} \quad v_B = \frac{M_0}{\rho N_A} \quad (3.7)$$

n is the number of PBO repeat units in the chain; M_0 is the molar mass of one repeat unit; ρ is the density of liquid PBO and N_A is Avogadro's number.

Booth and co-workers[119, 120] have shown that for diblocks and triblocks of the form $E_m B_n$, $E_m B_{2n} E_m$ and $B_n E_m B_n$, the association number varies as

$$N_w \propto n'^{1.19} m^{-0.63} \quad \text{where} \quad n' = (n - n_{cr}) \quad (3.8)$$

n_{cr} is the critical micellization length, that is the value of n below which micelles do not form under the specified conditions. In very strongly segregated systems, such as PEO-alkyl block copolymers $n_{cr} = 0$. Aqueous solutions of EB diblocks and triblocks are not quite so strongly segregated and it has been determined that $n_{cr} \approx 4$ [120]. In liquid epoxy, one would expect n_{cr} to be higher than in aqueous systems as PBO is more soluble in the former, particularly at raised temperatures. However, since we know that phase separation processes can be enhanced as cross-linking of the epoxy proceeds it is reasonable to think that, in the cured sample n_{cr} may be low.

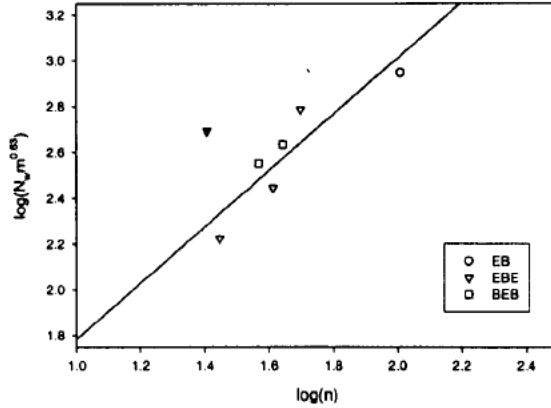


Figure 3.32 – Graph showing fitting of data obtained from PYR fitting of 10wt% block copolymer in epoxy to Booth's model for micellar size as a function of block-length. The slope of the line is 1.22 ± 0.54 . The filled symbol indicates a datum that was excluded from the fit as an outlier.

Thus, in the plot presented in Figure 3.32, it is assumed that $n_{cr} = 0$. This assumption is also convenient for practical reasons. In aqueous systems, n_{cr} is determined through dynamic light-scattering or surface tension measurements. Clearly, neither of these can be applied to cured samples, indeed, even in the liquid state, the viscosity of epoxy resin is too high to successfully exploit these techniques. The limit of detection of micelles by SAXS is poor, it might be possible to obtain a value from transmission electron micrographs on a series of polymers with fixed E-block length, but the range of polymers studied here does not allow an accurate value to be determined.

Using this assumption, and excluding the value for $E_{126}B_{51}E_{126}$ as an outlier, a plot of $\log(N_w m^{0.63})$ as a function of $\log(n)$ for the 10wt% samples fits moderately well to a straight line of gradient 1.22 ± 0.54 . This is in agreement with the value of 1.19 ± 0.25 given by Booth *et al.* in ref. [120] for aqueous PEO-PBO systems assuming $n_{cr} = 4$.

On the basis of the available data it appears that micellar association number of EB, EBE and BEB block copolymers in cured epoxy systems scales in the same manner as in aqueous solution except that n_{cr} can be considered as equal to zero due to enhanced phase separation in the cured system. Hence we can state that

$$N_w \propto m^{-0.63} n^{1.2} \quad (3.9)$$

3.3.2.5 Variation of micelle size with concentration

As concentration increases, an increase in the total volume fraction of interacting hard-spheres is accompanied by a decrease in their radius. This is expected given that r_{hs} is an interaction radius, not directly related to the size of the micelles. As the number density of micelles increases, the distance between interacting micelles will decrease.

In the case of block copolymer micelles formed in aqueous solution, it has been shown that the association number is essentially independent of concentration [125, 126]. The data presented above suggest that the core radius, which should be proportional to $\sqrt[3]{N_w}$, increases with concentration. This change might also be due to swelling of the core for some other reason, not associated with increased aggregation. Alternatively, the apparent increase in r_c , being small, might be an artefact of the fitting.

In an attempt to provide confirmation of the increase in association number with concentration, the following model was used. If it is assumed that all block copolymer added to the system forms micelles, rather than simply being present as unimolecular species, then any polymer not involved in increasing the association number of existing micelles must form new micelles. With reference to the hard-sphere model described above, each hard sphere will be centred on one micelle. In some volume, V_∞ , the volume fraction occupied by M spheres of radius r_{hs} may be written as:

$$\phi_{hs} = \frac{MV_{hs}}{V_\infty} \quad (3.10)$$

where the volume of a single hard-sphere, $V_{hs} = 4\pi r_{hs}^3 / 3$. Hence, for the case of two samples, a and b , of different concentration we can write:

$E_{115}B_{102}$ ($^{10\%}/5\%$)	2.0	$E_{90}B_{82}E_{90}$ ($^{10\%}/5\%$)	2.0	$B_{44}E_{127}B_{44}$ ($^{20\%}/10\%$)	0.98
$E_{43}B_{100}E_{43}$ ($^{10\%}/5\%$)	1.9	$E_{91}B_{56}E_{91}$ ($^{20\%}/10\%$)	1.4	$B_{37}E_{150}B_{37}$ ($^{10\%}/5\%$)	1.1
$E_{43}B_{100}E_{43}$ ($^{20\%}/10\%$)	1.6	$E_{126}B_{51}E_{126}$ ($^{10\%}/5\%$)	1.8	$B_{37}E_{150}B_{37}$ ($^{20\%}/10\%$)	1.2

Table 3.4 – Ratio of the number of micelles (M_a/M_b) at varying polymer concentrations ($^a/b$). Calculated from Percus-Yevick hard-sphere fitting using Equation 3.8.

$$\frac{M_a}{M_b} = \frac{v_a}{v_b} \quad \text{where } v = \frac{\phi_{hs}}{r_{hs}^3} \quad (3.11)$$

Values of M_a/M_b calculated using the data above are presented in Table 3.4.

At the lowest concentration ($^{10\%}/5\%$) $E_{115}B_{102}$ and the EBEs basically show a doubling of micelle number density with doubling of concentration. This indicates that, as in aqueous systems, all of the additional polymer is involved in forming new micelles. The deviation from the expected doubling for $E_{43}B_{100}E_{43}$ ($^{20\%}/10\%$) is attributed to the number density of micelles being too great to allow all of the additional polymer to form new micelles. Instead some polymer merges with existing micelles and a significant shift in the core scattering minima is observed, corresponding to an increase in r_c . This is the beginning of the process whereby the PBO domains increase in size relative to the (PEO/Epoxy) domains and that will eventually lead to ordered morphologies as shown earlier.

It is interesting to note that the degree of deviation from expected ideal behaviour ($N_a / N_b = 2$) appears to be greatest for those polymers which show no structure in their SAXS patterns prior to cure. As discussed in section 3.3.2.6, this is believed to be due to reaction-induced microphase separation (i.e. in this case, reaction-induced micellization). Samples which show the greatest degree of microphase separation prior to cure would be considered most likely to reach equilibrium before vitrification occurs. In those samples where microphase separation does not begin until the sample is partially cured, it is reasonable to think that the final structure observed in the cured sample may be a kinetically trapped, non-equilibrium, structure.

The behaviour of the BEB samples does not fit well to this model. In $B_{44}E_{127}B_{44}$, this is unsurprising since the evidence, presented earlier, suggests that the 10wt% sample has macrophase separated copolymer-rich regions which are locally more concentrated than the homogenous 20wt% sample. The reasons for the behaviour of the $B_{37}E_{150}B_{37}$ system are unclear but it is noted that this system also undergoes reaction-induced microphase separation.

3.3.2.6 Observations during cure – Reaction-Induced Micellization

In their work on the modification of epoxy resins with block copolymers, Bates and co-workers have observed that micellar structures can form in the uncured epoxy solution and persist, without change, throughout curing yielding nanostructured thermosets. They have demonstrated this through SAXS for systems of BADGE + MDA modified with PEO-PEP[40] and with reactive block copolymers[49].

SAXS patterns for the uncured solutions of block copolymer in BADGE + DETDA were obtained using a liquid cell. The cell consisted of a PTFE washer, around 2mm thick, sandwiched between two mica windows and sealed by clamping in a machined brass assembly. The results obtained are compared with those for cured samples in Figure 3.33. In the case of $E_{115}B_{102}$ patterns were also obtained after placing the liquid cell, with sample, into an oven at 75°C. At 8 and 16 hours curing time, the cell was removed from the oven and allowed to cool to room temperature, before submitting the sample to SAXS.

It is noted that, in their study of EB diblocks in a BADGE + PN epoxy system, Wu *et al.* reported difficulty in obtaining useful SAXS patterns from their uncured samples[39]. They attributed this to a lack of contrast difference between PBO and the resin. It is possible that their epoxy system was more closely contrast matched to PBO than the one used here. Indeed, the low T_g exhibited by Wu's unmodified epoxy (<90°C) suggests a significantly lower cross-linking density than BADGE + DETDA. ($T_g \approx 200^\circ\text{C}$ – the density of the cured resin was determined to be 1.166g.cm^{-3} using a helium pycnometer. The density of liquid PBO is 0.923g.cm^{-3} .)

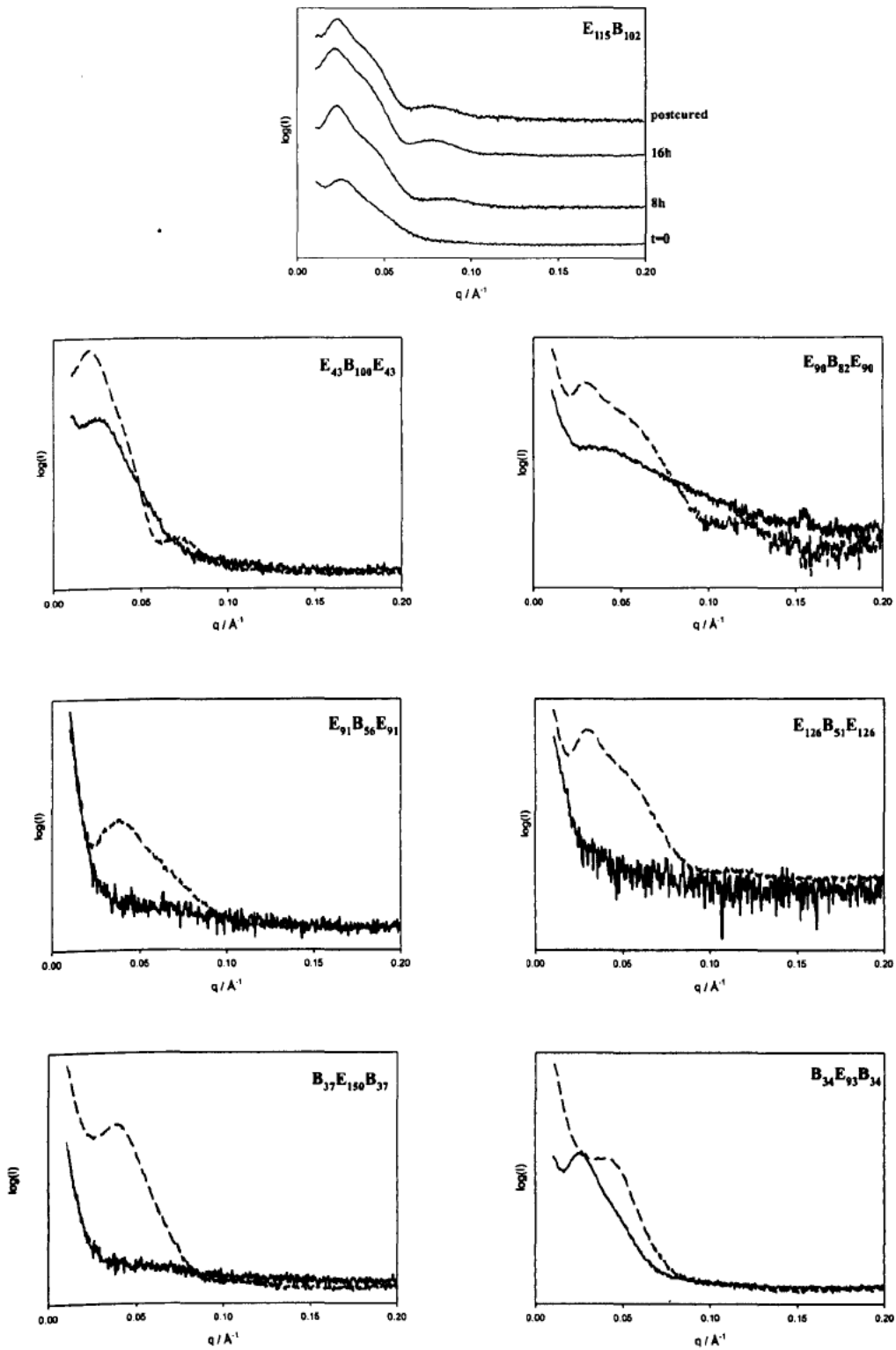


Figure 3.33 – Changes in SAXS patterns during cure for some micelle forming block copolymer-epoxy systems at 5wt% in BADGE + DETDA. In the plots for the triblocks, solid lines represent patterns prior to curing, dashed lines are after 72 hours at 75°C followed by a 2 hour postcure at 180°C. All data acquired at 25°C.

It is also possible that the more complex structures that are formed by Wu's block copolymers simply do not produce easily interpreted scattering data. Finally, it may be that Wu's system also demonstrates the behaviour shown here, where clear patterns only arise after curing. Data for cured samples is not presented in Wu's paper as SAXS analysis was not essential to the main aims of the work.

Returning to the data above, it can be seen that all of the samples which exhibit micellization at 5wt% show some degree of change in their nanoscale structure as they cure. The degree of microphase separation in uncured samples, as judged empirically from peak breadth and intensity, can be seen to increase with decreasing PEO volume fraction. This is consistent with the increased tendency to phase separate as the fraction of matrix immiscible block increases.

It is probable that some of the variation is due to an increase in contrast between the PBO and the matrix which will occur due to the increase in density of the epoxy with extent of reaction. However, it is clear from the samples with low ϕ_E that PBO and the matrix are not contrast matched in the uncured state. Thus we can be confident that the lack of scattering observed in uncured samples with higher ϕ_E indicates a lack of structure on the appropriate length scales.

The data suggest that reaction-induced microphase separation is occurring. One might expect this to be driven by the same mechanism as reaction-induced macrophase separation. For the purpose of this discussion three Flory-Huggins interaction parameters are defined. $\chi_{(BR)}$ relates to the interaction between the PBO block and the epoxy resin, $\chi_{(ER)}$ to the interaction between PEO and epoxy resin and $\chi_{(EB)}$ to the interaction between blocks of the copolymer. In the extreme case, the uncured samples consist of a disordered solution of block copolymer in epoxy. As the reaction progresses and the molecular weight of the matrix increases, the increase in $\chi_{(BR)}N$ will eventually lead to phase separation of the PBO block from the resin. Micelles will form in order to minimize the enthalpic penalty associated with PBO-matrix interaction by the minimization of contact surface area.

For block copolymer $B_{44}E_{127}B_{44}$ ($\phi_E = 0.43$, $M_n = 11900\text{g}\cdot\text{mol}^{-1}$), macrophase separation is observed at 75°C . The lower molecular weight analogue $B_{34}E_{93}B_{34}$ ($\phi_E = 0.42$, $M_n = 9000\text{g}\cdot\text{mol}^{-1}$) forms micelles when cured at 75°C (as observed by TEM) and appears, from the SAXS data above, to have some microphase structure in the uncured solution. However, as shown later, when cured at elevated temperature (e.g. 175°C), $B_{34}E_{93}B_{34}$ also macrophase separates by spinodal decomposition. The simplest explanation for this macrophase separation would be that $\chi_{(ER)}N$, where N is dependent on the molecular weights of the E-block and of the growing epoxy network, has reached some critical value and the E-block has been expelled from the resin prior to gelation. However, were this the case, one would expect macrophase separation to occur for all block copolymers with long E-blocks. Since it does not, the interactions of E and B blocks with the resin cannot be treated independently.

If $\chi_{(PR)}$ is defined as the interaction parameter between the matrix and the diblock copolymer, then reaction-induced macrophase separation would be expected to occur when $\chi_{(PR)}N$ reaches some critical value. One might expect $\chi_{(PR)}$ to vary as some combination of $\chi_{(ER)}$ and $\chi_{(BR)}$, perhaps scaled by volume fraction or block size. This may be true within a given architecture but it is clear that polymers of different architectures display differing behaviour. Whereas the BEBs with $\phi_E \approx 0.42$ show reaction-induced macrophase separation, no such behaviour is observed for $E_{43}B_{100}E_{43}$ ($\phi_E = 0.31$, $M_n = 11000\text{g}\cdot\text{mol}^{-1}$) or $E_{115}B_{102}$ ($\phi_E = 0.37$, $M_n = 12500\text{g}\cdot\text{mol}^{-1}$). From the available data it is not possible to draw any further conclusions except to say that $\chi_{(PR)}$ is clearly dependent on architecture as well as composition.

We can say that the final observed structure will depend on a balance between $\chi_{(PR)}$ – which determines the onset of reaction-induced macrophase separation, $\chi_{(BR)}$ which determines the onset of reaction-induced micellization and vitrification which acts to freeze-in the structure. If, at vitrification, $\chi_{(BR)}N < (\chi N)_{\text{crit}}$ then phase separation will not be observed on any scale. If $\chi_{(PR)}N < (\chi N)_{\text{crit}} < \chi_{(BR)}N$ then reaction-induced

microphase separation will be observed (formation of micelles in this work). Finally, if $(\chi N)_{\text{crit}} < \chi_{(\text{PR})}N$ then reaction-induced macrophase separation will be observed.

Curing Time / h	r_c / nm	r_{hs} / nm	ϕ_{hs}
8	6.5	13.5	0.30
16	7.1	12.8	0.20
∞	6.8	12.8	0.21

Table 3.5 – Rayleigh-Percus-Yevick fit values for $E_{115}B_{102}$ in BADGE + DETDA at various points during curing at 75°C.

The data acquired during curing of the $E_{115}B_{102}$ sample were fitted using the RPY model as before. Optimum fitting parameters are presented in Table 3.5. The initially increased r_{hs} and ϕ_{hs} values suggest that the micelles become less swollen as curing progresses. This might be due to partial expulsion of PEO from the resin, or it may be due to increased cross-linking in that part of the resin which is mixed with PEO. An apparent increase in r_c is observed between 8 and 16 hours followed by a small decrease on postcuring. It is suggested that the initial increase is due to continuing phase separation of PBO from solution and the subsequent decrease is due to an increase in cross linking during the high temperature post-cure.

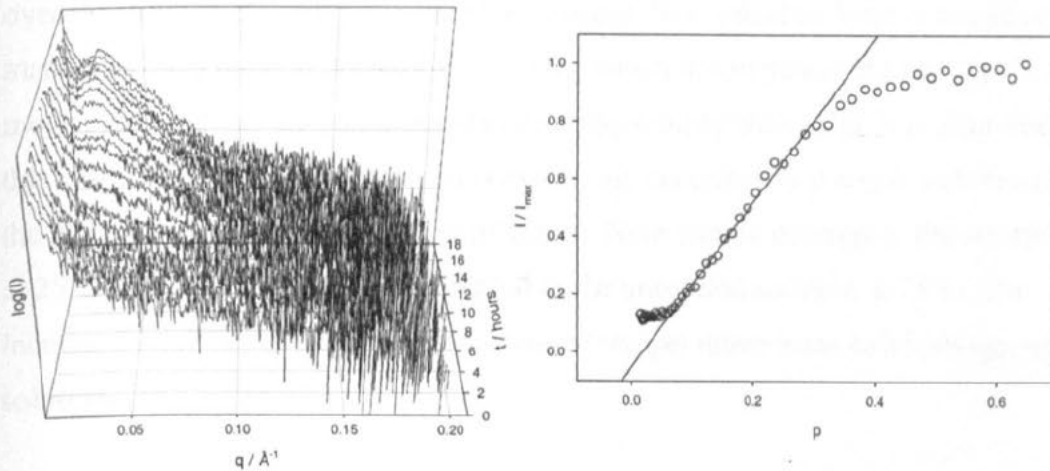


Figure 3.34 - (Left) Time resolved SAXS patterns showing the progression of reaction-induced microphase separation in a 5wt% sample of $E_{90}B_{82}E_{90}$ in BADGE + DETDA. Only one pattern in three is shown so as to reduce clutter. (Right) Variation of normalized peak intensity as a function of extent of reaction. The slope of the line is 2.85; $R^2=0.993$.

Time resolved SAXS was attempted on the NanoStar laboratory based SAXS system. A disposable cell was constructed by fixing a piece of 25 μ m thick mica on either side of an M4 washer using commercial rapid-curing epoxy adhesive. Once the adhesive had cured, the cell was filled with sample, via a channel that had been cut into the washer before constructing the cell, using a syringe and needle. The cell was placed into the heating stage on the NanoStar system and heated to 75°C. A series of frames of 20 minutes duration were acquired over 18 hours. Each frame was azimuthally integrated and a background subtracted from the resulting one-dimensional pattern.

Results for a 5wt% sample of E₉₀B₈₂E₉₀ are shown in Figure 3.34. The NanoStar instrument is not ideally suited to time-resolved measurements because of its comparatively weak beam intensity. This is reflected in the poor signal-to-noise ratio in this experiment. The patterns are too noisy to provide useful data about micelle parameters from an RPY fit, however it is still possible to obtain useful information about the rate of phase separation by looking at the increase in scattering intensity. Scattering intensity scales directly with the number of scattering centres. When intensity (normalized to its maximum value) is plotted as a function of extent of reaction (obtained from FTIR experiments) it is clear that the relationship is linear over the majority of the phase separation process. New micelles form in a regular manner as the reduction in entropy of mixing which accompanies the increase in molecular weight of the matrix reduces its compatibility with PBO. It is clear that, in this case, the microphase separation is essentially complete by $p = 0.4$, well before the gel point and certainly before vitrification. Note that, in contrast to the situation at 25°C, no scattering pattern is observed in the unreacted solution at 75°C. The increased solubility of PBO in epoxy at raised temperatures leads to a homogenous solution.

Very recently, Meng and co-workers have observed reaction-induced microphase separation in MOCA cured BADGE resins modified with PCL-PB-PCL[60] and PEO-PS[59]. In the former, only micellar type structures were observed. In the later case, they suggest that their observations are consistent with the formation of

structures with long-range order *via* reaction-induced microphase separation, although no data are presented to confirm the lack of structure prior to cure at higher copolymer concentrations. The SAXS data presented for lower concentrations may indeed indicate long range structure, however experience gained from the present work suggests that such scattering is typical of interacting micellar structures which can be characterized by RPY fitting. It is suggested that for 10-30wt% PEO-PS in BADGE + MOCA the data, reproduced below, corresponds to interacting micelles. By 40wt%, a cubic-packed structure appears to have formed, as suggested in the original paper.

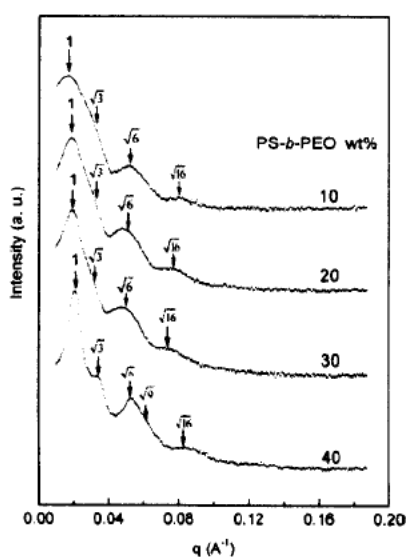


Figure 3.35 – SAXS patterns from cured samples of PS-PEO diblock copolymer at various concentrations in BADGE + MOCA. Reproduced from ref.[59].

3.3.2.7 Changing the cross-linking agent

The choice of curing agent has been shown to have a significant effect on the miscibility of block-copolymers and epoxy resins throughout cure. Therefore it may have a significant effect on nanostructure formation, particularly in the case of structures formed by reaction-induced microphase separation.

Samples of BADGE + MDA resin containing 5wt% of each of the block copolymers were prepared according to the same method as the DETDA cured samples. SAXS

patterns were acquired from the cured samples and fitting to the RPY model was performed as before. Fitted parameters for those samples for which the data were successfully fitted are presented in Table 3.6.

Polymer	r_c / nm	r_{hs} / nm	ϕ_{hs}
E ₁₁₅ B ₁₀₂	7.0	14.0	0.25
E ₄₃ B ₁₀₀ E ₄₃	7.5	12.5	0.20
E ₉₀ B ₈₂ E ₉₀	4.7	10.0	0.23
B ₃₇ E ₁₅₀ B ₃₇	5.0	8.5	0.45

Table 3.6 – Rayleigh-Percus-Yevick parameters for cured samples of block copolymer at 5wt% in BADGE + MDA cured resin. Cured at 75°C and post-cured at 180°C.

The values for samples containing E₁₁₅B₁₀₂, E₄₃B₁₀₀E₄₃ and E₉₀B₈₂E₉₀ are very close to those observed in the DETDA cured system. The B₃₇E₁₅₀B₃₇ sample shows a significant increase in both r_{hs} and ϕ_{hs} . The samples containing E₉₀B₈₂E₉₀ and E₁₂₆B₅₁E₁₂₆ both show broad scattering at low q , to which a sensible fit cannot be made. It is probable that the differences observed are due to variations in the tendency to microphase separate caused by differing interactions of the PBO copolymer with the mixture of resin and hardener when the later is changed. The data are consistent with the situation where the equilibrium micelle parameters are determined solely by the block copolymer structure but non-equilibrium structures may be observed when vitrification occurs before the microphase separation process is completed. Those systems where, with both cross-linking agents, the micelle formation process is complete before vitrification show similar values of the micelle parameters in both cases. The progress of the microphase separation process as a function of extent of reaction would be expected to change when the interaction between the copolymer and the matrix is changed by, for example, changing one component of the matrix. Thus the extent of microphase separation will vary between epoxy systems at a given extent of reaction, therefore differing structures may be frozen in place at vitrification. (It is assumed here that the extent of reaction required for vitrification is identical for both hardener-resin systems, since both hardeners used here are tetrafunctional aromatic amines. However this mechanism remains plausible even if that assumption is not valid.)

3.3.2.8 Effect of the curing temperature

The SAXS patterns obtained previously for 5wt% E₁₁₅B₁₀₂ after high-temperature curing were fitted using the RPY model and the resulting parameters are given in Table 3.7. It is clear that r_c , r_{hs} and ϕ_{hs} all increase with increasing curing temperature. At raised temperatures, the PBO core may be partially swollen by epoxy resin as PBO has been shown to be increasingly soluble at higher temperatures. The observations in higher concentration systems shown earlier indicate that, if this is the case, swelling of the PEO domains must increase with temperature at a greater rate to that of PBO in order to maintain the hexagonally packed structure at higher concentrations. Alternatively, the PBO domains may remain unswollen with only swelling of the PEO domains increasing with temperature. The change observed in r_c would then be due to the need for a larger core in order to accommodate swelling of the PEO in the micellar corona.

$T_{cure} / ^\circ C$	r_c / nm	r_{hs} / nm	ϕ_{hs}
75	6.8	12.8	0.21
100	7.3	13.6	0.25
150	8.5	15.0	0.27

Table 3.7 – Rayleigh-Percus-Yevick parameters from SAXS patterns of 5wt% E₁₁₅B₁₀₂ in BADGE + DETDA, after curing at different temperatures.

3.3.3 Reaction-Induced Macrophase Separation

Reaction-induced macrophase separation is observed on curing at 75°C in the system containing 5wt% B₄₄E₁₂₇B₄₄ and at elevated temperature (175°C) in systems containing 5wt% B₃₄E₉₃B₃₄ and B₃₇E₁₅₀B₃₇. Bulk samples of these systems are optically transparent prior to cure but are completely opaque afterwards, due to the presence of phase separated domains with length scales on the order of microns. Phase separation in the cured product can be seen clearly by optical microscopy to exhibit a bicontinuous structure, typical of a system which has separated by spinodal decomposition. Typical optical micrographs are shown in Figure 3.36.

The development of structure during the curing process can be observed using time-resolved small-angle light-scattering (SALS). Attempts to monitor phase separation in the B₄₄E₁₂₇B₄₄ system when cured at 75°C were unsuccessful. This is believed to be due to the system being incompletely microphase separated on vitrification at this temperature. It can be seen in Figure 3.36 that the contrast between the domains is poor in the sample cured at 75°C when compared to the one cured at 175°C. The domain sizes are similar in the two cases. The domains are defined by copolymer-rich and copolymer-poor regions, as the spinodal decomposition process progresses, these regions will become more highly copolymer-rich and -poor respectively and optical contrast between the domains will increase.

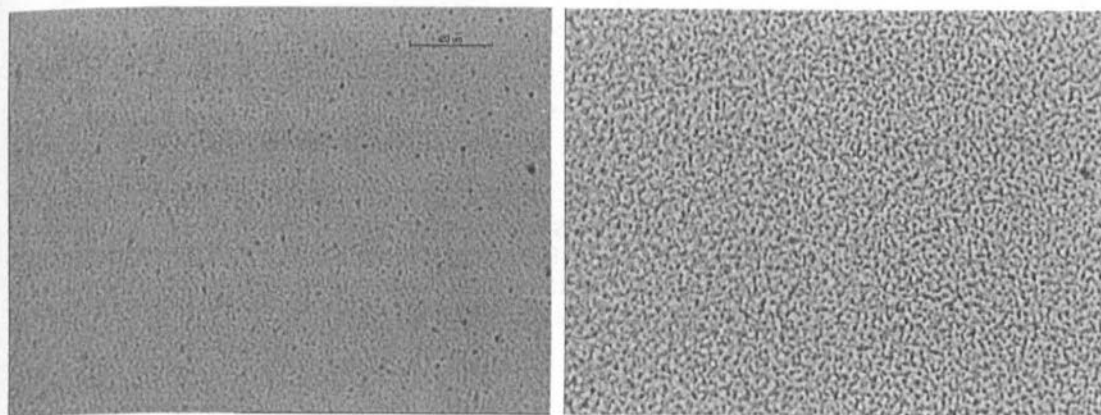


Figure 3.36 – Optical micrographs of 5wt% B₄₄E₁₂₇B₄₄ in BADGE + DGEBA after curing at 75°C (left) and 175°C (right).

In the sample cured at 75°C, vitrification has occurred at an earlier stage in the phase separation process due to the higher viscosity of the system at lower temperatures inhibiting diffusion. The lack of contrast is also indicated by the fact that, after curing at 75°C, the thin samples used for SALS analysis are still largely transparent, samples cured at the higher temperature are nearly opaque.

Time-resolved SALS was performed during cure of 5wt% $B_{44}E_{127}B_{44}$ and 5 & 10wt% $B_{34}E_{93}B_{34}$ systems at 175°C. Because spinodal decomposition leads to phase separated structures which display a characteristic wavelength over comparatively large distances, it can lead to a peak in the SALS pattern, where the peak maximum is indicative of the characteristic length scale of the domains.

A 3d-plot of typical data obtained during separation is shown for 5wt% $B_{34}E_{93}B_{34}$ in Figure 3.37, together with a plot showing how peak intensity at q_{max} varies throughout the entire curing process.

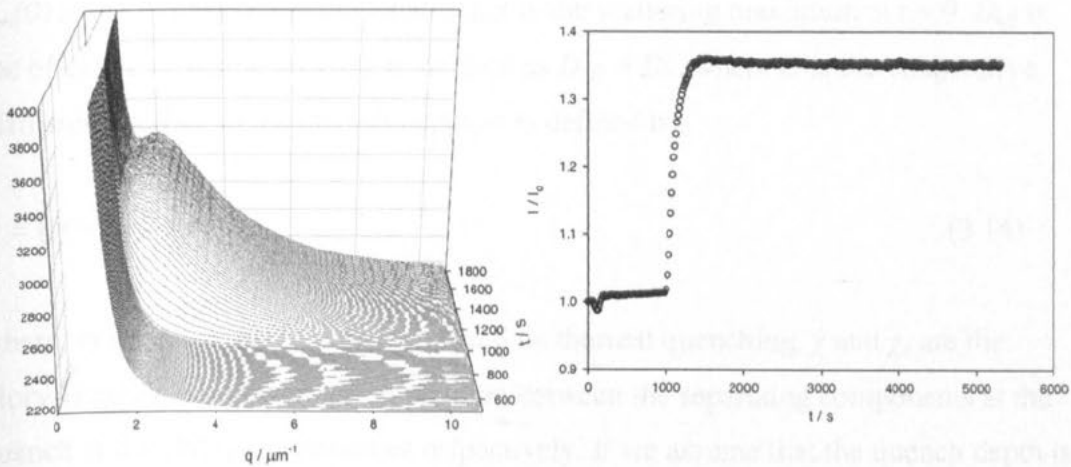


Figure 3.37 – Reaction-induced macrophase separation as observed by SALS during curing of a sample of BADGE + DETDA containing 5wt% $B_{34}E_{93}B_{34}$. (Left) Evolution of the scattering pattern over the time-period where separation occurs. (Right) Evolution of normalized peak intensity over time, throughout the entire curing process.

Thermally induced spinodal decomposition can be modelled using the Cahn-Hilliard theory[127]. Ishii[102, 128] has successfully applied this model to the reaction-induced phase separation of poly(2,6-dimethyl-1,4-phenylene ether) homopolymer from a DGEBA + DETDA epoxy system.

In Cahn-Hilliard theory the scattering structure factor, $S(q,t)$ for a binary mixture undergoing spinodal decomposition varies as:

$$S(q,t) = S_x(q) + [S(q,0) - S_x(q)]e^{2R(q)t} \quad (3.12)$$

where S_x is a virtual structure factor arising from thermal noise; q is the scattering vector; $R(q)$ is termed the amplification factor and is defined as below.

$$R(q) = D_{eff} q^2 \left[1 - \frac{1}{2} \left(\frac{q}{q_m(0)} \right)^2 \right] \quad (3.13)$$

$q_m(0)$ is the initial correlation length, that is the scattering maximum at $t = 0$. D_{eff} is the effective diffusion coefficient defined as $D_{eff} = D\varepsilon$, where D is the cooperative diffusion coefficient the quench depth, ε , is defined by:

$$\varepsilon = (\chi - \chi_s) / \chi_s \quad (3.14)$$

where, in a system where cure is induced by thermal quenching, χ and χ_s are the Flory-Huggins parameters for interaction between the separating components at the quench and stability temperatures respectively. If we assume that the quench depth is large, we can neglect $S_x(q)$ and write the observed scattering intensity as:

$$I(q,t) = I(q,0)e^{2R(q)t} \quad (3.15)$$

Thus a plot of $\ln(I/I_0)$ as a function of time will be linear in the early stages of spinodal decomposition and the slope of the line will be equal to $2R(q)$.

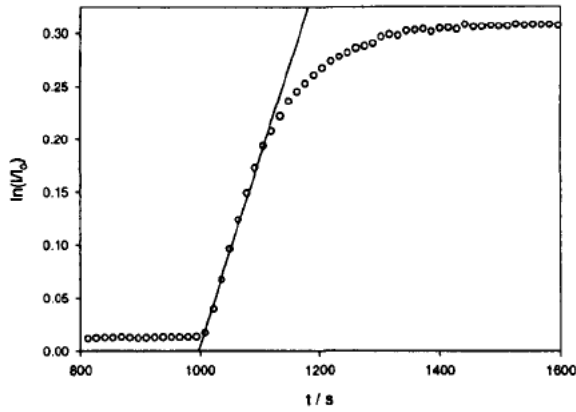


Figure 3.38 – Plot of the natural log of normalized intensity as a function of time from SALS measurements during cure of 5wt% $B_{34}E_{93}B_{34}$ in BADGE + DETDA at 175°C. The linear section shows where the Cahn-Hilliard linear theory is valid and is used to extract $R(q)$ for use in subsequent calculations.

If values of R are determined over a range of q then it is clear from Equation 3.13 that a plot of $R(q)/q^2$ as a function of q^2 should allow the determination of D_{eff} and $q_m(0)$ from a linear fit. Figure 3.39 shows a plot of such data for 5wt% $B_{34}E_{93}B_{34}$ cured at 175°C, demonstrating the validity of the fit at low q .

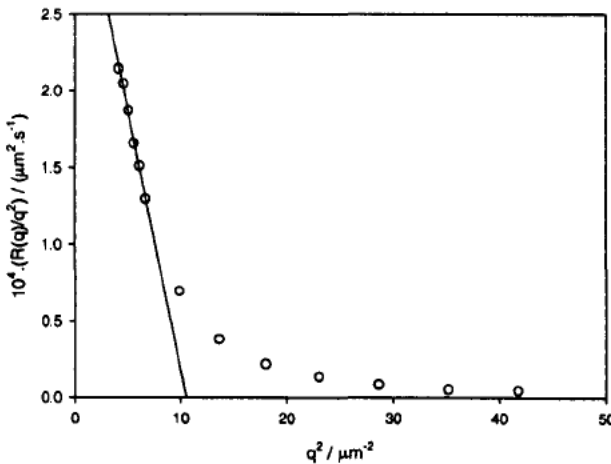


Figure 3.39 – Plot to determine $q_m(0)$ (from slope) and D_{eff} (from intercept) using the Cahn-Hilliard model for early-stage spinodal decomposition.

A summary of parameters obtained in the systems studied here is given in Table 3.8.

Sample	Onset of phase separation t / s	$10^4 D_{eff} / \mu\text{m}^2 \cdot \text{s}^{-1}$	$q_m(0) / \mu\text{m}^{-1}$
5wt% B ₃₄ E ₉₃ B ₃₄	1008	3.58	2.29
10wt% B ₃₄ E ₉₃ B ₃₄	1022	3.17	3.40
5wt% B ₄₄ E ₁₂₇ B ₄₄	810	0.70	3.28

Table 3.8 – Onset times of phase separation and Cahn-Hilliard parameters for the systems studied by SALS.

The similar onset times for both B₃₄E₉₃B₃₄ samples suggest that, at these concentrations, the extent of reaction and the Flory-Huggins parameter for interaction between the block copolymer and the resin, $\chi_{(PR)}$, dictate the onset of phase separation, independently of concentration. The earlier onset time in B₄₄E₁₂₇B₄₄ is what would be expected from the influence of molecular weight.

It was not possible to fit the data with models of late-stage spinodal decomposition such as those of Langer *et al.* [129] and Binder [130]. These models suggest changes in the q value of maximum intensity in the later phase of spinodal decomposition process and such changes were not observed. This is likely to be because vitrification occurred before the phase separation process was complete, kinetically trapping the interpenetrating structures that have been observed by microscopy.

It is interesting to note that, whilst the BEB systems show reaction-induced macrophase separation, no such behaviour is observed in EBE or EB systems at accessible curing temperatures. It is suggested that this may be due to break down of a bridged micellar network as PEO is expelled from the resin – as described in section 3.3.1.12. Expulsion of the PEO bridge leads to dissociation of the micelles within which PBO is solubilized.

3.4 Bulk Properties of Cured Samples

Most of the work performed to date involving investigation of nanostructure formation in epoxy resins has been driven by the desire to modify the properties of the bulk material in a commercially useful manner. This might include increasing the glass transition temperature or improving the fracture properties of the material.

3.4.1 Glass Transition Temperature

The glass transition temperatures of 5wt% samples cured at 75°C and post-cured at 180°C were determined by DSC, T_g was taken as the midpoint of the step. DSC thermographs are shown in Figure 3.40 and the values of T_g obtained are summarized in Table 3.9.

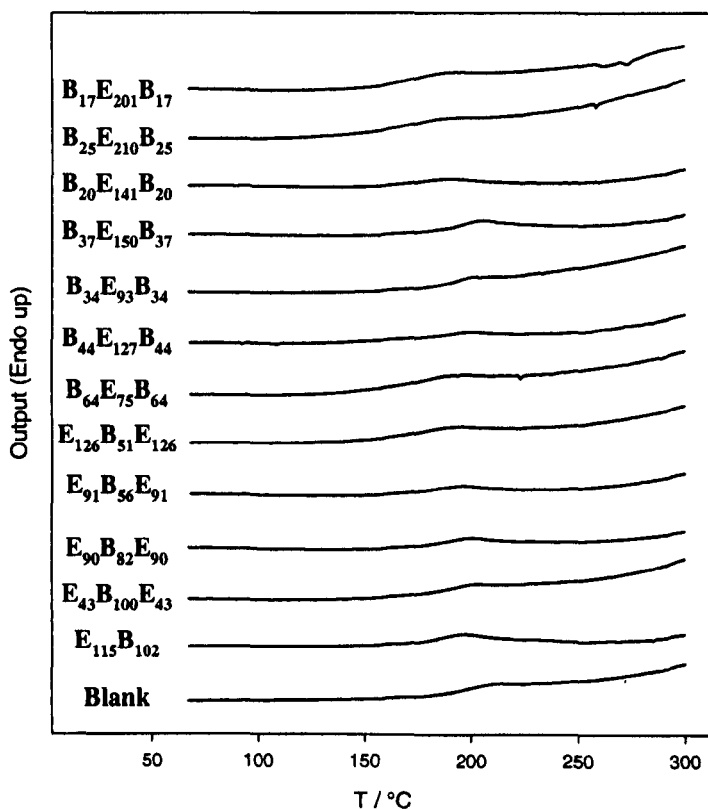


Figure 3.40 – DSC thermographs obtained from 5wt% samples of various block copolymers cured in BADGE + DETDA at 75°C. The heating rate was 20°C / min.

Modifier	T _g / °C	Modifier	T _g / °C	Modifier	T _g / °C
Unmodified	195	E ₉₁ B ₅₆ E ₉₁	170	B ₃₇ E ₁₅₀ B ₃₇	186
		E ₁₂₆ B ₅₁ E ₁₂₆	171	B ₂₀ E ₁₄₁ B ₂₀	169
E ₁₁₅ B ₁₀₂	180			B ₂₅ E ₂₁₀ B ₂₅	166
		B ₆₄ E ₇₅ B ₆₄	169	B ₁₇ E ₂₀₁ B ₁₇	170
E ₄₃ B ₁₀₀ E ₄₃	184	B ₄₄ E ₁₂₇ B ₄₄	169		
E ₉₀ B ₈₂ E ₉₀	177	B ₃₄ E ₉₃ B ₃₄	187		

Table 3.9 – Glass-transition temperatures for BADGE + DETDA epoxy resins modified with 5wt% of various block copolymers and cured at 75°C.

Clearly, the addition of block copolymer causes a decrease in T_g. If we assume that the PBO block is completely phase separated from the resin, in which case it should have a negligible effect on T_g of the matrix, then we might consider this reduction to be due to dilution of the resin by PEO.

The glass-transition temperature of a mixture, *M*, consisting of two fully miscible polymers, *A* and *B*, can be predicted using the Fox equation[131]:

$$\frac{1}{T_g(M)} = \frac{W_A}{T_g(A)} + \frac{W_B}{T_g(B)} \quad (3.16)$$

where *T_g* is the absolute temperature of the glass-transition and *W* is the weight fraction of the component in the system.

For a system consisting of PEO from a block copolymer, denoted *E*, and epoxy resin, denoted *R*, the weight fraction of PEO in the whole system will be proportional to the weight fraction of PEO in the block copolymer, *w_E*.

$$W_E = W_P w_E \quad \text{where} \quad w_E = \frac{n_E}{n_E + (72n_B/44)} \quad (3.17)$$

W_P is the weight fraction of block copolymer in the system and, in the present case, is constant at 0.05. *n_E* and *n_B* are, respectively, the number of PEO and PBO repeat units in the block copolymer.

Equation 3.16 can be applied to this system and rearranged to give:

$$\frac{1}{T_g(M)} = \frac{1}{T_g(R)} + W_E \left(\frac{1}{T_g(E)} - \frac{1}{T_g(R)} \right) \quad (3.18)$$

Thus, if the epoxy is being diluted solely by the PEO and the Fox equation is valid in this system, a plot of $1/T_g(M)$ against W_E should be linear. It can be seen from the plot presented in Figure 3.41 that, at least for systems modified by EB and EBE copolymers, this is indeed the case.

The data for BEB copolymers is included on the plot but was excluded from the fit. The samples containing BEBs with high PEO content are in reasonable agreement with the fit, but were excluded since the lack of micellar scattering in these systems suggests that the PBO block may be dissolved in the matrix which would complicate the diluent effect. Data for $B_{64}E_{75}B_{64}$ and $B_{44}E_{127}B_{44}$ are not plotted since these samples are macrophase separated. The T_g observed at 169°C in these samples is assumed to be that of the epoxy rich phase. A second T_g at much lower temperature, belonging to the block copolymer rich phase, would be expected in these samples but no attempt was made to observe this. Data for $B_{34}E_{93}B_{34}$ ($W_E = 0.0230$) and $B_{37}E_{150}B_{37}$ ($W_E = 0.0275$) indicate that T_g for these systems is significantly higher than predicted. This suggests that some of the PEO is not interacting with the resin. One possible explanation for this is that, if networks of bridging micelles are formed, then the micelle centres may be sufficiently close together so as to prevent proper interpenetration by the epoxy network.

From the gradient of the fitted line $T_g(E)$ can be calculated to be -88°C. Values for T_g of PEO in the literature vary widely depending on the molecular weight and what end groups are present. However, this value is well within the range of -40 to -115°C quoted in the compendium by Mark[132].

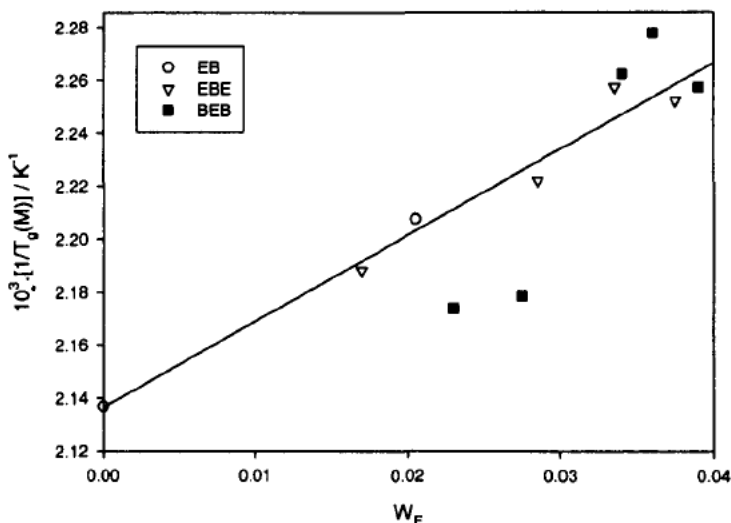


Figure 3.41 – Plot showing a fit of glass-transition data to the Fox equation. Samples consist of 5wt% of block copolymer in BADGE + DETDA, cured at 75°C. Only data plotted as open markers (EB and EBE) were fitted to the line.

Using the calculated values of $T_g(E)$ and $T_g(R)$ and the measured $T_g(M)$ for the macrophase separated systems (169°C) together with equation 3.13, the weight fraction of epoxy resin in the epoxy rich phase of these samples can be estimated to be approximately 0.80.

Bates, Wu and Thio[39, 71, 72] have observed an *increase* in the glass-transition of a phenol-novolac cured BADGE epoxy resin system after addition of PEO-PBO or PEO-PHO diblock copolymer. These systems form vesicles as well as wormlike and spherical micelles, but some increase is observed in all cases. It is unclear why this occurs, but the present results suggest that this behaviour is highly dependent on the curing agent in use. The cured resins produced by Bates *et al.* have relatively low glass-transition temperatures in their unmodified states (90-115°C).

3.4.2 Mechanical Properties

Figures 3.43 - 3.45 show the measured values for tensile and flexural modulus, K_{Ic} , and flexural stress at fracture for epoxy resins modified with various block copolymers. Where included, error bars indicate maximum and minimum values since only two or three samples were examined in each case.

Little can be inferred from this data. There is clearly a decrease in flexural modulus after addition of any block copolymer and this appears, unsurprisingly, to be inversely related to flexural stress at fracture. There is no indication of any sizeable effect on fracture toughness (K_{Ic}). This may be because of difficulty encountered in obtaining reproducible initial cracks in the fracture toughness samples. The samples were sufficiently brittle that crack initiation tended to lead to complete fracture. This might be fixed by using larger samples in order to allow the initial crack to propagate further without reaching the edge of the sample. This has not been tried since supplies of material are limited. It may well be that the micellar systems simply do not toughen this resin system.

Bates *et al.* [39, 71, 72] have reported enhanced fracture toughness in micelle containing systems of PEO-PBO and PEO-PHO in phenol novolac cured BADGE. They have typically observed a doubling of K_{Ic} in the presence of spherical micelles. As noted above, their epoxy resin system is significantly different to that employed here and it is known that changing the cross-linking agent in an epoxy system can dramatically affect its susceptibility to toughening [1].

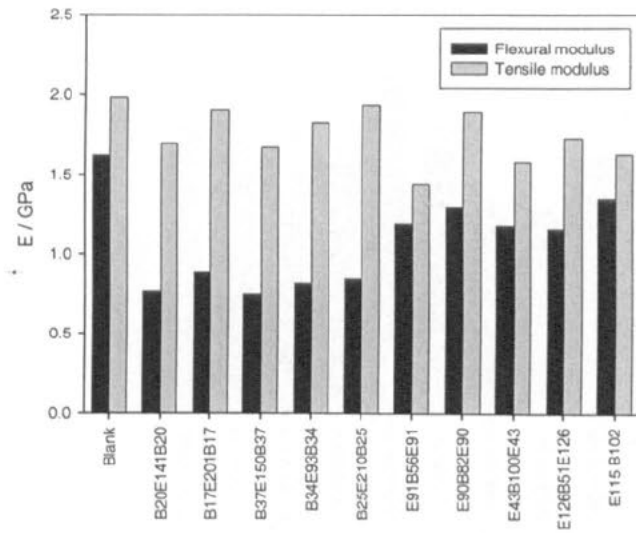


Figure 3.42 – Flexural and tensile modulus values for cured samples of BADGE + DETDA modified with 5wt% of various block copolymers

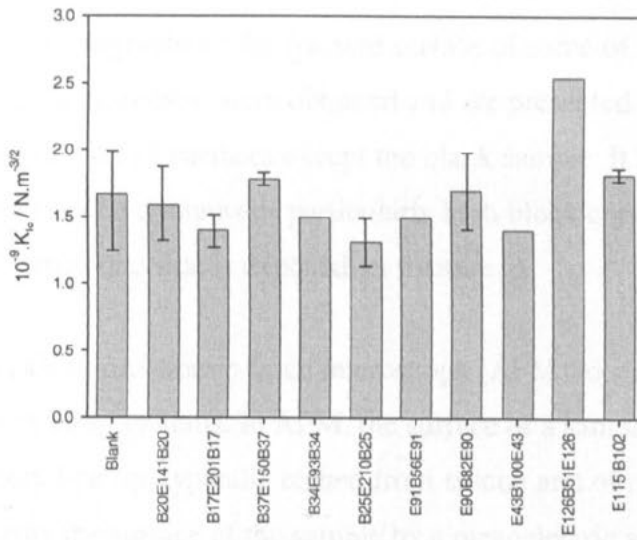


Figure 3.43 – K_{1c} (fracture toughness) values determined for cured samples of BADGE + DETDA modified with 5wt% of various block copolymers

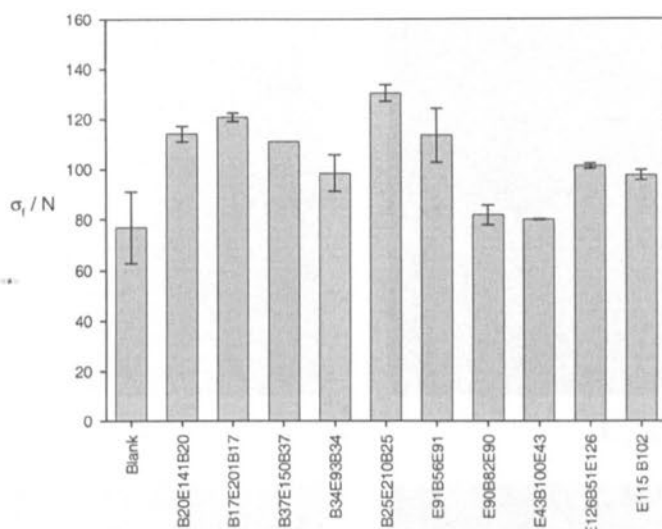
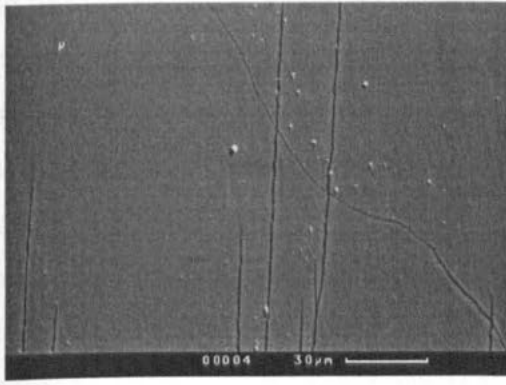


Figure 3.44 – Flexural stress at fracture for cured samples of BADGE + DETDA modified with 5wt% of various block copolymers

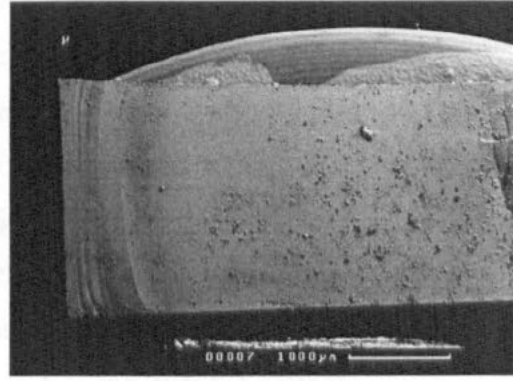
3.4.3 Other Observations

Scanning electron micrographs of the fracture surface of some of the samples used in fracture toughness measurement were obtained and are presented in Figure 3.45. Protrusions are visible on all surfaces except the blank sample. It is unclear what these are, but they may be domains of particularly high block copolymer concentration of which one side is exposed on fracture.

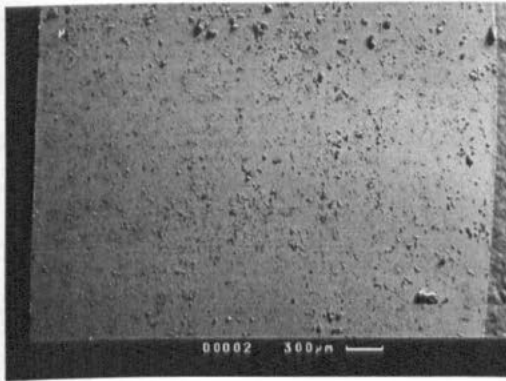
Attempts were made to use atomic force microscopy (AFM) to study the nanoscale phase separation in these systems. In AFM, the surface of a sample is mechanically probed using a very fine tip, typically etched from silicon and of radius ~ 10 nm. The tip is rastered across the surface of the sample by a piezoelectric actuator. The vertical deflection of the tip is determined by monitoring the displacement of a laser beam reflected from the top side of the cantilever on which the tip is located. In this way, surface features having lateral dimensions on the order of nanometres can be imaged with sub-nanometre vertical resolution.



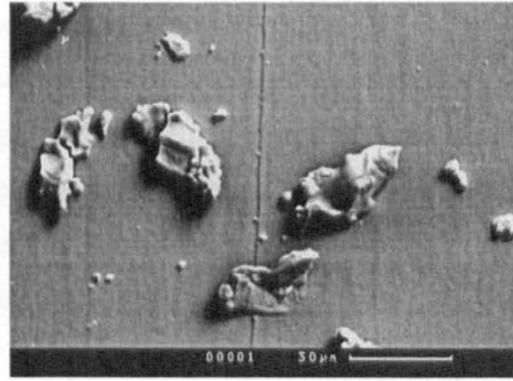
Blank Sample



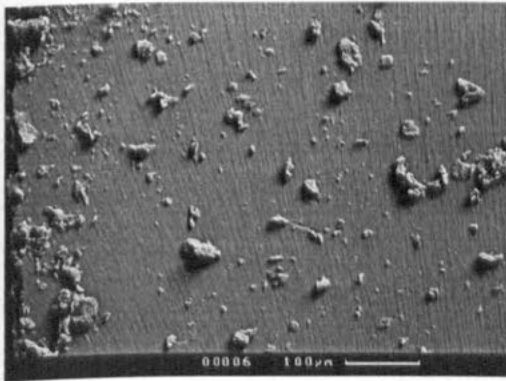
$E_{115}B_{102}$



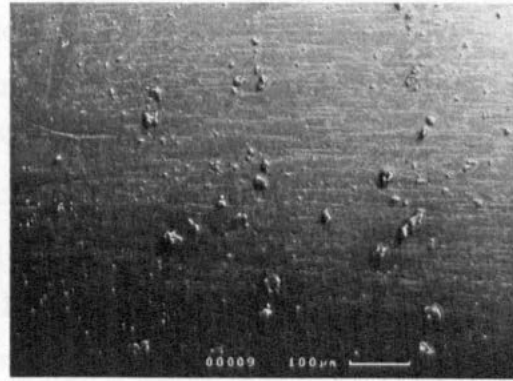
$E_{126}B_{51}E_{126}$ - 'Wide angle'



$E_{126}B_{51}E_{126}$ - 'Close-up'



$B_{34}E_{93}B_{34}$



$B_{25}E_{210}B_{25}$

Figure 3.45 – Scanning electron micrographs from fracture surfaces of modified epoxy samples which had been cured at 75°C, post-cured at 180°C and fractured using a razor blade to initiate the crack then bending to propagate the crack.

In this case 'tapping mode' AFM was used. Here the tip is vibrated such that it resonates at some frequency and the shift in that frequency is monitored as the surface is scanned. The frequency changes depending on how heavily damped the vibrations are on interaction with the surface. Hence 'hard' regions of the surface can be distinguished from 'soft' regions by viewing the phase-contrast image. An additional advantage of the tapping mode technique in polymer studies is that the reduced contact of the tip with the surface minimizes damage to the sample (as compared with 'contact mode' where the tip is dragged over the surface).

Figure 3.46 shows AFM images obtained from a sample containing 20wt% $B_{25}E_{210}B_{25}$. The first time that the AFM tip passes over an area on the sample, large soft, dark, areas are visible in the phase image. When the tip is passed over the same region for a second time, these structures appear to have been crushed and dragged to one side by the tip. It is possible that these structures are composed PEO chains which have crystallized as they are exposed on the surface. Contact with the tip leads to disruption of the crystallites.

Figure 3.47 shows the phase image for a cured sample containing 20wt% of $B_{20}E_{141}B_{20}$. This appears to show the existence of structure on nanometre length scales. It was hoped that AFM would be complimentary to SAXS and allow characterization of those samples where SAXS patterns are not well defined. Unfortunately, experimental difficulties were encountered in the form of repeated fouling of the AFM tip. This made obtaining good quality images impossible without frequent replacement of the costly AFM tip. Presumably, this was due to the tip 'picking up' some part of the sample, such as the surface features described above. AFM imaging was abandoned after repeated attempts to overcome this problem were unsuccessful.

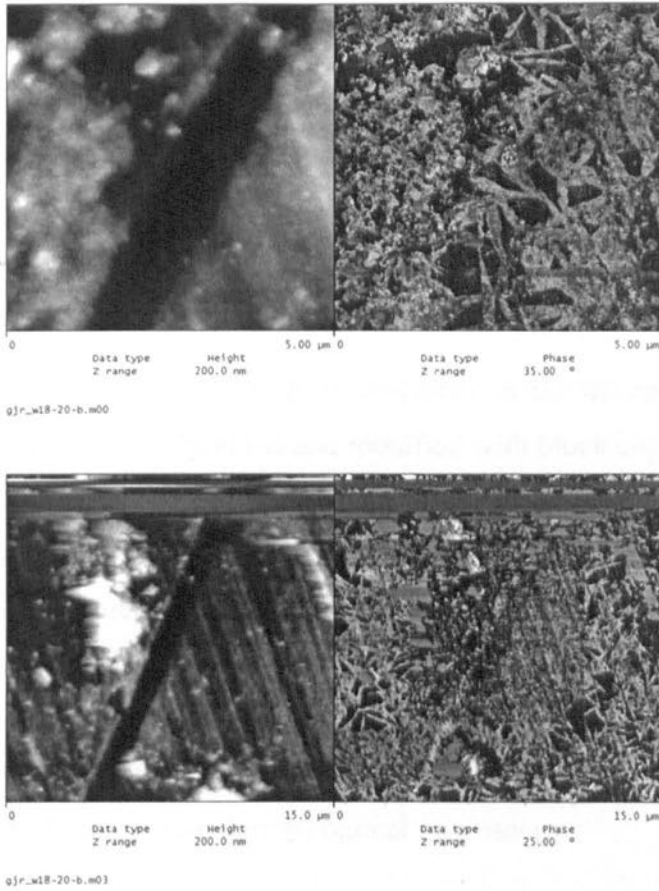


Figure 3.46 – AFM height (left) and phase (right) images from a sample of BADGE+DETDA containing 20wt% $B_{25}E_{210}B_{25}$ cured at 75°C. The upper image is the first scan and the lower image is a second, subsequent, scan centred on the same area.

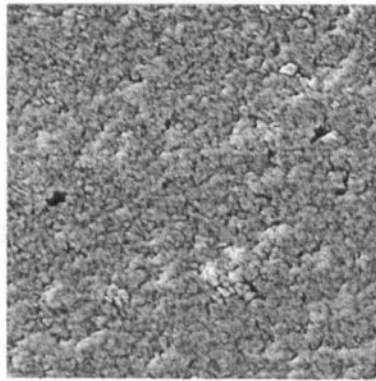


Figure 3.47 – AFM phase image of a sample containing 20wt% of $B_{20}E_{141}B_{20}$. The image is 2μm wide.

4 Conclusions and Future Work

4.1 Summary & Conclusions

Systems consisting of a bisphenol-A, diglycidyl ether (BADGE) epoxy resin cured with diethyltoluenediamine (DETDA) and modified with block copolymers composed of poly(ethylene oxide) (PEO) and poly(butylene oxide) (PBO) have been investigated. Samples were prepared containing a range of concentrations of block copolymers having different architectures (EB diblocks, EBE and BEB triblocks), and differing compositions, as measured by the volume fraction of one component in the block copolymer. The morphology of the cured samples on micron and nanometre length scales was investigated using a range of techniques, including SAXS, SALS, TEM and cross-polarized optical microscopy.

Initial experiments demonstrated that PBO homopolymer displays an upper critical solution temperature (UCST) in BADGE. The ability of some of the BEB triblocks used to form bridged micellar networks in aqueous solution was also confirmed by dynamic light-scattering. It was hoped that the formation of bridged micellar networks of block copolymer in the epoxy resin might lead to significant improvement in mechanical properties of the cured epoxy.

The curing kinetics of a diblock containing system that is known to form micelles in the cured resin at low block copolymer concentration was investigated by FTIR spectroscopy. Other workers have observed a retardation of the reaction rate in PEO containing systems[45, 47]. They attribute this to hydrogen-bonding between PEO and the epoxy system interfering with the auto-catalytic reaction mechanism. Such behaviour was not observed in this system, possibly because the interaction between PEO and the resin is limited by geometric constraints imposed by the confinement of PEO to the micellar corona. A marked reduction in reaction rate was observed at

high concentrations. This was attributed to the transition from a solution of block copolymer in a reactive solvent to a block copolymer gel swollen by a reactive diluent.

Optical observation of the cured samples, both by microscopy and with the naked eye, demonstrated a number of features. PEO crystallites are clearly observed at higher concentrations. In lower concentration samples, turbidity indicates the presence of structures with size similar to that of the wavelength of visible light; this was attributed to flocculation of micellar particles. Reaction-induced macrophase separation was observed in one BEB containing system, but not in an EBE system of similar composition.

Small angle X-ray scattering (SAXS) experiments revealed microphase separation on the nanometre scale in many of the samples. Taking the results for all samples in combination, the following general pattern was observed. At low concentrations interacting micellar structures may be formed in an epoxy matrix. As expected, the degree of interaction between micelles increases as concentration is increased. When the concentration gets sufficiently high, packed cubic structures are observed and the system becomes more like a swollen block copolymer gel. Further increases in block copolymer concentration result in phase transitions from cubic packed spheres to hexagonally packed cylinders and then on, sometimes through a gyroid phase, to lamellar structures. This is the sequence of transitions which has been observed in block copolymer systems when a solvent which is selective for one of the blocks is added, similar behaviour has also been reported in one of the modified epoxy systems investigated by Dean[40]. The behaviour is consistent with selective swelling of the PEO block by the epoxy resin, thereby increasing the volume fraction of the (PEO + epoxy) component at lower block copolymer concentrations. SAXS patterns obtained from samples cured at elevated temperature suggest that the tendency of the epoxy to preferentially swell PEO over PBO increases with increased temperature.

The tendency to microphase separate is dependent on the architecture of the block copolymer and on the PBO content. Systems having copolymers with low PBO content do not microphase separate from the resin at low concentrations.

The micellar structure in low concentration samples was confirmed by transmission electron microscopy (TEM). The Rayleigh-Percus-Yevick model allows the determination, from SAXS data, of characteristic parameters for micellar systems, such as those observed here, where the interactions between micelles are sufficiently close to those expected between a set of hard spheres. Those samples for which the data were a good fit to the model were analyzed and trends in their respective parameters were determined.

It is clear from SAXS experiments performed before and after curing that some of the low concentration systems undergo reaction-induced micellization. That is, starting from a homogenous, or poorly ordered, system the PBO blocks phase separate during curing so that the cured product contains micelles. The degree of microphase separation prior to cure, and the probability of reaction-induced microphase separation occurring in those systems with no structure prior to cure, was found to be dependent on the volume fraction of PBO in the copolymer. Time-resolved SAXS data, combined with kinetics data from the FTIR experiments, shows that the maximum scattering intensity increases linearly with extent of reaction until a maximum is reached. This is consistent with a linear increase in the number of micelles up to the point where all of the PBO has phase separated.

In some cases, where the volume fraction of PBO in the block copolymer is too low, vitrification sets in before the reaction-induced micellization process is complete and non-equilibrium structures are observed. This is supported by data from samples cured using a more reactive curing agent. Micelle dimensions were shown to be reasonably independent of curing agent for those systems where the microphase separation process is complete before vitrification occurs.

The ratio of the number of micelles present in pairs of samples was estimated from the fitted SAXS data. In systems where the microphase separation process had gone to completion before vitrification occurred, and at low concentrations, the number of micelles doubles on doubling the concentration. At higher concentrations the relationship between block copolymer concentration and number density of micelles becomes non-linear. This is consistent with the onset of the situation where some of the additional block copolymer is consumed in swelling the existing structures, which will eventually lead to long-range order and observation of the sequence of structures described above.

From measurements of the micellar core radius, the association number, N , of the micelles has been determined to scale with block copolymer composition in a very similar manner to that observed for PEO/PBO copolymers in water. For $E_m B_n$, $E_m B_{2n} E_m$ and $B_n E_m B_n$ systems, the association number was found to scale as $m^{-0.61} n^{1.22}$. This was found to be in good agreement with the value determined by Booth and co-workers for aqueous systems[120].

Increasing the curing temperature was found to increase the observed radius of the micelles.

Reaction-induced macrophase separation was observed in one BEB sample on curing at 75°C and in others at elevated temperature. The process was characterized by optical microscopy and time-resolved small-angle light scattering (SALS). The observations were found to be consistent with phase separation by spinodal decomposition in accordance with the Cahn-Hilliard linear theory in the early stage. Vitrification occurs before the process is complete, yielding a cured sample with an interpenetrating network of phase separated domains.

The glass transition temperature of cured epoxy resin was shown to decrease after the addition of low concentrations of block copolymer. By fitting data from samples with a constant weight fraction of block copolymer in the system to the Fox equation, it was determined that, in most cases, the decrease is the result of dilution of the resin

by PEO and is independent of PBO content. Two BEB samples showed anomalously high T_g s given their compositions – although they were still lower than the value for the unmodified resin. It is suggested that this may be due to flocculation of micelles.

The modulus of bulk samples was determined to decrease after addition of block copolymer and a corresponding increase in the flexural stress at break was observed. Fracture toughness did not appear to be improved by any significant degree, although this could be due to inadequacies in the testing process. It is noted that the only experiments where a significant increase in fracture toughness is observed in a system containing spherical micelles are those of the Bates group[39, 71] using a specific phenol-novolac cured epoxy resin system which also displays anomalous T_g behaviour.

4.2 Future Work

The results obtained in the present work suggest a number of further series of experiments which might provide interesting results.

Reaction kinetics in micelle forming systems

Further experiments could be carried out to compliment the results obtained here which demonstrate that micelle forming systems do not exhibit the same degree of retardation displayed by PEO + Epoxy and non-micellizing block copolymer + epoxy systems. If the experimental procedure used herein can be modified so as to improve the signal-to-noise ratio and therefore improve resolution then it would be possible to perform a series of experiments using a range of micellizing systems so as to confirm the behaviour observed here and to fully determine the factors affecting the reaction rate. It would be interesting to observe the effect of differing degrees of microphase separation prior to cure on the curing kinetics (i.e. from systems which are fully microphase separated prior to cure, through those which are initially partially separated to those which show no evidence of microphase separation until the reaction is partially complete.)

Reaction-induced microphase separation

The process of reaction-induced micellization observed here appears worthy of further investigation. It is hoped that time-resolved SAXS at a synchrotron radiation facility might allow improved observations of the process. In particular it would be useful to determine at what point in the separation process the scattering data becomes a good fit to the RPY, and whether this would allow a mechanism for the process to be deduced.

It would also be interesting to observe the effect of concentration on reaction-induced microphase separation. Although Meng *et al.*[59] have reportedly observed reaction-induced formation of a structure showing long range cubic symmetry, however, little data is available to confirm this observation.

Micellar network formation and mechanical properties

It was hoped that it might be possible to observe the effect of a bridging micellar structure on the mechanical properties of an epoxy system. This has not proved to be achievable with these systems. It might be possible to make such a system using epoxy reactive triblocks as described in the introduction. Alternatively, if a triblock was synthesised with a low volume fraction of epoxy-immiscible end groups, but a large overall molecular weight, then it might form these structures prior to cure and maintain the structure throughout cure. For example, in Wu's work with PEO-PBO diblocks in epoxy resins[39], copolymers with much larger PBO blocks were used (together with a corresponding increase in the size of the PEO block).

References

1. B. Ellis; *Chemistry and technology of epoxy resins*. 1993: Blackie Academic & Professional
2. C. A. May; *Epoxy resins : chemistry and technology*. 2nd ed. rev. and expanded / edited by Clayton A. May. ed. 1988, New York, N.Y.: Dekker
3. P. Alexandridis and B. r. Lindman; *Amphiphilic block copolymers : self-assembly and applications*. 2000, Amsterdam ; Oxford: Elsevier
4. N. Hadjichristidis; S. Pispas, and G. Floudas; *Block copolymers : synthetic strategies, physical properties, and applications*. 2003, New York: Wiley
5. I. W. Hamley; *The physics of block copolymers*. 1998, Oxford: Oxford University Press
6. I. W. Hamley; *Developments in block copolymer science and technology*. 2004, Chichester: J. Wiley
7. I. W. Hamley; *Block copolymers in solution : fundamentals and applications*. 2005, Chichester: John Wiley
8. M. A. Hillmyer; P. M. Lipic; D. A. Hajduk; K. Almdal, and F. S. Bates; *Self-Assembly and Polymerization of Epoxy Resin-Amphiphilic Block Copolymer Nanocomposites*. *Journal of the American Chemical Society*, 1997. **119**(11): p. 2749-2750.
9. P. J. Flory; *Molecular size distribution in three-dimensional polymers. I. Gelation*. *Journal of the American Chemical Society*, 1941. **63**: p. 3083-90.
10. P. J. Flory; *Fundamental principles of condensation polymerization*. *Chem. Rev.*, 1946. **39**: p. 137-97.
11. W. H. Stockmayer; *Theory of molecular size distribution and gel formation in branched-chain polymers*. *Journal of Chemical Physics*, 1943. **11**: p. 45-55.
12. W. H. Stockmayer; *Theory of molecular size distribution and gel formation in branched polymers. II. General cross linking*. *Journal of Chemical Physics*, 1944. **12**: p. 125-31.
13. B. A. Rozenberg; *Kinetics, Thermodynamics and Mechanism of Reactions of Epoxy Oligomers with Amines*. *Advances in Polymer Science*, 1986. **75**: p. 113-165.
14. K. Horie; H. Hiura; M. Sawada; I. Mita, and H. Kambe; *Calorimetric investigation of polymerization reactions. III. Curing reaction of epoxides with amines*. *Journal of Polymer Science, Polymer Chemistry Edition*, 1970. **8**(6): p. 1357-72.
15. G. Wisanrakkit and J. K. Gillham; *The glass transition temperature (T_g) as an index of chemical conversion for a high-T_g amine/epoxy system: chemical and diffusion-controlled reaction kinetics*. *Journal of Applied Polymer Science*, 1990. **41**(11-12): p. 2885-929.
16. Y. Ishii and A. J. Ryan; *Processing of poly(2,6-dimethyl-1,4-phenylene ether) with epoxy resin. 2. Gelation mechanism*. *Macromolecules*, 2000. **33**(1): p. 167-176.

17. J. G. Williams; *Fracture mechanics of polymers*. Ellis Horwood series in mechanical engineering. 1984, Chichester: Ellis Horwood
18. A. Griffith; *The Phenomena of Rupture and Flow in Solids*. Philosophical Transactions of the Royal Society of London. Series A, Containing Papers of a Mathematical or Physical Character (1896-1934), 1921. **221**: p. 163-198.
19. Y. Huang and A. J. Kinloch; *The sequence of initiation of the toughening micromechanisms in rubber-modified epoxy polymers*. *Polymer*, 1992. **33**(24): p. 5338-40.
20. Y. Huang and A. J. Kinloch; *The role of plastic void growth in the fracture of rubber-toughened epoxy polymers*. *Journal of Materials Science Letters*, 1992. **11**(8): p. 484-7.
21. J. M. G. Cowie; *Polymers : chemistry and physics of modern materials*. 2nd ed ed. 1991, Glasgow: Blackie
22. P. I. Flory; *Thermodynamics of high polymer solutions*. *Journal of Chemical Physics*, 1942. **10**(1): p. 51-61.
23. P. J. Flory; *Principles of polymer chemistry*. The George Fisher Baker non-resident lectureship in chemistry at Cornell University. 1953, Ithaca, N.Y. ; London: Cornell University Press
24. M. L. Huggins; *Some properties of solutions of long-chain compounds*. *Journal of Physical Chemistry*, 1942. **46**(1): p. 151-158.
25. M. L. Huggins; *Theory of solutions of high polymers*. *Journal of the American Chemical Society*, 1942. **64**: p. 1712-1719.
26. M. L. Huggins; *Thermodynamic properties of solutions of long-chain compounds*. *Annals of the New York Academy of Sciences*, 1942. **43**(Art. 1): p. 1-32.
27. R. Kenzler; F. Eurich; P. Maass; B. Rinn; J. Schropp; E. Bohl, and W. Dieterich; *Phase separation in confined geometries: Solving the Cahn-Hilliard equation with generic boundary conditions*. *Computer Physics Communications*, 2001. **133**(2-3): p. 139-157.
28. R. J. J. Williams; B. A. Rozenberg, and J.-P. Pascault; *Reaction-induced phase separation in modified thermosetting polymers*. *Advances in Polymer Science*, 1997. **128**: p. 95-156.
29. J. Arnauts and H. Berghmans; *Amorphous thermoreversible gels of atactic polystyrene*. *Polymer Communications*, 1987. **28**(3): p. 66-8.
30. V. M. Nace; *Nonionic surfactants : polyoxyalkylene block copolymers*. Surfactant science series ; v. 60. 1996, New York: M. Dekker
31. I. W. Hamley; *Introduction to soft matter : polymers, colloids, amphiphiles, and liquid crystals*. 2000, Chichester ; New York: Wiley
32. D. E. Discher and A. Eisenberg; *Polymer Vesicles*. *Science*, 2002. **297**(5583): p. 967-973.
33. M. W. Matsen; *Phase Behavior of Block Copolymer/Homopolymer Blends*. *Macromolecules*, 1995. **28**(17): p. 5765-73.
34. A. E. Likhtman and A. N. Semenov; *Theory of Microphase Separation in Block Copolymer/Homopolymer Mixtures*. *Macromolecules*, 1997. **30**(23): p. 7273-7278.
35. L. Konczol; W. Doll; U. Buchholz, and R. Mulhaupt; *Ultimate properties of epoxy resins modified with a polysiloxane-polycaprolactone block copolymer*. *Journal of Applied Polymer Science*, 1994. **54**(6): p. 815-26.

36. P. M. Lipic; F. S. Bates, and M. A. Hillmyer; *Nanostructured Thermosets from Self-Assembled Amphiphilic Block Copolymer/Epoxy Resin Mixtures*. *Journal of the American Chemical Society*, 1998. **120**(35): p. 8963-8970.
37. J. Mijovic; M. Shen; J. W. Sy, and I. Mondragon; *Dynamics and Morphology in Nanostructured Thermoset Network/Block Copolymer Blends during Network Formation*. *Macromolecules*, 2000. **33**(14): p. 5235-5244.
38. Q. Guo; K. Wang; L. Chen; S. Zheng, and P. J. Halley; *Phase behavior, crystallization, and nanostructures in thermoset blends of epoxy resin and amphiphilic star-shaped block copolymers*. *Journal of Polymer Science, Part B: Polymer Physics*, 2006. **44**(6): p. 975-985.
39. J. Wu; Y. S. Thio, and F. S. Bates; *Structure and properties of PBO-PEO diblock copolymer modified epoxy*. *Journal of Polymer Science, Part B: Polymer Physics*, 2005. **43**(15): p. 1950-1965.
40. J. M. Dean; P. M. Lipic; R. B. Grubbs; R. F. Cook, and F. S. Bates; *Micellar structure and mechanical properties of block copolymer-modified epoxies*. *Journal of Polymer Science, Part B: Polymer Physics*, 2001. **39**(23): p. 2996-3010.
41. J. M. Dean; N. E. Verghese; H. Q. Pham, and F. S. Bates; *Nanostructure Toughened Epoxy Resins*. *Macromolecules*, 2003. **36**(25): p. 9267-9270.
42. Q. Guo; R. Thomann; W. Gronski, and T. Thurn-Albrecht; *Phase Behavior, Crystallization, and Hierarchical Nanostructures in Self-Organized Thermoset Blends of Epoxy Resin and Amphiphilic Poly(ethylene oxide)-block-poly(propylene oxide)-block-poly(ethylene oxide) Triblock Copolymers*. *Macromolecules*, 2002. **35**(8): p. 3133-3144.
43. P. Sun; Q. Dang; B. Li; T. Chen; Y. Wang; H. Lin; Q. Jin; D. Ding, and A.-C. Shi; *Mobility, Miscibility, and Microdomain Structure in Nanostructured Thermoset Blends of Epoxy Resin and Amphiphilic Poly(ethylene oxide)-block-poly(propylene oxide)-block-poly(ethylene oxide) Triblock Copolymers Characterized by Solid-State NMR*. *Macromolecules*, 2005. **38**(13): p. 5654-5667.
44. M. Larrañaga; P. Arruti; E. Serrano; K. Caba; P. M. Remiro; C. C. Riccardi, and I. Mondragon; *Towards microphase separation in epoxy systems containing PEO/PPO/PEO block copolymers by controlling cure conditions and molar ratios between blocks. Part 2. Structural characterization*. *Colloid and Polymer Science*, 2006. **284**(12): p. 1419-1430.
45. M. Larrañaga; M. D. Martin; N. Gabilondo; G. Kortaberria; A. Eceiza; C. C. Riccardi, and I. Mondragon; *Towards microphase separation in epoxy systems containing PEO-PPO-PEO block copolymers by controlling cure conditions and molar ratios between blocks: Part 1. Cure Kinetics*. *Colloid and Polymer Science*, 2006. **284**(12): p. 1403-1410.
46. M. Larrañaga; N. Gabilondo; G. Kortaberria; E. Serrano; P. Remiro; C. C. Riccardi, and I. Mondragon; *Micro- or nano-separated phases in thermoset blends of an epoxy resin and PEO-PPO-PEO triblock copolymer*. *Polymer*, 2005. **46**(18): p. 7082-7093.
47. M. Larrañaga; M. D. Martin; N. Gabilondo; G. Kortaberria; M. A. Corcuera; C. C. Riccardi, and I. Mondragon; *Cure kinetics of epoxy systems modified with block copolymers*. *Polymer International*, 2004. **53**(10): p. 1495-1502.
48. Q. Guo; J. M. Dean; R. B. Grubbs, and F. S. Bates; *Block copolymer modified novolac epoxy resin*. *Journal of Polymer Science, Part B: Polymer Physics*, 2003. **41**(17): p. 1994-2003.
49. R. B. Grubbs; J. M. Dean; M. E. Broz, and F. S. Bates; *Reactive Block Copolymers for Modification of Thermosetting Epoxy*. *Macromolecules*, 2000. **33**(26): p. 9522-9534.
50. Q. Guo; P. Figueiredo; R. Thomann, and W. Gronski; *Phase behavior, morphology and interfacial structure in thermoset/thermoplastic elastomer blends of poly(propylene glycol)-type epoxy resin and polystyrene-*b*-polybutadiene*. *Polymer*, 2001. **42**(26): p. 10101-10110.

51. E. Serrano; M. D. Martin; A. Tercjak; J. A. Pomposo; D. Mecerreyes, and I. Mondragon; *Nanostructured thermosetting systems from epoxidized styrene butadiene block copolymers*. *Macromolecular Rapid Communications*, 2005. **26**(12): p. 982-985.
52. E. Serrano; A. Tercjak; G. Kortaberria; J. A. Pomposo; D. Mecerreyes; N. E. Zafeiropoulos; M. Stamm, and I. Mondragon; *Nanostructured Thermosetting Systems by Modification with Epoxidized Styrene-Butadiene Star Block Copolymers. Effect of Epoxidation Degree*. *Macromolecules*, 2006. **39**(6): p. 2254-2261.
53. J. M. Dean; R. B. Grubbs; W. Saad; R. F. Cook, and F. S. Bates; *Mechanical properties of block copolymer vesicle and micelle modified epoxies*. *Journal of Polymer Science, Part B: Polymer Physics*, 2003. **41**(20): p. 2444-2456.
54. S. Ritzenthaler; F. Court; L. David; E. Girard-Reydet; L. Leibler, and J. P. Pascault; *ABC Triblock Copolymers/Epoxy-Diamine Blends. 1. Keys To Achieve Nanostructured Thermosets*. *Macromolecules*, 2002. **35**(16): p. 6245-6254.
55. S. Ritzenthaler; F. Court; E. Girard-Reydet; L. Leibler, and J. P. Pascault; *ABC triblock copolymers/epoxy-diamine blends. 2. Parameters controlling the morphologies and properties*. *Macromolecules*, 2003. **36**(1): p. 118-126.
56. H. Kosonen; J. Ruokolainen; P. Nyholm, and O. Ikkala; *Self-Organized Thermosets: Blends of Hexamethylenetetramine Cured Novolac with Poly(2-vinylpyridine)-block-poly(isoprene)*. *Macromolecules*, 2001. **34**(9): p. 3046-3049.
57. H. Kosonen; J. Ruokolainen; P. Nyholm, and O. Ikkala; *Self-organized cross-linked phenolic thermosets: thermal and dynamic mechanical properties of novolac/block copolymer blends*. *Polymer*, 2001. **42**(23): p. 9481-9486.
58. Q. Guo; R. Thomann; W. Gronski; R. Staneva; R. Ivanova, and B. Stuehn; *Nanostructures, Semicrystalline Morphology, and Nanoscale Confinement Effect on the Crystallization Kinetics in Self-Organized Block Copolymer/Thermoset Blends*. *Macromolecules*, 2003. **36**(10): p. 3635-3645.
59. F. Meng; S. Zheng; H. Li; Q. Liang, and T. Liu; *Formation of Ordered Nanostructures in Epoxy Thermosets: A Mechanism of Reaction-Induced Microphase Separation*. *Macromolecules*, 2006. **39**(15): p. 5072-5080.
60. F. Meng; S. Zheng; W. Zhang; H. Li, and Q. Liang; *Nanostructured Thermosetting Blends of Epoxy Resin and Amphiphilic Poly(ϵ -caprolactone)-block-polybutadiene-block-poly(ϵ -caprolactone) Triblock Copolymer*. *Macromolecules*, 2006. **39**(2): p. 711-719.
61. I. A. Zucchi; M. J. Galante, and R. J. J. Williams; *Comparison of morphologies and mechanical properties of crosslinked epoxides modified by polystyrene and polymethyl methacrylate or by the corresponding block copolymer polystyrene-*b*-poly(methyl methacrylate)*. *Polymer*, 2005. **46**(8): p. 2603-2609.
62. T. Fine; F. Lortie; L. David, and J.-P. Pascault; *Structures and rheological properties of reactive solutions of block copolymers. Part I. Diblock copolymers in a liquid epoxy monomer*. *Polymer*, 2005. **46**(17): p. 6605-6613.
63. V. Rebizant; V. Abetz; F. Tournilhac; F. Court, and L. Leibler; *Reactive Tetrablock Copolymers Containing Glycidyl Methacrylate. Synthesis and Morphology Control in Epoxy-Amine Networks*. *Macromolecules*, 2003. **36**(26): p. 9889-9896.
64. V. Rebizant; A.-S. Venet; F. Tournilhac; E. Girard-Reydet; C. Navarro; J.-P. Pascault, and L. Leibler; *Chemistry and Mechanical Properties of Epoxy-Based Thermosets Reinforced by Reactive and Nonreactive SBMX Block Copolymers*. *Macromolecules*, 2004. **37**(21): p. 8017-8027.
65. R. B. Grubbs; M. E. Broz; J. M. Dean, and F. S. Bates; *Selectively Epoxidized Polyisoprene-Polybutadiene Block Copolymers*. *Macromolecules*, 2000. **33**(7): p. 2308-2310.

66. A. S. Argon; R. E. Cohen, and T. M. Mower; *Mechanisms of toughening brittle polymers*. Materials Science & Engineering, A: Structural Materials: Properties, Microstructure and Processing, 1994. **176**(1-2): p. 79-90.
67. R. A. Pearson and A. F. Yee; *Toughening mechanisms in elastomer-modified epoxies. Part 2. Microscopy studies*. Journal of Materials Science, 1986. **21**(7): p. 2475-88.
68. R. A. Pearson and A. F. Yee; *Toughening mechanisms in elastomer-modified epoxies. Part 3. The effect of crosslink density*. Journal of Materials Science, 1989. **24**(7): p. 2571-80.
69. P. C. Yang; E. P. Woo; M. T. Bishop; D. M. Pickelman, and H. J. Sue; *Rubber toughening of thermosets - a system approach*. Polymeric Materials Science and Engineering, 1990. **63**: p. 315-21.
70. A. F. Yee and R. A. Pearson; *Toughening mechanisms in elastomer-modified epoxies. Part 1. Mechanical studies*. Journal of Materials Science, 1986. **21**(7): p. 2462-74.
71. Y. S. Thio; J. Wu, and F. S. Bates; *Epoxy Toughening Using Low Molecular Weight Poly(hexylene oxide)-Poly(ethylene oxide) Diblock Copolymers*. Macromolecules, 2006. **39**(21): p. 7187-7189.
72. F. S. Bates and S. F. Hahn; *Amphiphilic block copolymer-toughened epoxy resins*; WO2006052729.
73. Dow Chemicals Website; <http://www.dow.com/productsafety/finder/bisphenol.htm>; Access date: 20th August 2006.
74. G. King; *Estimation of Epoxides*. Nature, 1949. **164**: p. 706-707.
75. C. Chaibundit; W. Mingvanish; C. Booth; S.-M. Mai; S. C. Turner; J. P. A. Fairclough; A. J. Ryan, and P. Pissis; *Effect of Architecture on the Crystal Morphology of Block Copolymers. Small-Angle X-ray Scattering and Differential Scanning Calorimetry*. Macromolecules, 2002. **35**(12): p. 4838-4840.
76. C. Chaibundit; W. Mingvanish; S. C. Turner; S.-M. Mai; J. P. A. Fairclough; A. J. Ryan; M. W. Matsen, and C. Booth; *Microphase separation in oxyethylene/oxybutylene copolymers with diblock and triblock architectures*. Macromolecular Rapid Communications, 2000. **21**(14): p. 964-967.
77. S. M. Mai; J. P. A. Fairclough; I. W. Hamley; M. W. Matsen; R. C. Denny; B. X. Liao; C. Booth, and A. J. Ryan; *Order-Disorder Transition in Poly(oxyethylene)-Poly(oxybutylene) Diblock Copolymers*. Macromolecules, 1996. **29**(19): p. 6212-6221.
78. J. P. A. Fairclough; S.-M. Mai; M. W. Matsen; W. Bras; L. Messe; S. C. Turner; A. J. Gleeson; C. Booth; I. W. Hamley, and A. J. Ryan; *Crystallization in block copolymer melts: Small soft structures that template larger hard structures*. Journal of Chemical Physics, 2001. **114**(12): p. 5425-5431.
79. I. W. Hamley; M. L. Wallwork; D. A. Smith; J. P. A. Fairclough; A. J. Ryan; S. M. Mai; Y. W. Yang, and C. Booth; *Crystal thicknesses in semicrystalline oxyethylene/oxybutylene block copolymers by atomic force microscopy and SAXS*. Polymer, 1998. **39**(15): p. 3321-3326.
80. S.-M. Mai; J. P. A. Fairclough; N. J. Terrill; S. C. Turner; I. W. Hamley; M. W. Matsen; A. J. Ryan, and C. Booth; *Microphase Separation in Poly(oxyethylene)-Poly(oxybutylene) Diblock Copolymers*. Macromolecules, 1998. **31**(23): p. 8110-8116.
81. S.-M. Mai; J. P. A. Fairclough; K. Viras; P. A. Gorry; I. W. Hamley; A. J. Ryan, and C. Booth; *Chain folding in semicrystalline oxyethylene/oxybutylene diblock copolymers*. Macromolecules, 1997. **30**(26): p. 8392-8400.
82. A. J. Ryan; J. P. A. Fairclough; I. W. Hamley; S.-M. Mai, and C. Booth; *Chain folding in crystallizable block copolymers*. Macromolecules, 1997. **30**(6): p. 1723-1727.
83. A. J. Ryan; S.-M. Mai; J. P. A. Fairclough; I. W. Hamley, and C. Booth; *Ordered melts of block copolymers of ethylene oxide and 1,2-butylene oxide*. Physical Chemistry Chemical Physics, 2001. **3**(15): p. 2961-2971.

84. Y.-W. Yang; S. Tanodekaew; S.-M. Mai; C. Booth; A. J. Ryan; W. Bras, and K. Viras; *Structures of oxyethylene/oxybutylene diblock copolymers in their solid and liquid states*. *Macromolecules*, 1995. **28**(18): p. 6029-41.
85. S.-M. Mai; C. Booth, and V. M. Nace; *Specific volumes of poly(oxybutylene) and poly(oxyethylene) dimethyl ethers in the liquid state*. *European Polymer Journal*, 1997. **33**(7): p. 991-996.
86. S. C. Turner; *Architectural effects of block copolymer phase behaviour*. Thesis - University of Sheffield; 2000.
87. D. Campbell; R. A. Pethrick, and J. R. White; *Polymer characterization : physical techniques*. 2nd ed. 2000, Cheltenham: Stanley Thornes
88. D. B. Williams and C. B. Carter; *Transmission electron microscopy : a textbook for materials science*. 1996, New York ; London: Plenum
89. J. S. Trent; J. I. Scheinbeim, and P. R. Couchman; *Ruthenium tetraoxide staining of polymers for electron microscopy*. *Macromolecules*, 1983. **16**(4): p. 589-98.
90. C. N. Banwell; *Fundamentals of molecular spectroscopy*. 3rd ed. 1983, Maidenhead: McGraw-Hill
91. J. Mijovic and S. Andjelic; *A Study of Reaction Kinetics by Near-Infrared Spectroscopy. 1. Comprehensive Analysis of a Model Epoxy/Amine System*. *Macromolecules*, 1995. **28**(8): p. 2787-96.
92. J. Mijovic; A. Fishbain, and J. Wijaya; *Mechanistic modeling of epoxy-amine kinetics. 1. Model compound study*. *Macromolecules*, 1992. **25**(2): p. 979-85.
93. O. Glatter and O. Kratky; *Small angle x-ray scattering*. 1982, London: Academic Press
94. P. Lindner and T. Zemb; *Neutrons, X-rays and light : scattering methods applied to soft condensed matter*. North-Holland delta series, 09275029. 2002, Amsterdam ; Oxford: Elsevier
95. I. W. Hamley and V. Castelletto; *Small-angle scattering of block copolymers*. *Progress in Polymer Science*, 2004. **29**(9): p. 909-948.
96. This image is released under the GNU Free Documentation Licence. See <http://www.fsf.org/> for more details.
97. G. Margaritondo; *Elements of synchrotron light : for biology, chemistry, and medical research*. 2002, Oxford: Oxford University Press
98. R. J. Cernik; P. Barnes; G. Bushnell-Wye; A. J. Dent; G. P. Diakun; J. V. Flaherty; G. N. Greaves; E. L. Heeley; W. Helsby; S. D. M. Jacques; J. Kay; T. Rayment; A. Ryan; C. C. Tang, and N. J. Terrill; *The new materials processing beamline at the SRS Daresbury, MPW6.2*. *Journal of Synchrotron Radiation*, 2004. **11**: p. 163-170.
99. R. J. Cernik; P. Barnes; G. N. Greaves; T. Rayment, and A. J. Ryan; *Facilities for synchrotron X-ray materials processing on the SRS Daresbury*, in *Applied Crystalligraphy*, H. Morawiec and D. Stroz, Editors. 2004. p. 3-9.
100. C. C. Tang; C. M. Martin; D. Laundy; S. P. Thompson; G. P. Diakun, and R. J. Cernik; *X-ray beam characteristics on MPW6.2 at the SRS*. *Nuclear Instruments & Methods in Physics Research Section B-Beam Interactions with Materials and Atoms*, 2004. **222**(3-4): p. 659-666.
101. A. Berry; W. I. Helsby; B. T. Parker; C. J. Hall; P. A. Buksh; A. Hill; N. Clague; M. Hillon; G. Corbett; P. Clifford; A. Tidbury; R. A. Lewis; B. J. Cernik; P. Barnes, and G. E. Derbyshire; *The Rapid2 X-ray detection system*. *Nuclear Instruments & Methods in Physics Research Section a-Accelerators Spectrometers Detectors and Associated Equipment*, 2003. **513**(1-2): p. 260-263.

102. Y. Ishii; *Processing of polyphenylene ether with thermoset resins*. Thesis - University of Sheffield; 1999.
103. A. P. Hammersley; *FIT2D V9.129 Reference Manual V3.1*. ESRF Internal Report, 1998. **ESRF98HA01T**.
104. A. P. Hammersley; S. O. Svensson; M. Hanfland; A. N. Fitch, and D. Häusermann; *Two-Dimensional Detector Software: From Real Detector to Idealised Image or Two-Theta Scan*. High Pressure Research, 1996. **14**: p. 235-248.
105. *ASTM D5045 Plane-Strain Fracture Toughness and Strain Energy Release Rate of Plastic Materials*.
106. J. E. Srawley; *Wide range stress intensity factor expressions for ASTM E 399 standard fracture toughness specimens*. International Journal of Fracture, 1976. **12**(3): p. 475-476.
107. *ASTM D790 Flexural Properties of Unreinforced and Reinforced Plastics and Electrical Insulating Materials*.
108. J. W. Goodwin and R. W. Hughes; *Rheology for chemists : an introduction*. 2000, Cambridge: Royal Society of Chemistry
109. G. Ronca and T. P. Russell; *Thermodynamics of phase separation in polymer mixtures*. Macromolecules, 1985. **18**(4): p. 665-670.
110. Z. Sixun; Z. Naibin; L. Xiaolie, and M. Dezhu; *Epoxy-Resin Poly(Ethylene Oxide) Blends Cured with Aromatic Amine*. Polymer, 1995. **36**(18): p. 3609-3613.
111. T. Liu; Z. Zhou; C. Wu; V. M. Nace, and B. Chu; *Dominant factors on the micellization of BnEmBn-type triblock copolymers in aqueous solution*. Journal of Physical Chemistry B, 1998. **102**(16): p. 2875-2882.
112. T. Liu; Z. Zhou; C. Wu; V. M. Nace, and B. Chu; *Effects of block lengths on the association numbers and micellar sizes of BnEmBn type triblock copolymer micelles in aqueous solution*. Macromolecules, 1997. **30**(24): p. 7624-7626.
113. Z. Zhou; Y.-W. Yang; C. Booth, and B. Chu; *Association of a Triblock Ethylene Oxide (E) and Burylene Oxide (B) Copolymer (B12E260B12) in Aqueous Solution*. Macromolecules, 1996. **29**(26): p. 8357-8361.
114. Z. Zhou; B. Chu; V. M. Nace; Y.-W. Yang, and C. Booth; *Self-assembly characteristics of BEB-type triblock copolymers*. Macromolecules, 1996. **29**(10): p. 3663-4.
115. B. J. Berne and R. Pecora; *Dynamic light scattering : with applications to chemistry, biology, and physics*. 2000, Mineola, N.Y.: Dover Publications
116. J.-T. Xu; J. P. A. Fairclough; S.-M. Mai; C. Chaibundit; M. Mingvanish; C. Booth, and A. J. Ryan; *Crystallization behavior of oxyethylene/oxybutylene diblock and triblock copolymers*. Polymer, 2003. **44**(22): p. 6843-6850.
117. G. Battaglia; *Amphiphilic polymeric membranes*. Thesis - Sheffield; 2006.
118. G. Battaglia and A. J. Ryan; *The evolution of vesicles from bulk lamellar gels*. Nature Materials, 2005. **4**(11): p. 869-876.
119. C. Booth and D. Attwood; *Effects of block architecture and composition on the association properties of poly(oxyalkylene) copolymers in aqueous solution*. Macromolecular Rapid Communications, 2000. **21**(9): p. 501-527.

120. C. Booth; D. Attwood, and C. Price; *Self-association of block copoly(oxyalkylene)s in aqueous solution. Effects of composition, block length and block architecture*. Physical Chemistry Chemical Physics, 2006. **8**(31): p. 3612-3622.
121. G. E. Yu; H. Li; J. P. A. Fairclough; A. J. Ryan; N. McKeown; Z. Ali-Adib; C. Price, and C. Booth; *A Study of Lyotropic Mesophases of Concentrated Solutions of a Triblock Copolymer of Ethylene Oxide and 1,2-Butylene Oxide, E16B10E16, Using Rheometry, Polarized Light Microscopy, and Small-Angle X-ray Scattering*. Langmuir, 1998. **14**(20): p. 5782-5789.
122. J. K. Percus and G. J. Yevick; *Analysis of Classical Statistical Mechanics by Means of Collective Coordinates*. Physical Review, 1958. **110**(1): p. 1.
123. D. J. Kinning and E. L. Thomas; *Hard-sphere interactions between spherical domains in diblock copolymers*. Macromolecules, 1984. **17**(9): p. 1712-18.
124. K. Mortensen; *Structural studies of aqueous solutions of PEO-PPO-PEO triblock copolymers, their micellar aggregates and mesophases; a small-angle neutron scattering study*. Journal of Physics: Condensed Matter, 1996. **8**(25A): p. A103-A124.
125. K. Mortensen and W. Brown; *Poly(ethylene oxide)-poly(propylene oxide)-poly(ethylene oxide) triblock copolymers in aqueous solution. The influence of relative block size*. Macromolecules, 1993. **26**(16): p. 4128-35.
126. K. Mortensen and J. S. Pedersen; *Structural study on the micelle formation of poly(ethylene oxide)-poly(propylene oxide)-poly(ethylene oxide) triblock copolymer in aqueous solution*. Macromolecules, 1993. **26**(4): p. 805-12.
127. J. W. Cahn and J. E. Hilliard; *Free Energy of a Nonuniform System .I. Interfacial Free Energy*. Journal of Chemical Physics, 1958. **28**(2): p. 258-267.
128. Y. Ishii and A. J. Ryan; *Processing of poly(2,6-dimethyl-1,4-phenylene ether) with epoxy resin. I. Reaction-induced phase separation*. Macromolecules, 2000. **33**(1): p. 158-166.
129. J. S. Langer; M. Bar-on, and H. D. Miller; *New computational method in the theory of spinodal decomposition*. Physical Review A, 1975. **11**(4): p. 1417.
130. K. Binder; *Nucleation barriers, spinodals, and the Ginzburg criterion*. Physical Review A, 1984. **29**(1): p. 341.
131. T. G. Fox; *Influence of diluent and of copolymer composition on the glass temperature of a polymer system*. Bull. Am. Phys. Soc. [2], 1956. **1**: p. 123.
132. J. E. Mark; *Polymer data handbook*. 1999, Oxford: Oxford University Press